Eta Decays with Emphasis on Rare Neutral Modes: The JLab Eta Factory (JEF) Experiment

June 1, 2014

(The GlueX Collaboration and Other Participants)

M. Dugger,[1] B. Ritchie,[1] I. Senderovich,[1] E. Anassontzis,[2] P. Ioannou,[2] C. Kourkoumeli,[2] G. Vasileiadis,[2] G. Voulgaris,[2] N. Jarvis,[3] W. Levine,[3] P. Mattione,[3] W. McGinley,[3] C. A. Meyer,[3] R. Schumacher,[3] M. Staib,[3] F. Klein,[4] D. Sober,[4] N. Sparks,[4] N. Walford,[4] D. Doughty,[5] A. Barnes,[6] R. Jones,[6] J. McIntyre,[6] F. Mokaya,[6] B. Pratt,[6] W. Boeglin,[7] L. Guo,[7] E. Pooser,[7] J. Reinhold,[7] H. Al Ghoul,[8] V. Crede,[8] P. Eugenio,[8] A. Ostrovidov,[8] N. Sparks,[8] A. Tsaris,[8] D. Ireland,[9] K. Livingston,[9] D. Bennett,[10] J. Bennett,[10] J. Frye,[10] M. Lara,[10] J. Leckey,[10] R. Mitchell,[10] K. Moriya,[10] M. R. Shepherd,[10] O. Chernyshov,[11] A. Dolgolenko,[11] A. Gerasimov,[11] V. Goryachev,[11] I. Larin,[11] V. Matveev,[11] V. Tarasov,[11] F. Barbosa,[12] E. Chudakov,[12] M. Dalton,[12] A. Deur,[12] H. Egiyan,[12] S.Furletov,[12] M. Ito,[12] D. Lawrence,[12] M. McCaughan,[12] L. Pentchev,[12] Y. Qiang,[12] E. S. Smith,[12] A. Somov (Cospokesperson),[12] S. Taylor (Cospokesperson),[12] T. Whitlatch,[12] B. Zihlmann,[12] R. Miskimen,[13] B. Guegan,[14] J. Hardin,[14] J. Stevens,[14] M. Williams,[14] V. Berdnikov,[15] G. Nigmatkulov,[15] D. Romanov,[15] S. Somov,[15] I. Tolstukhin,[15] C. Salgado,[16] P. Ambrozewicz,[17] S. Danagoulian,[17,*] A. Gasparian,[17] R. Pedroni,[17] T. Black,[18] L. Gan (Spokesperson),[18] S. Dobbs,[19] K. Seth,[19] X. Ting,[19] A. Tomaradze,[19] T. Beattie,[20] G. Huber,[20] G. Lolos,[20] Z. Papandreou,[20] A. Semenov,[20] I. Semenova,[20] W. Brooks,[21] H. Hakobyan,[21] S. Kuleshov,[21] O. Soto,[21] A. Toro,[21] I. Vega,[21] N. Gevorgyan,[22] H. Hakobyan,[22] V. Kakoyan,[22] J. Benesch,[12,*] D. Mack (Cospokesperson),[12] X. Chen (Cospokesperson),[23,*] P. Zhang,[23,*] J. He,[23,*] D. Chen,[23,*] H. Yang,[23,*] R. Wang,[23,*] D. Armstrong,[24,*] W. Deconinck,[24,*] W. Briscoe,[25,*] A. Opper,[25,*] I. Strakovsky,[25,*] N. Semicevic,[26] S. Wells,[26] J. Dunne,[27,*] D. Dutta,[27,*] P. King,[28,*] J. Roche,[28,*] K.E. Myers,[29,*] S. Gevorkyan,[30,*] L. Roca,[31,*] S. Fang,[32,*] H. Lui,[32,*] X.Z. Bai,[33,*] H.X. He,[33,*] J. Feng,[33,*] S.Y. Hu,[33,*] S. Y. Jian,[33,*] X.M. Li,[33,*] C. Shan,[33,*] H.H. Xia,[33,*] L. Ye,[33,*] J. Yuan,[33,*] J. Zhou,[33,*] S.H. Zhou,[33,*] B. Hu,[34,*] Y. Zhang,[34,*] L. Ma,[34,*] S. Barkanova,[35,†] G. Colangelo,[36,†] B. Kubis,[37,†] B. Martemyanov,[11,†] E. Passemar,[38,†] J. Bijnens,[39,†] B. Holstein,[40,†] M. Ramsey-Musolf,[40,†] A.Aleksejevs,[41,†] S. Tulin,[42,†] and J. Goity[43,†]

[1] *Arizona State University, Tempe, Arizona 85287, USA*

[2] *University of Athens, GR-10680 Athens, Greece*

[3] *Carnegie Mellon University, Pittsburgh, Pennsylvania 15213, USA*

[4]*Catholic University of America, Washington, D.C. 20064, USA*

[5]*Christopher Newport University, Newport News, Virginia 23606, USA*

[6]*University of Connecticut, Storrs, Connecticut 06269, USA*

[7]*Florida International University, Miami, Florida 33199, USA*

[8]*Florida State University, Tallahassee, Florida 32306, USA*

[9]*University of Glasgow, Glasgow G12 8QQ, United Kingdom*

[10]*Indiana University, Bloomington, Indiana 47405, USA*

[11]*Moscow Institute for Theoretical and Experimental Physics (ITEP), Moscow, Russia*

[12]*Thomas Jefferson National Accelerator Facility, Newport News, Virginia 23606, USA*

[13]*University of Massachusetts, Amherst, Massachusetts, 01003, USA*

[14]*Massachusetts Institute of Technology, Cambridge, Massachusetts 02139, USA*

[15]*National Research Nuclear University (MEPhI), Moscow, Russia*

[16]*Norfolk State University, Virginia, 23504, USA*

[17]*North Carolina A&T State University, Greensboro, North Carolina 27411, USA*

[18]*University of North Carolina, Wilmington, North Carolina 28403, USA*

[19]*Northwestern University, Evanston, IL, 60208, USA*

[20]*University of Regina, Regina, SK S4S 0A2, Canada*

[21]*Universidad Técnica Federico Santa María, Casilla 110-V Valparaíso, Chile*

[22]*Yerevan Physics Institute, Yerevan, Armenia*

[23]*Institute of Modern Physics, Lanzhou, P.R.China*

[24]*College of William and Mary, Williamsburg, VA*

[25]*The George Washington University, Washington, DC, USA*

[26]*Louisiana Tech University, Ruston, LA, USA**

[27] *Mississippi State University, Mississippi State, MS, USA*

[28] *Ohio University, Athens, OH, USA*

[29] *Rutgers University, Piscataway, NJ*

[30] *Joint Institute for Nuclear Research, Dubna, Russia*

[31] *Universidad de Murcia, E-30071 Murcia, Spain*

[32] *Institute of High Energy Physics, Beijing, P.R. China*

[33] *Chinese Institute of Atomic Energy, Beijing, P.R.China*

[34] *Lanzhou University, Lanzhou, P.R.China*

[35] *Acadia University, Wolfville, Nova Scotia, Canada*

[36] *University of Bern, Sidlerstrasse 5, CH3012, Switzerland*

[37] *University of Bonn, D-53115 Bonn, Germany*

[38] *Theoretical Division, Los Alamos National Laboratory, Los Alamos, NM*

[39] *Lund University, SE 223-62 Lund, Sweden*

[40] *University of Massachusetts, Amherst, Massachusetts 01003, USA*

[41] *Memorial University, Grenfell Campus, Canada*

[42] *University of Michigan, Ann Arbor, MI, 48109, USA*

[43] *Thomas Jefferson National Accelerator Facility and*
Hampton University, Newport News, Virginia 23606, USA

---

*Other participant

†Theory adviser

Executive Summary

Decays of the η meson provide a unique, flavor-conserving laboratory to probe the isospin violating sector of low energy QCD and search for physics beyond the Standard Model. Because G parity conservation prevents the η from rapidly decaying to pions by the isospin-conserving strong interaction, it has an unusually small decay width ($\Gamma_{tot} = 1.3$ keV), four orders of magnitude smaller than the ω total decay width. A branching ratio of $O(10^{-6})$ in an η decay therefore probes rare processes within several orders of magnitude of the weak scale. Our priority physics campaigns are centered around neutral decays of the η:

• A search for a leptophobic dark boson (B) coupled to baryon number is complementary to ongoing searches for a dark photon. The decay $\eta \to \gamma + B(\to \gamma + \pi^0)$, will cover the B mass range 0.14-0.54 GeV. Our measurement will improve on existing bounds by two orders of magnitude, with sensitivity to the baryonic fine structure constant α_B as low as 10^{-7}, indirectly constraining the existence of anomaly cancelling fermions at the TeV-scale.

• A low-background measurement of the rare decay $\eta \to \pi^0 2\gamma$ provides a clean, rare window into $\mathcal{O}(p^6)$ in chiral perturbation theory. This is the only known meson decay which proceeds via a polarizability type mechanism. With sufficient precision to explore the role of scalar meson dynamics in this channel for the first time, our measurement will test the ability of models such as meson resonance saturation to calculate the many unknown $\mathcal{O}(p^6)$ coefficients.

• Reduction of the uncertainty on the quark mass ratio, $\mathcal{Q} \equiv (m_s^2 - \hat{m}^2)/(m_d^2 - m_u^2)$ with $\hat{m} \equiv (m_u + m_d)/2$, will be achieved by increasing the world datasets for both the charged and neutral $\eta \to 3\pi$ channels by a factor of 2.7 while controlling systematic uncertainties due to our relatively flat acceptance over phase space.

• A search for the SM forbidden decay $\eta \to 3\gamma$ (as well as $\eta \to 2\pi^0\gamma$) will allow the best direct constraints on new C violating, P conserving reactions, reducing the branching ratio upper limits by 1-1.5 orders of magnitude.

In general,we anticipate a reduction in backgrounds for rare η decays to neutral modes of 1-2 orders of magnitude. Although η decay measurements to neutral modes have historically been limited by the problem of missing photons from $\eta \to 3\pi^0 \to 6\gamma$ (BR = 32.6%), we resolve this problem by the fact that η's are significantly boosted, the kinematics are over-determined (with recoil proton detection), and the decay photons are measured in an upgraded forward calorimeter (FCAL-II) with a central region of high-granularity, high-resolution lead tungstate crystals with flash ADC readout.

Contents

I. OVERVIEW AND RESPONSE TO PAC40 COMMENTS

The Standard Model (SM) is successful in describing a wide range of phenomena in nuclear and particle physics. Its success has been crowned with the discovery of the Higgs boson at CERN in 2012, the last missing fundamental particle in the SM. However, in addition to the obvious lack of gravity, there are other indications that the SM is incomplete. The theory needs 19 input parameters, and does not explain the origin of the three fermion families, nor why their masses are widely different. Furthermore, the SM fails to explain the dominance of matter over anti-matter in the universe, and the dark matter relic density. Extending the SM to resolve these questions is a high priority.

Another high priority is to better understand the rich complexity of confinement QCD. For example, can we confirm predictions for low energy phenomenology such as the meson spectrum with explicit gluonic degrees of freedom, or correct for strong rescattering well enough to accurately determine basic SM parameters like $m_u - m_d$? Special techniques must be used for these difficult but interesting problems, among them Chiral Perturbation Theory (ChPT) based on the chiral symmetry of QCD in the massless quark limit, the numerical simulation of QCD on the lattice (LQCD), and dispersion theory. In recent years, significant progress has been made in these and other complementary techniques. [50],[51]

Decays of the neutral and long lived η meson provide a unique, flavor-conserving laboratory to probe the isospin violating sector of low energy QCD and search for physics beyond the SM. Spontaneously broken chiral symmetry in QCD gives birth to the η as one of the Goldstone Bosons. The η is an eigenstate of P, C, CP, and G ($I^G J^{PC} = 0^+0^{-+}$) whose strong and electromagnetic decays are either anomalous or forbidden to the lowest order due to P, C, CP, G-parity and angular momentum conservation [59]. This enhances the relative importance of higher order contributions, making η decays a sensitive hadronic probe for searching for rare processes or testing discrete symmetries.

Table I summarizes various η decays in the scope of this proposal. In addition to our priority channels, the upgraded calorimeter will permit improved limits for other rare or SM forbidden channels leading to all-neutral final states.

In 2013, we submitted an earlier version of the present proposal (now heavily revised) to Jlab PAC40 to measure η decays to all-neutral final states (PR12-13-004).[1] The three physics foci of

Mode	**Branching Ratio**	**Physics Highlight**	**Photons**
priority:			
$\pi^0 2\gamma$	$(2.7 \pm 0.5) \times 10^{-4}$	χPTh at $\mathcal{O}(p^6)$	4
$\gamma + B$	beyond SM	leptophobic dark boson	4
$3\pi^0$	$(32.6 \pm 0.2)\%$	$m_u - m_d$	6
$\pi^+\pi^-\pi^0$	$(22.7 \pm 0.3)\%$	$m_u - m_d$, CV	2
3γ	$< 1.6 \times 10^{-5}$	CV, CPV	3
ancillary:			
4γ	$< 2.8 \times 10^{-4}$	$< 10^{-11}$[112]	4
$2\pi^0$	$< 3.5 \times 10^{-4}$	CPV, PV	4
$2\pi^0\gamma$	$< 5 \times 10^{-4}$	CV, CPV	5
$3\pi^0\gamma$	$< 6 \times 10^{-5}$	CV, CPV	6
$4\pi^0$	$< 6.9 \times 10^{-7}$	CPV, PV	8
$\pi^0\gamma$	$< 9 \times 10^{-5}$	CV, Ang. Mom. viol.	3
normalization:			
2γ	$(39.3 \pm 0.2)\%$	anomaly, η-η' mixing PR12-10-011	2

TABLE I: The η decays highlighted in this proposal, plus related ancillary channels. [8] Rare neutral channels will be measured with unparalleled sensitivity due to our technological solution for the "missing photon problem" which affects rare η decays to all-neutral final states with < 6 photons. The PDG branching ratio for $\pi^0 2\gamma$ is the average of several widely inconsistent measurements as suggested in Figure 11. All branching ratio upper limits in this proposal are quoted at 90% confidence level.

the proposal were:

- Cleanly probing chiral perturbation theory at $\mathcal{O}(p^6)$ through a precise, low background measurement of the rare decay $\eta \to \pi^0 2\gamma$ with an uncertainty on the Branching Ratio (BR) of $\sim 4\%$ and with sufficient sensitivity in the Dalitz distribution to constrain scalar meson dynamics;

- Improved *direct* limits on new C and CP violating interactions by reducing the BR upper limits by 1-2 orders of magnitude for several SM forbidden η decays to all-neutral final states;

- An improved determination of the quark mass ratio (closely related to $m_u - m_d$) by providing

a new $\eta \to 3\pi$ Dalitz distribution with smaller statistical errors and significantly different systematics than published datasets.

The PAC40 report [2] commented on the feasibility: *"The proposed measurements appear to be feasible and the experiment is well suited for the tagged Hall D photon beam."*

The PAC40 report also pointed out issues: *"The PAC recognizes the scientific interest of performing new measurements of rare eta decays with improved sensitivity to test the SM. However, the PAC identified some issues, mainly related to the theoretical implications of these measurements. For the SM forbidden decays more work should be done to identify physics scenarios which could imply branching ratios closer to the experimental sensitivities. The PAC suggests that these issues be addressed in close collaboration with the theory community working in this field, which should be involved in helping strengthen the physics case. In addition, the projected results should be discussed in the context of similar or competing measurements at other facilities. Similar remarks apply to the impact the $\eta \to \pi^0 2\gamma$ decay (as well as the main background channel $\eta \to 3\pi^0$ which is offered as a means to constrain the light quark mass ratio from the slope of the Dalitz distribution) would have on chiral perturbation theory.*

Finally, the PAC feels that the compatibilities and synergies with GlueX should be discussed in more detailed, in particular concerning the running configurations and the possibility of a staged running approach."

Based on these recommendations, a workshop entitled "Hadronic Probes of Fundamental Symmetries" [3][4] was held at the new Amherst Center for Fundamental Interactions (ACFI), University of Massachusetts, Amherst, MA, on March 6-8, 2014. Theory experts from the Chiral Perturbation Theory (ChPT) and Beyond Standard Model (BSM) communities, as well as experimentalists from JLab, KLOE/WASA, and Mainz came together for three days to discuss and address the above PAC issues. At the workshop, the physics goals were sharpened for the ChPT test based on the rare decay $\eta \to \pi^0 2\gamma$. A new opportunity to search for a dark-sector, leptophobic vector boson (B) coupled to baryon number was identified (which ironically can mimic the rare decay $\eta \to \pi^0 2\gamma$). The European experimentalists summarized their rich programs and forthcoming results. Applications of η decays beyond the scope of this proposal were also discussed (hadronic light by light scattering, partially visible η decays, etc.). Two new working groups were formed. One working

group is being led by Professor M. Ramsey-Musolf and Dr. S. Tulin to study BSM opportunities. The other working group, of ChPT/dispersion theorists, will be directly involved in the data analysis of $\eta \to 3\pi$ used for the quark mass ratio determination. A follow-up meeting is planned for Fall 2014 at the ACFI center to prepare a white paper on the topic of hadronic probes of fundamental symmetries.

In the following, we respond to questions from PAC40. While the answers provide a short summary of the physics motivations of this proposal, more details can be found in Section II.

A. What is the expected impact of JEF's BSM physics searches?

1. It will provide a stringent constraint on a new leptophobic gauge boson (B) coupled to baryon number in the mass region 0.14-0.54 GeV: [5],[6]

This is a new discovery window for forces beyond the SM that is not covered by ongoing dark photon searches and can provide the strongest limit on a new vector boson in the mass range of 140-540 MeV [6]. The decay of this boson, referred to as the B, would mimic the SM rare decay $\eta \to \pi^0 2\gamma$ by the two-step process $\eta \to B\gamma \to \pi^0 2\gamma$. The B would be identified as a resonance peak in the $M_{\gamma\pi^0}$ invariant mass distribution.

Additional $U(1)'$ gauge symmetries and associated vector gauge bosons were proposed soon after the electroweak $SU(2) \times U(1)_Y$ model and are one of the best motivated extensions of the SM [7]. The existence of dark matter is non-controversial due to its significant gravitational influence in galaxies and clusters of galaxies. New gauge symmetries are well-motivated from the point of view of dark matter since its stability can be explained by a conserved charge. Experimental searches for new gauge bosons at hadron colliders have set upper limits on their couplings for masses in the 50 GeV to 3 TeV range [8]. Masses smaller than the MeV scale also have very strong constraints from searches for long-range nuclear forces. However masses around the QCD scale have been less intensively investigated due to large backgrounds [9].

A dark-sector gauge vector boson, the B, was proposed nearly three decades ago and subsequently discussed extensively in the literature [13]-[14]. The B-boson couples to baryon number at tree level and arises from a new $U(1)_B$ symmetry. Many different dark matter models have been proposed

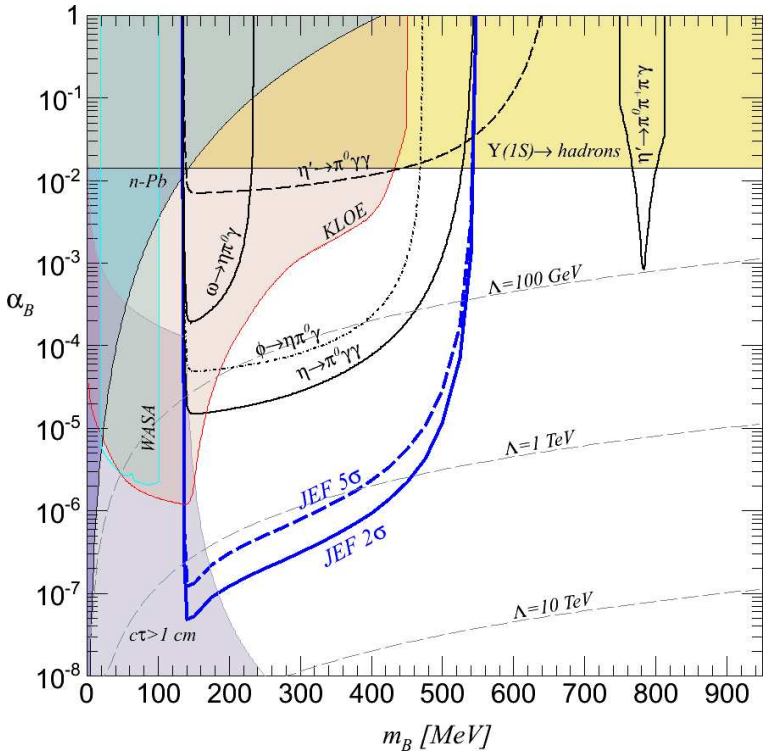

FIG. 1: Current exclusion regions for a leptophobic gauge boson, the B [6], with our proposed search region labelled "JEF" for the coupling vs mass plane. Shaded regions are exclusion limits from low energy n-Pb scattering [15] and hadronic $\Upsilon(1S)$ decay [16]. The pink and blue shaded regions are from A' searches (KLOE [63] and WASA [64]). A' limits applied to B are model-dependent, constraining possible leptonic B couplings. Limits shown here is for $\epsilon = 0.1 \times eg_B/(4\pi)^2$. The black contours are current exclusion limits from radiative light meson decays based on their total rate (assuming the QCD contribution is zero). The light purple shaded region shows where the B has a macroscopic decay length $c\tau > 1$ cm. Projected JEF sensitiviity is shown as blue curves for 2σ (solid) and 5σ (dashed). Dashed gray contours denote the upper bound on the mass scale Λ for new electroweak fermions needed for anomaly cancellation.

where the stability of the dark matter particle is ensured by its being charged under the $U(1)_B$ symmetry.[11] These models have been motivated in part by the similar cosmological abundances of dark matter and baryonic matter in the Universe, which may point toward a unified baryogenesis mechanism for both types of matter.[12]

Tulin demonstrated in a recent article [6] that the leading decay channel for a leptophobic B-boson is $B \to \pi^0 + \gamma$ for $m_\pi \leq m_B \leq 620$ MeV. The rare η doubly radiative decay $\eta \to \pi^0 2\gamma$, which our proposed experiment is designed to measure with low background, is ideally suited to search for

the B-boson in this mass range. (See section VI B 2.) The partial width for the SM "background" in this case is only 0.4 eV and will be measured by us with an uncertainty of less than 0.018 eV ; binning in the $M_{\gamma\pi^0}$ invariant distribution increases our sensitivity further.

The experimental limits on the B-boson coupling α_B and mass m_B are shown in Fig. 1 along with our projected exclusion limits. Because baryon number has an electro-weak anomaly, there must be new fermions with a mass scale of Λ to cancel all gauge anomalies [13]. The dashed gray contours denote the upper bound on the mass scale Λ for new electroweak fermions needed for anomaly cancellation. As shown in the figure, the observation of a B-boson would imply new fermions with masses around the TeV-scale or below. Although such new fermions may have escaped detection at colliders thus far, they are likely to be within the reach for discovery at the LHC or future high energy colliders.

2. The possibility of new C-Violating, P-Conserving (CVPC) interactions is worthy of further exploration: [36]

There is insufficient CP violation in the SM to account for the observed dominance of matter over anti-matter. Searching for new sources of CP violation is therefore a high priority. New sources of CP violation accompanied by P violation are constrained by Electric Dipole Moment (EDM) measurements. Yet C-violation is also among the Sakharov criteria for baryogenesis. We believe η decays provide the best *direct* constraints on new sources of CP violation accompanied by P conservation (and thus C violation).

Although C is generally assumed to be an exact symmetry in non-weak reactions involving photons and hadrons, direct experimental bounds at the amplitude level are only 0.3%- 0.5%.[38] Decay of the η into pions and photons is a readily available system for testing C.

The suggestion that there may be new CVPC interactions is an old one. Bernstein, Feinberg and Lee proposed a new C- and T-violating, and P-conserving interaction in the mid 60's [34]. Tarasov predicted the branching ratio of $\pi^0 \to 3\gamma$ induced by the new CVPC interaction [35]. Replacing the mass of the π^0 with the η in Tarasov's calculation, his model would have allowed the $\eta \to 3\gamma$ branching ratio to be large as 10^{-2}. If this is still the case, our proposed experimental sensitivity of 10^{-6} for the branching ratio upper limit for C-violating η neutral decays should offer powerful constraints on new CVPC interactions. On the other hand, experimental constraints have tightened

since the 1960's. These early investigations must be re-opened.

As pointed out by Ramsey-Musolf [36], CVPC interactions are a largely unexplored area of fundamental symmetry tests. Analyzing their effects for light quark systems requires an Effective Field Theory (EFT) approach, as they do not arise at tree-level via renormalizable gauge interactions. In general, EDM measurements place stringent constraints on new CVPC interactions via Electro-Weak (EW) radiative corrections from the standpoint of short distance parity restoration and/or naturalness. Exceptions may exist in the presence of a conspiracy or new symmetry at the T-violating and P-conserving (TVPC) matching scale [36] (equivalent to CVPC due to the CPT theorem). If parity remains broken at short distances, the experimental EDM limits do not constrain the existence of a new CVPC interaction. Since the mass hierarchy is a priori unknown (ie, whether the scale of C invariance restoration is above or below the scale of P invariance restoration), only direct searches for CVPC interactions such as we propose are unambiguous. [37]

The C-violating η decays such as $\eta \to 3\gamma$ represent some of the few opportunities nature has provided to test C invariance. The small decay width of the η suggests these are the most sensitive flavor-conserving *direct* tests involving hadrons. Our experiment proposes to measure these channels as a natural part of our program emphasizing rare η decays to all-neutral final states. In the meantime, our theory colleagues in the BSM working group plan to explore the relationship between direct measurements and indirect EDM constraints on new CVPC interactions. Ramsey-Musolf has already assigned two graduate students to work on $\eta \to 3\gamma$.

B. What is the expected impact of the SM $\eta \to \pi^0 2\gamma$ measurement on ChPT?

A rare window to test the role of scalar dynamics in high order ChPT: [17].

The $\eta \to \pi^0 2\gamma$ channel is one of the rare windows that nature offers to test the role of scalar dynamics in high order ChPT [17]. This decay is dominated by higher order contributions, starting at $\mathcal{O}(p^6)$. Comparing our clean measurement with models will allow theorists to estimate and/or reduce the uncertainties for the more frequent case where channels are dominated by the lower order $\mathcal{O}(p^4)$ contributions.

The major contributions to $\eta \to \pi^0 2\gamma$ are two $\mathcal{O}(p^6)$ counter-terms associated with two Low

Energy Constants (LEC's) in the chiral Lagrangian [18]. The values of these LEC's can be fixed by experimental data or, equivalently, calculated assuming that they are saturated by the exchange of known meson resonances. The proposed JEF experiment will measure the $\eta \to \pi^0 2\gamma$ branching ratio and Dalitz distribution, providing a model-independent determination of two LEC's at $\mathcal{O}(p^6)$.

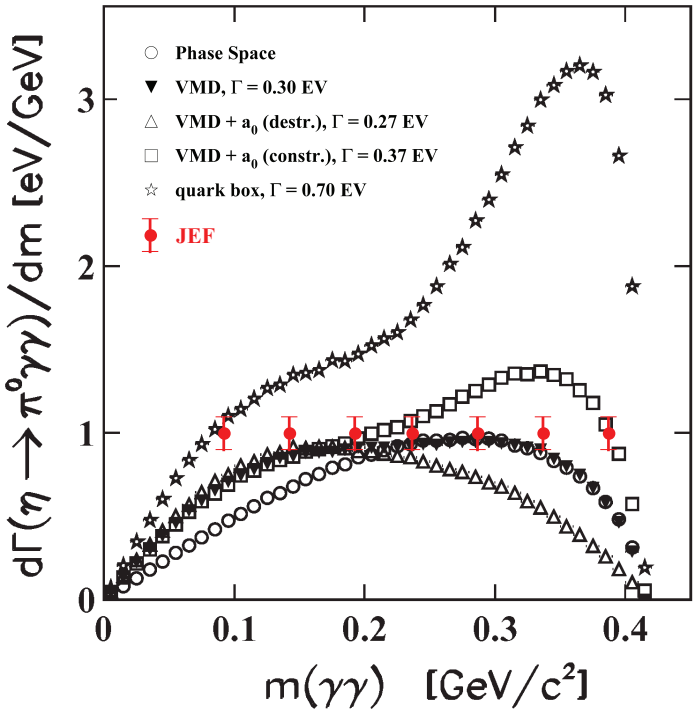

FIG. 2: Predicted $\gamma\gamma$ invariant mass distributions from $\eta \to \pi^0\gamma\gamma$ [20] and projected JEF result from section VI B 1. This figure demonstrates how our projected uncertainties could effectively discriminate between constructive and destructive interference with the a_0 amplitude. (This is an older calculation. See also our projected uncertainties compared to a state-of-the-art model shown in Figure 10.)

As pointed out by Bijnens at the ACFI workshop [17], the physics impact of $\eta \to \pi^0 2\gamma$ goes far beyond these two LEC's. There are 56-94 LEC's at $\mathcal{O}(p^6)$, depending on the numbers of flavors included in the Lagrangian. Some combinations of those LEC's are known from curvature of the scalar and vector form factors and from $\pi\pi$ scattering, but the only option for many LEC's will be calculation rather than experiment. The most widely used theoretical approach to calculate LEC's uses the meson resonance approximation. Vector Meson Dominance (VMD) has been tested and is well understood [19]; however, scalar meson contributions are poorly understood since they contribute mostly where loop contributions are also important. As shown in Fig. 2, the projected JEF precision would be sufficient to determine the scalar contribution and distinguish it from

the VMD mechanism alone. Note that the scalar contribution not only affects the magnitude of $d\Gamma/dM_{\gamma\gamma}$ but also the shape; for constructive interference it produces a "hump" near $M_{\gamma\gamma} = 0.35$ GeV. This will have direct impact on our understanding of high order ChPT.

C. What is the expected impact of the $\eta \to 3\pi$ measurement(s)?

1. They will provide a better determination of the Light Quark Mass Ratio: [17][21][22]

The fundamental SM parameter $\mathcal{Q} \equiv (m_s^2 - \hat{m}^2)/(m_d^2 - m_u^2)$, with $\hat{m} \equiv (m_u + m_d)/2$, has a wide-ranging impact. It drives isospin violation which is usually a higher order process in low energy QCD, but which is nevertheless important for frontier studies requiring precise corrections for strong interaction effects. Examples include the extraction of V_{us} in K_{l3} decays to refine tests of first row CKM unitarity[23–25], two-nucleon contributions to the EDM of the deuteron[26], and searches for supersymmetric effects in the highly suppressed flavor-changing neutral current decay, the Standard Model $B \to \rho\gamma$[27].

The relative uncertainty on $\mathcal{Q}$ from the dispersive analysis discussed below, and using presently available experimental inputs, is arguably in the range 2.5% - 5%. A realistic goal of our program is to first demonstrate through cross-checks between different precision experiments that the uncertainty is indeed at the lower end of that range, then try to reduce the uncertainty further. It is essential to work in close collaboration with theorists to ensure that the data are expressed in a form which is maximally useful to them.

For a few strong interaction observables, symmetry forbids a contribution directly proportional to $\Lambda_{\rm QCD}$, or even to $m_u + m_d$, which implies a sensitivity to the quark mass difference. In most cases, however, these isospin-violating observables are also affected by electromagnetic effects, so that if one wants to extract information on $m_u - m_d$, one has to first calculate and disentangle the contribution due to electromagnetic interactions. For example, in the proton–neutron or K^+–K^0 mass differences, this is problematic and it is therefore difficult to extract phenomenological information on $m_u - m_d$.

By contrast, the $\eta \to 3\pi$ decay is due to almost exclusively to the isospin symmetry breaking part of the Hamiltonian $\sim (m_u - m_d)(u\bar{u} - d\bar{d})/2$. Moreover, Sutherland's theorem [28, 29] forbids

electromagnetic contributions in the chiral limit: contributions of order α are also suppressed by $(m_u + m_d)/\Lambda_{\rm QCD}$. This singles out this decay as the best potential source of phenomenological information on the up-down quark mass difference. The amplitude is proportional to $m_u - m_d$ and is given by

$$A(s,t,u) = \frac{1}{\mathcal{Q}^2}\frac{m_K^2}{m_\pi^2}\frac{\mathcal{M}(s,t,u)}{3\sqrt{3}F_\pi^2}, \quad \mathcal{Q} = \frac{m_s^2 - \hat{m}^2}{m_d^2 - m_u^2}, \quad \hat{m} = (m_u + m_d)/2 \tag{1}$$

where $\mathcal{M}(s,t,u)$ is a dimensionless factor which is theoretically calculable, and s, t and u are Mandelstam variables.

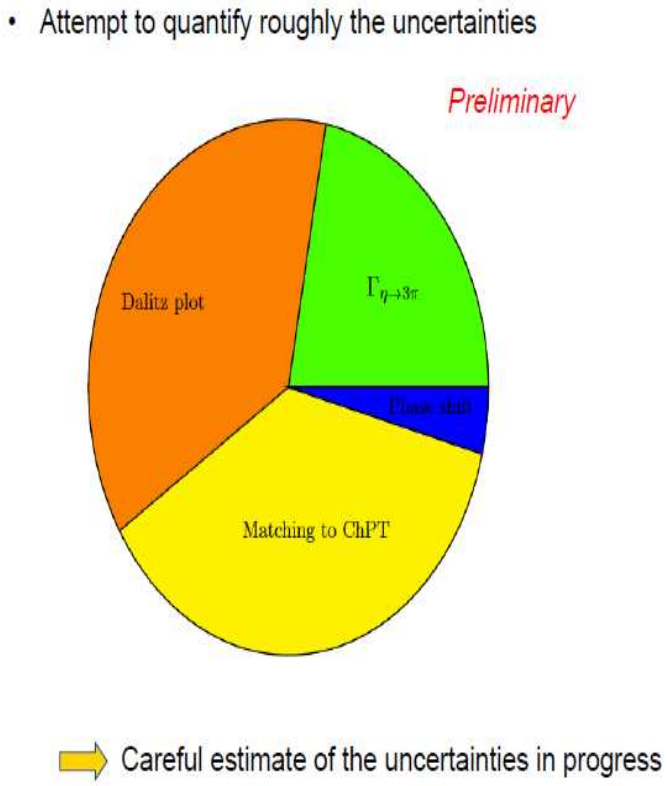

FIG. 3: A preliminary breakdown of the contributions to the uncertainty in the quark mass ratio. Our experiment will address the experimental contribution from the "Dalitz Plot". [21]

To determine the quark mass ratio, $\mathcal{Q}$, one needs a precision measurement of the decay width $\Gamma(\eta \to 3\pi)$, which is determined using the measured BR and the decay width of the normalization channel $\Gamma(\eta \to 2\gamma)$.[1] On the theoretical side, a precise calculation of $\mathcal{M}(s,t,u)$ is required, but

[1] A reduced uncertainty for the $\Gamma(\eta \to 2\gamma)$ normalization channel is the motivation for the approved Primakoff

this is not easy because the chiral expansion for this decay amplitude does not converge very fast. The main difficulty is the re-scattering effects of pions in the $S, I = 0$ wave.

The best solution at hand is to combine ChPT with a dispersion analysis. Some unknown constants, called subtraction constants, enter the calculation and can be fixed from a fit to the experimental Dalitz distribution for $\eta \to 3\pi$. The uncertainty due to the experimental Dalitz distributions makes the largest contribution to the experimental error in extracting the quark mass ratio $\mathcal{Q}$ [21]. (See Figure 3.) The constraints from use of the KLOE Dalitz distribution not only reduce the uncertainty in $\mathcal{Q}$ but also shift the central value [21][30] *by more than the original error bar* of $\sim$3% as shown from the bottom two points in Fig. 4. Precise measurements of the $\eta \to 3\pi$ Dalitz distributions with a precision comparable to (or superior to) KLOE are critical.

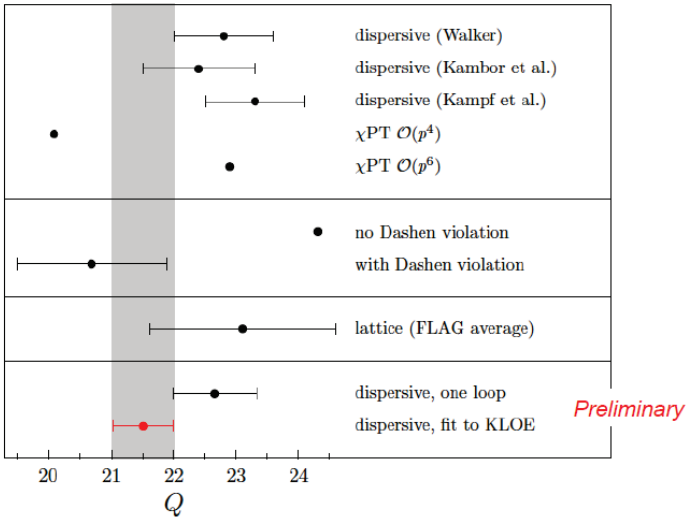

FIG. 4: Determinations of the quark mass ratio $\mathcal{Q}$ [21]. The bottom two points show $\mathcal{Q}$ determined with and without the constraint from the KLOE $\eta \to \pi^0\pi^+\pi^-$ Dalitz distribution. Note that the addition of the "fit to KLOE" constraint moved the central value more than the original error bar of $\sim$3%.

There have been several experimental results published in the recent years from the KLOE, Crystal Ball, and WASA collaborations. The results for the slope parameter, α, in $\eta \to 3\pi^0$ are consistent- [100], [101], [102], [103]. However, working to a given order, the neutral channel provides fewer constraints on theory due to identical final state particles. The Dalitz distribution for the charged

experiment (PR12-10-11) in Hall D.

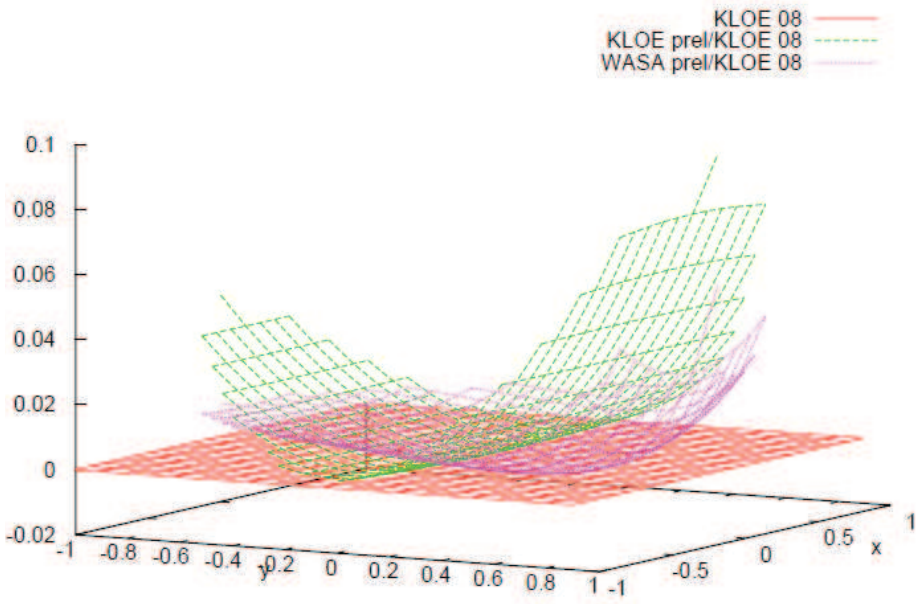

FIG. 5: Relative difference in the $\eta \to \pi^0\pi^+\pi^-$ Dalitz distributions in the X vs Y plane from different experiments [17]. There are systematic differences of typically 5% between experiments for larger absolute values of Y.

channel $\eta \to \pi^0\pi^+\pi^-$ is at least as important as the neutral channel, so it was added to the present version of this proposal. In combination with GlueX-IV running, we would be able to accumulate a world-class dataset as summarized in Table II. We would not only acquire the largest individual 3π datasets, but would increase the size of the world datasets for each channel by about a factor of 2.7 .

Current experimental results from the charged channel have significant discrepancies, as shown in Fig. 5. These experiments were performed with relatively unboosted η's hence the detection efficiency was more sensitive to the detector threshold. Our proposed measurement with more highly boosted η's will be less sensitive to the detection threshold (see Figure 42) and will offer a new result with significantly different systematics in addition to higher statistics. Such cross checks on the systematics are important for understanding the final uncertainty on $\mathcal{Q}$, a fundamental QCD parameter[31].

2. The 3π data offer an opportunity to directly constrain new C violating interactions through fits to the Dalitz distribution of $\eta \to \pi^0\pi^+\pi^-$: [32]

The Dalitz distribution for $\eta \to \pi^0\pi^+\pi^-$ can be searched for a C violating left-right asymmetry (isospin change indeterminate), sextant asymmetry ($\Delta I = 1$), and quadrant asymmetry ($\Delta I = 2$).[33] Existing statistical and systematic uncertainties on these asymmetries are each only at the level of $\pm 0.1\%$ [97]. We could reduce the statistical error a factor of 3 by combining our charged 3π dataset with GlueX-IV. Gardner pointed out at the ACFI workshop that "The background reduction associated with boosted η decay at the JEF should help control systematics" [32]. Because such asymmetries would be proportional to C violating amplitudes, they provide complementary information to that from searches such as $\eta \to 3\gamma$ which are proportional to a C violating amplitude *squared*. Further investigation of the outlook for the charged 3π system is on the task list for our BSM working group.

D. Compatabilities and synergies with GlueX and other Hall D experiments

No negative impacts on other Hall D experiments are anticipated. The upgraded FCAL-II would be in the same location as the existing FCAL. Upgrading the central region of the current FCAL with $PbWO_4$ crystals would benefit the general Hall D program by providing high radiation resistant material near the beamline needed for high beam intensity running (10^8 γ/s) as well as improving the energy and position resolutions for forward neutral particle reconstruction.

Synergies between GlueX and JEF include increased manpower/talent and larger/better datasets for both programs:

- For the GlueX program, some interesting final states for exotics searches are 3π, $2\pi\omega$, and $2\pi\eta$. Since the π^0, η, and ω widths are rather narrow, and have significant branches to final states yielding photons, the higher resolution calorimeter is expected to reduce combinatoric backgrounds and improve purity of the datasets. See Appendix A for a $\pi(1400)$ example of the improvement of the missing energy resolution, as well as the invariant mass resolution for π^0 and η reconstruction due to the calorimeter upgrade.

- For non-rare decays where the η decay products do not have to be boosted into the relatively

small, high resolution section of FCAL-II, the figure of merit for running at the lower GlueX photon beam energy is 20% higher than JEF's. (See Table VII.) The combination of 100 days of JEF and 200 days of GlueX-IV running would enable a revolutionary increase in the world $\eta \to 3\pi$ dataset, the channel used to determine the quark mass ratio.

Another approved experiment in Hall D, E-10-011, will measure the η radiative decay width, $\Gamma(\eta \to 2\gamma)$, via the Primakoff effect. The total uncertainty on the radiative width is expected to decrease from 3% to 2% if the calorimeter upgrade is carried out (due to a combination of background reduction and improved angle resolution). [151][152] Since all other decay widths of the η are ultimately normalized to $\Gamma(\eta \to 2\gamma)$, the upgrade would positively impact the interpretation of other measurements such as $\eta \to 3\pi$ used to determine the quark mass ratio.

A recently approved experiment in Hall D will measure the charged pion polarizability. The upgraded calorimeter should assist with the separation of charged pions from the muon background. The downstream muon detection capability they are building would allow JEF to extend our η decay program to channels such as $\eta \to \mu^+\mu^-$.

The η' radiative width measurement has been identified as one of the physics projects driving the Jlab 12 GeV upgrade in the past decade[39]. Development of this future experiment will definitely benefit from the high resolution, high granularity FCAL-II.

E. JLab's η decay program in the context of other facilities

Ongoing investigations of η decays around the world are quite vigorous. Generally speaking, JEF's niche is rare, all-neutral η decays where our solution for the missing photon background will give us a figure of merit superior to facilities with a much larger number of detected events.

An example of a recently completed program is the KLOE-I collaboration at the Frascati ϕ factory. They accumulated large η datasets using ϕ production in e^+e^- collision at the center of mass energy of 1.02 GeV. By detecting a mono-energetic photon from the decay of the ϕ, they tagged η production with backgrounds at the part per thousand level. The status of the broad and successful KLOE(-II) η decay experimental program was recently summarized at the ACFI workshop [130]. The KLOE-I program was very competitive for η decays to final states involving charged particles.

After luminosity and detector upgrades, the program is continuing as KLOE-II.[126] But even if KLOE-II succeeds in increasing production to $1{\times}10^8$ η's, we believe their lack of significantly boosted η's and lack of high quality, large acceptance calorimetry means they cannot reach the sensitivity of JEF for rare or forbidden all neutral final states like $\eta \to \pi^0 2\gamma$, 3γ, etc.

After completing a rich experimental program on the η physics at Brookhaven National Laboratory AGS where they enjoyed extremely high η production rates from $\pi^- + p \to \eta + n$ (as well as high backgrounds), the Crystal Ball collaboration moved their photon spectrometer to the Mainz Microtron facility in 2002. Using a bremsstrahlung photon beam from a 1.5 GeV electron beam, they are continuing a rare η decay program using the same reaction as us, $\gamma p \to \eta p$. Their η production rates are reportedly over an order of magnitude higher than that expected in JEF, but the backgrounds in the $\pi^0 2\gamma$ channel are only moderately better than what was obtained with the CB at the AGS [86][84]. They have made cutting edge measurements of the η mass, have measured the Dalitz distribution slope parameter in $\eta \to 3\pi^0$ (BR = 33%), the $\eta \to \gamma + \gamma_v$ form factor, searched for C violation in ω decays, are beginning measurements of η' decays, and have a pre-print of their new $\eta \to \pi^0 2\gamma$ result. The status of the MAMI η decay experimental program was recently summarized at the ACFI workshop [131].

Another large acceptance photon detector that has gained a new life by emigration is the Wide Angle Shower Apparatus (WASA). Originally located at Uppsala, Sweden, it is now at the COoler SYnchrotron (COSY) facility in Germany [125]. A 1.0 GeV proton produces η's via the $p + d \to {}^3He + \eta$ or $p + p \to p + p + \eta$ reaction. One clear niche of WASA whether at CELSIUS or at COSY has been η decays to final states with e^+e^- pairs. This is because it has an extremely clever cryogenic pellet target that avoids the problem of $\eta \to 2\gamma$ (BR 39%) followed by pair production in a thick target. The have also made $\eta \to 3\pi$ measurements which have provided cross checks on other experiments.

The BES-III collaboration [115] at the Beijing Electron Positron Collider got into the η rare decay business using $J/\psi \to \gamma\eta$. Possibly because of the large J/ψ mass and the small branching ratio to $\gamma\eta$, they did not obtain a competitive result for the difficult $\eta \to 2\pi^0$ channel, although they dramatically lowered the BR upper limits for $\eta', \eta_c \to \pi^+\pi^-$ decays.

Finally, there is a CLAS Approved Analysis (CAA) which is mining data from the g11 and g12 experiments. [116]. All of their stated channels of interest involve the detection of charged particles,

including several million $\eta \to \pi^+\pi^-\pi^0$ events. If systematic errors can be controlled at the required few percent level, the latter channel may allow CLAS to make an important determination of the Dalitz parameters used to help extract the quark mass ratio, as well as cross checking KLOE published and forthcoming results. Generally speaking, our proposal avoids η decays to charged final states due to serious competition from KLOE and now KLOE-II. However, we added the channel $\eta \to \pi^+\pi^-\pi^0$ due to synergies with GlueX running, as well as the channel's priority in reducing the quark mass ratio uncertainties. The dataset we plan to acquire in concert with GlueX running should be thought of as a next generation measurement, with almost an order of magnitude larger statistics than the CAA, and a very flat acceptance in the variables X and Y which should allow us to control systematic errors at the required level.

What all these groups have in common is that η's are produced nearly at rest in the laboratory and then detected in a nominally 4π detector. As discussed above, this leads to fierce backgrounds in rare decays to 4γ final states due to $\eta \to 3\pi^0$ with missing or merged photons. Using the high energy η production and high-resolution, high-granularity $PbWO_4$ γ detector in this proposal, we will be able to reduce the background by orders of magnitude compared to our competitors, while maintaining a healthy η production rate.

II. DETAILED DISCUSSION OF η DECAY PHYSICS CAMPAIGNS IN THIS PROPOSAL

Our proposed experiment will search for evidence of leptophobic dark matter which couples to baryon number, directly probe chiral perturbation theory at high order to provide a benchmark for models of the many undetermined parameters at $\mathcal{O}(p^6)$, dramatically increase the size of the world dataset used to determine the quark mass ratio, and place the best direct constraints on the existence of new C violating, P conserving interactions. Three physics campaigns in this proposal highlight JEF's ability to make unparalleled improvements in rare η decays to all neutral final states. The remaining physics campaign, an improved determination of the quark mass ratio from $\eta \to 3\pi$, is not a rare decay but is a must-do for us due to synergies with GlueX and the potential to extend our C violation searches from branching ratios to asymmetries.

A. Search for a leptophobic dark B boson in the 0.14-0.54 GeV mass range

$\eta \to \gamma + B(\to \pi^0 + \gamma)$

Here we discuss a search for a new boson at the 0.14-0.54 GeV scale which might have escaped notice due to its relatively feeble couplings (particularly to leptons) and relatively large SM backgrounds in its branch to $\pi^0\gamma$. Note that this reaction would mimic the rare SM process $\eta \to \pi^0 2\gamma$.

Dark Matter (DM) dominates the matter density in our universe, but very little is known about it. Its existence and stability provides a strong hint that there may be a dark sector, consisting of rich symmetry structure with new forces and new particles that do not interact with the known strong, weak, and electromagnetic forces, except gravity. Discovery of any of these particles and new forces would redefine our worldview and have a profound impact. There are only a few well-motivated interactions with four-dimension operators that provides a "portal" from the SM sector into the dark sector [40]. These portals include: "dark vector", "Axion pseudoscalar", "Higgs-singlet scalar", and "neutrino Yukawa coupling". The Axion, Higgs, and neutrino portals are best explored at low-energy, high intensity light sources, high-energy colliders, and neutrino facilities, respectively. The "Vector " portal has inspired a global effort in recent years at intermediate-energy, high intensity frontier centers, such as Jefferson Lab.

The conserved vector currents are uniquely positioned to avoid the violation of the Glashow-Iliopoulos-Maiani (GIM) mechanism for suppression of Flavor Changing Neutral Currents (FCNC) [13]. One model in the "Vector" portal that has been widely considered is a new force mediated by an abelian $U(1)'$ gauge boson A' (dark photon) that couples very weakly to electrically charged particles through "kinetic mixing" with the photon [41]. The mixing angle ε controls the coupling of the DM sector to the SM. The A' has been intensively investigated in recent years. Most of experimental searches for the A' are through its decays to e^+e^- or $\mu^+\mu^-$, which rely on the leptonic coupling of the new force. Alternative signals based on invisible decays to neutrinos or light dark matter have been proposed [42]-[46].

Another model in the "Vector" portal is a gauge B-boson that couples predominantly to quarks and arises from a new $\mathrm{U}(1)_B$ gauge symmetry [13][14][6]. Since quarks experience all known interactions, it is fitting to ask whether additional interactions of quarks exist [9]. A new $\mathrm{U}(1)_B$ gauge symmetry also provides a natural frame-work for the Peccei-Quinn mechanism in the quark sector for solving the strong CP problem [47]. Since $\mathrm{U}(1)_B$ is spontaneously broken by a new Higgs field, the B-boson is massive. In addition, new baryonic fermions with electroweak quantum numbers are required to cancel the $SU(2)_L^2 \times U(1)_B$ and $U(1)_Y^2 \times U(1)_B$ anomalies. The new fermions acquire masses (Λ) via a $U(1)_B$-breaking Higgs field, with $m_B/\Lambda \geq g_B/(4\pi)$ [48], where g_B is the $U(1)_B$ gauge coupling. As a result, a positive signal for B will imply new fermions at a large mass scale. A general Lagrangian for the interaction is [6]

$$\mathcal{L}_{int} = (\frac{1}{3} g_B + \varepsilon Q_q e)\bar{q}\gamma^\mu q B_\mu - \varepsilon e \bar{l}\gamma^\mu l B_\mu \tag{2}$$

where l is a charged lepton, and ε is a dark photon-like coupling through the kinetic mixing. The most important effect of ε is allowing for the decay $B \to e^+e^-$, which dominates when pion decays are kinematically forbidden. In this case, A' searches are sensitive to B, although B production may be modified compared to A'.

Tulin demonstrated in his recent article [6] that the leading decay channel of the B-boson is $B \to \pi^0 + \gamma$ for $m_\pi \leq m_B \leq 620$ MeV. (See Fig. 6.) This offers a great experimental opportunity to search for the B-boson in this mass range through the η doubly-radiative decay $\eta \to \pi^0\gamma\gamma$. The new physics decay $\eta \to B\gamma \to \pi^0\gamma\gamma$ would reveal a resonance peak at m_B in the $\pi^0\gamma$ invariant mass distribution, while the Standard Model allowed $\eta \to \pi^0\gamma\gamma$ decay with a branching ratio of

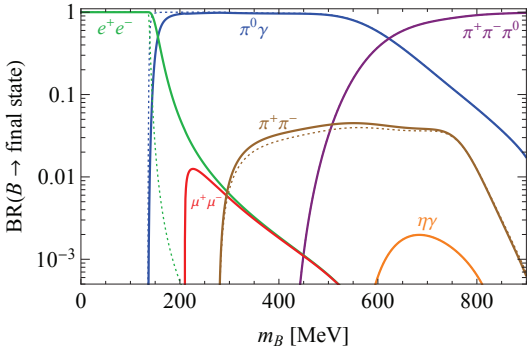

FIG. 6: Predicted branching ratio for B boson decays (independent of α_B) [6]. For most of the mass range probed by $\eta \to \gamma + B$, the dominant B decay branch is $B \to \pi^0\gamma$. For $\eta' \to \gamma + B$, the dominant B decay branch is $B \to \pi^0\pi^+\pi^-$. Thick lines have kinetic mixing between B and the photon $\varepsilon = eg_B/(4\pi)^2$; thin dotted lines have $\varepsilon = 0.1 \times eg_B/(4\pi)^2$.

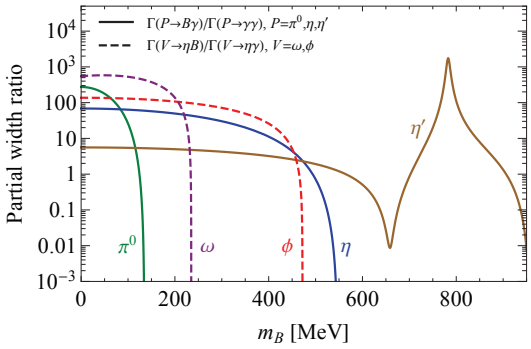

FIG. 7: Predicted partial decay width ratios [6]. Solid lines show $\Gamma(P \to B\gamma)/\Gamma(P \to 2\gamma)$ for $P = \pi^0$, η, and η'. Dashed lines show $\Gamma(V \to B\eta)/\Gamma(V \to \gamma\eta)$ for $V = \omega$, ϕ, normalized to $\alpha_B = 1$.

$\sim 2.7 \times 10^{-4}$ [8] would be present as the irreducible background in the signal window.

As pointed out by Pospelov [49], searching for light new physics at the intensity frontier is still gathering momentum, but it is time to diversify. Proposed searches for the B-boson in three-photon final states ($B \to \pi^0 + \gamma$) are complementary to the many searches for A' in charged final states ($A' \to l^+l^-$). While the limits for $A' \to l^+l^-$ will continue to improve, the more difficult neutral decay modes in ~ 1 GeV range are currently unexplored territory. JEF's background reduction in the detection of multi-photon final states offers a superior opportunity to probe this "untouched" new physics domain.

The partial decay width of $\eta \to B\gamma$ decay is given by [6]:

$$\frac{\Gamma(\eta \to B\gamma)}{\Gamma(\eta \to 2\gamma)} = 2\frac{\alpha_B}{\alpha_{em}}(1 - \frac{m_B^2}{m_\eta^2})^3 |\frac{(\frac{1}{3}c_\theta - \frac{\sqrt{2}}{3}s_\theta)F_\omega(m_B^2) + (\frac{2}{3}c_\theta + \frac{\sqrt{2}}{3}s_\theta)F_\phi(m_B^2)}{c_\theta - 2\sqrt{2}s_\theta}|^2, \quad (3)$$

where $c_\theta = \cos(\theta)$ and $s_\theta = \sin(\theta)$, and θ is the mixing angle of η-η'. $F_{\omega,\phi}(s) \sim (1 - s/m^2_{\omega,\phi})^{-1}$ are the form factors. The α_B and α_{em} are the baryonic and electromagnetic fine structure constants respectively. The partial decay width ratios normalized to $\alpha_B = 1$ are shown in Fig 7.

For a given value of m_B, the signal window is given by $\delta m_B = 2.5\sigma$ where σ is the resolution of the invariant mass $m_{\pi^0\gamma}$. The sensitivity for a resonance search is determined by $\frac{S}{\sqrt{N_{bin}}}$, where S

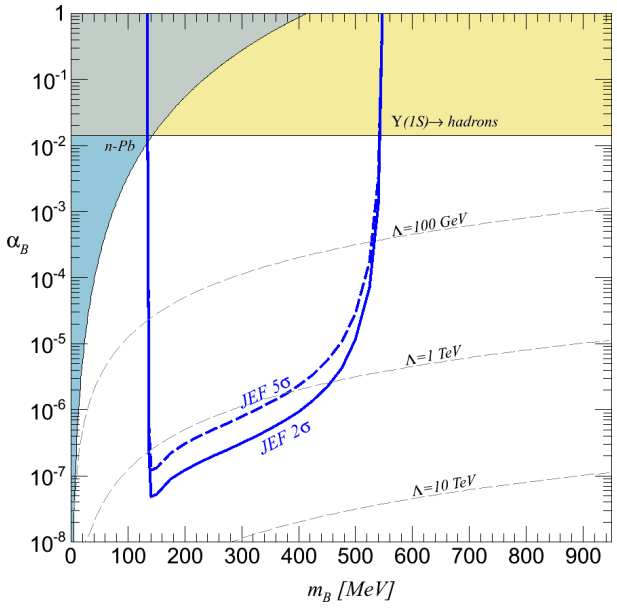

FIG. 8: Existing B-boson exclusion regions [6] and proposed search region for the JEF experiment in the B-boson mass-coupling plane. Shaded regions are exclusion limits from low energy n-Pb scattering [15] and hadronic $\Upsilon(1S)$ decay [16]. The blue solid (dash) curve corresponds to the 2σ (5σ) sensitivity. Dashed gray contours denote the upper bound on the mass scale Λ for new electroweak fermions needed for anomaly cancellation.

is the number of BSM signal events and N_{bin} is the number of SM background events, both within the signal window. The current experimental limits on the B-boson coupling α_B and mass m_B parameter landscape and the projected JEF search limit are shown in Fig. 8. The shaded regions are experimental constraints from low energy n-Pb scattering and hadronic $\Upsilon(1S)$ decay. Dashed gray contours denote the upper bound on the mass scale Λ for new electroweak fermions needed for anomaly cancellation. The solid blue curve is the exclusion limit for 2σ sensitivity and the dash-dotted blue curve corresponds to the 5σ sensitivity.

Fig. 1 is similar to Fig. 8, but Fig. 1 has additional constraints. The pink and blue shaded regions are from A' searches (KLOE [63] and WASA [64]). A' limits applied to the B-boson are model-dependent, constraining possible leptonic B couplings. Limits shown here assumed that the kinetic mixing between B and the photon is $\epsilon = 0.1 \times e g_B/(4\pi)^2$. The black contours are current exclusion limits from radiative light meson decays based on their total rate (assuming the QCD contribution is zero). As shown in Fig. 1, the projected JEF limits reach the region where B has a long lifetime and a small mass with a macroscopic decay length $c\tau > 1$ cm. The displaced B decay vertices may

smear the event reconstruction, thereby reducing the sensitivity in that region.

B. A clean window on $\mathcal{O}(p^6)$ in ChPT via $\eta \to \pi^0 2\gamma$

$\eta \to \pi^0 2\gamma$ theory

The "doubly radiative" η decay has a history spanning more than four decades [65]. This channel is sufficiently suppressed (BR $= 2.7 \times 10^{-4}$) that, while it has been possible for all recent experiments to observe a non-zero signal, measurements accurate enough to challenge theory have proven elusive.

Chiral Perturbation Theory (ChPT) is a rigorous low-energy effective field theory of non-perturbative QCD based only on the chiral invariance of QCD. The ChPT Lagrangian depends on a number of Low Energy Constants (LEC) that are not constrained by the chiral symmetry. They are in principle determined by the underlying QCD dynamics. Meson resonances and other hadronic states can contribute to these LEC's; direct short-distance contributions are also possible [76]. It is fundamentally important to understand which hadronic states dominate in determining the LEC's in a consistent chiral framework.

Many years of phenomenological analysis in both nuclear and particle physics have provided ample evidence for the special role of vector mesons, and therefore they have been included in the chiral Lagrangians since the early days [78]. Ecker and collaborators systematically investigated all LEC's at $\mathcal{O}(p^4)$ [76]. They concluded that vector meson exchanges completely dominate the relevant coupling constants whenever they can contribute. The octet scalars dominate the constants L_5 and L_8 where vector meson contributions are zero. A chiral version of vector meson dominance is thus clearly established. The question is, what is the role of meson resonances at the next order ($\mathcal{O}(p^6)$) of ChPT? Bijnens and Ecker have taken a fresh look at the evidence for resonance saturation of LEC's at both $\mathcal{O}(p^4)$ and $\mathcal{O}(p^6)$ orders in the strong sector [77]. Their results confirm the earlier study at $\mathcal{O}(p^4)$ by Ecker et. al. [76], and by comparing with LQCD predictions find qualitative support for resonance saturation for some of the LEC's at $\mathcal{O}(p^6)$ as well. Clearly, more experimental tests of $\mathcal{O}(p^6)$ in ChPT are needed.

The $\eta \to \pi^0\gamma\gamma$ channel offers a clean window for understanding the interplay of meson resonances at $\mathcal{O}(p^6)$ ChPT [79]. This is the only known meson decay which proceeds via a polarizability type of mechanism. This unique window has inspired many theoretical and experimental studies

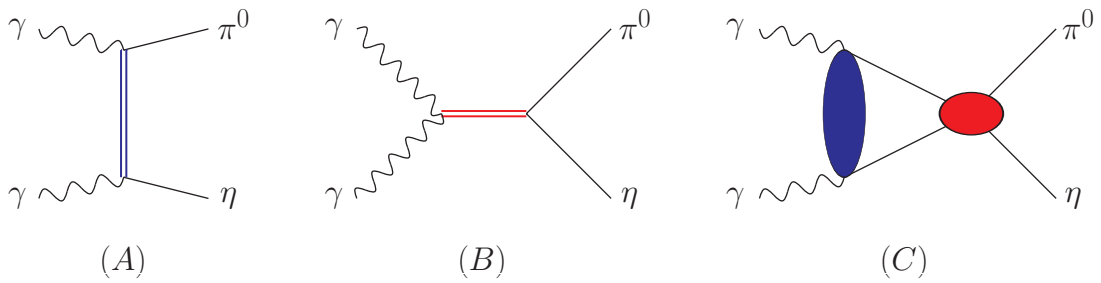

FIG. 9: Schematic form of Feynman diagrams contributing to $\eta \to \pi^0\gamma\gamma$; (A) t-channel resonance exchange (*e.g.* of vectors); (B) s-channel resonance exchange (predominantly $a_0(980)$ and $a_2(1320)$); (C) a generic loop diagram. See text for details.

(nicely reviewed in [65]). Theoretical calculations include vector-meson dominance (VMD), Nambu-Jona-Lasinio models and constituent quark models [65]-[67]. This interplay of meson resonances in $\eta \to \pi^0\gamma\gamma$ is investigated most comprehensively in Refs. [66][69], where the crossed process $\gamma\gamma \to \pi^0\eta$ is studied in parallel: the amplitudes of the two reactions are linked by crossing symmetry and analytic continuation, the decay being restricted to diphoton invariant masses in the range $0 \leq M_{\gamma\gamma} \leq M_\eta - M_{\pi^0}$, while $\pi^0\eta$ production in photon–photon fusion can be accessed above threshold, $M_\eta + M_{\pi^0} \leq M_{\gamma\gamma}$. Fig. 9 illustrates the various mechanisms for both processes.

Tree-level contributions to $\eta \to \pi^0\gamma\gamma$ vanish both at $\mathcal{O}(p^2)$ (due to both η and π^0 being uncharged) and at $\mathcal{O}(p^4)$ in the chiral expansion. The leading non-vanishing contribution that does exist at $\mathcal{O}(p^4)$ are meson loop graphs, with either $\pi^+\pi^-$ or K^+K^- intermediate states in Fig. 9(C). However, rescattering $\pi^+\pi^- \to \pi^0\eta$ requires isospin breaking and is strongly suppressed, while kaon loops turn out to be small for this decay due to combinatorial factors and the large kaon mass in the denominator [18]. The smallness of pure loop contributions is maintained beyond one-loop order as illustrated by the partial two-loop calculation in Ref. [70]. The bulk of the $\eta \to \pi^0\gamma\gamma$ decay width at $\mathcal{O}(p^6)$ is reproduced by counterterms (which corresponds to two-loop level).

The size of counterterm contributions in ChPT can be phenomenologically understood by resonance exchanges [71]. The time-honored concept of vector-meson dominance (VMD) is therein resurrected by the observation that vector mesons tend to contribute most to those counterterms (where allowed by quantum numbers). This turns out to be true also for $\eta \to \pi^0\gamma\gamma$: the largest contribution to the decay width stems from t-channel ρ- and ω-exchange (as in Fig. 9(A)). As has been pointed out in Ref. [18], the details on how to implement those vector meson exchanges matter significantly:

the full vector meson propagators lead to a $\eta \to \pi^0\gamma\gamma$ width almost a factor of 2 larger than what is found by employing resonance saturation in the strict sense, *i.e.* replacing the propagators by point interactions; the difference is of $\mathcal{O}(p^8)$ in the chiral counting. On the other hand, adjusting the coupling constants to the measured individual decays $\rho/\omega \to \pi^0/\eta\gamma$, as opposed to using SU(3) symmetric couplings, reduces the width by almost a factor of 2; updated measurements of those radiative vector decays have allowed to somewhat reduce the error in the theory prediction, with the central value cut once more by almost 20% [66].

However, the pure VMD prediction is significantly modified by the $\pi\eta$ S-wave. Through coupled-channel effects with $K\bar{K}$, this includes the $a_0(980)$ resonance near the $K\bar{K}$ threshold (the $a_0(980)$ is often said to be "dynamically generated" by coupled-channel meson–meson rescattering in the isospin $I = 1$ S-wave). In this way, no scalar resonance needs to be put into the calculation "by hand" (as in Fig. 9(B)): it occurs naturally, with the relative sign/phase of the corresponding amplitude fixed by the low-energy couplings of two photons to the two channels $\pi^0\eta$ and $K\bar{K}$. This mechanism is what is denoted by Fig. 9(C). The red blob denotes the two-channel rescattering matrix, which is calculated in unitarized ChPT (solving a Bethe–Salpeter equation with a momentum cutoff). Production (as in the blue blob in Fig. 9(C)) is assumed to proceed via ρ and ω for the $\pi^0\eta$ meson pair, and via K^+ pole terms, vector $K^*(890)$, and axial vector $K_1(1270)$ resonances for $K\bar{K}$ in Refs. [66, 69]. Non-strange axial vectors (b_1 and h_1 resonances) coupling to π^0 and η are not retained, but included in the uncertainty estimate. t-channel loops with $\pi\pi$ and $K\bar{K}$ intermediate states, involving two anomalous vertices, are only included perturbatively, *i.e.* without s-channel rescattering. The $a_0(980)$ resonance signal thus generated can be tested favorably against $\gamma\gamma \to \pi^0\eta$ data [72, 73], where the D-wave $a_2(1320)$ is added in a phenomenological way [74]. Note that Refs. [66, 69] neglect the $a_2(1320)$ in the decay amplitude for $\eta \to \pi^0\gamma\gamma$.

A similar approach to $\eta \to \pi^0\gamma\gamma$ and $\gamma\gamma \to \pi^0\eta$ (as well as other photon–photon fusion reactions) has been studied more recently in Ref. [75], with a potentially more sophisticated unitarization procedure to generate the $a_0(980)$; however, only the tree-level amplitudes with vector-meson exchange (using a different Lagrangian scheme) have been retained for the *decay* amplitude, such that the interplay with scalars is not made as transparent.

The shape of the two-photon invariant mass spectrum from $\eta \to \pi^0\gamma\gamma$, $d\Gamma/dM_{2\gamma}$, depends on the role of meson resonances in the decay; therefore it probes the underlying dynamics. The

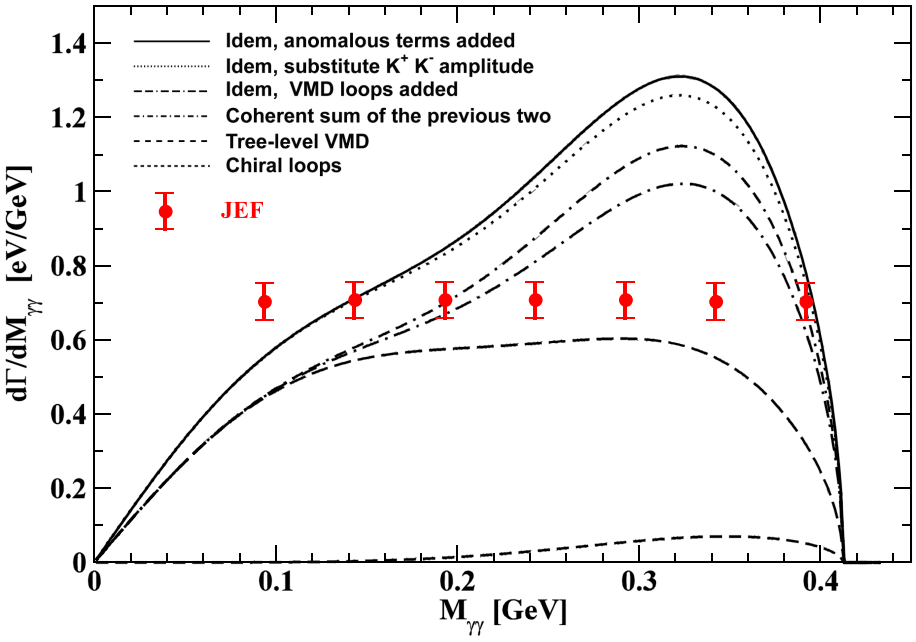

FIG. 10: Predicted two-photon invariant mass distribution from $\eta \to \pi^0 2\gamma$ [66]. From bottom to top: the short-dashed line is for chiral loops, the long-dashed line is only tree-level VMD, the dashed-dotted line is the coherent sum of the previous two, the double dashed-dotted line is the same but with resummed VMD loops added, the solid line - the full model - is the same but with the anomalous terms added. The error bars indicate our projected sensitivity from section VI B 1. The projected JEF precision would be sufficient to determine the scalar-VMD interference contribution and distinguish it from the VMD mechanism alone. (The dotted line is the full model substituting the $K^+K^- \to \eta\pi^0$ amplitude by its lowest order.)

resulting spectrum for $\mathrm{d}\Gamma/\mathrm{d}M_{\gamma\gamma}$ from Ref. [66] is shown in Fig. 10. To be noted in particular is the different *shape* for the full distribution (solid line), with a significant enhancement due to $\pi\eta$ S-wave effects at higher diphoton invariant masses, as compared to the flatter pure VMD prediction (long-dashed). The projected JEF precision would be sufficient to determine the scalar-VMD interference contribution and distinguish it from the VMD mechanism alone. This clearly demonstrates that a precision measurement of the two-photon invariant mass spectrum would help to elucidate the best theoretical description for $\eta \to \pi^0\gamma\gamma$ [81], and give deep insight into the role of meson resonances in high order ChPT.

Finally, the $\eta \to \pi^0\gamma\gamma$ channel is also an important CP-conserving "door-way" channel for searches for new sources for C- and CP-violation. An example in the kaon sector is $K_L \to \pi^0 l^+ l^-$. There is a significant SM CP-conserving background from $K_L \to \pi^0\gamma\gamma \to \pi^0 l^+ l^-$ due to re-scattering

of the photons in the vacuum. Long before $K_L \to \pi^0\gamma\gamma$ data became available from KTeV to help constrain this, Sehgal showed that the backgrounds could be estimated from η decay via $\eta \to \pi^0\gamma\gamma$ [82], where the initial K_L makes a transition by the known weak interaction to an intermediate η. Thus precise measurements of $\eta \to \pi^0\gamma\gamma$ would provide a cross-check on some of the same low energy constants now used in interpreting rare kaon decays. In the η sector, $\eta \to \pi^0 l^+ l^-$ is a C-violating search channel with possibly high sensitivity due to the lack of suppression factors. Again, there is a Standard Model background from $\eta \to \pi^0\gamma\gamma \to \pi^0 l^+ l^-$ [83]. The branching ratio of $\eta \to \pi^0\gamma\gamma$ alone is insufficient to determine both the real and imaginary parts of this background amplitude; constraints from the Dalitz distribution are required [83].

Previous $\eta \to \pi^0 2\gamma$ data

About two dozen experiments have been performed to measure this decay width since 1966. The first significant result was published by the GAMS-2000 collaboration [68] in 1984 yielding $\Gamma(\eta \to \pi^0\gamma\gamma) = 0.84 \pm 0.18$ eV, more than twice the ChPT prediction in Figure 11. By contrast, more recent results from the Crystal Ball and KLOE collaborations are significantly lower. The Crystal Ball results are consistent with the prediction by Oset [66]. However, the preliminary result from KLOE is lower than the Crystal Ball result by a factor of 3.

The discrepancies are almost certainly due to large backgrounds in the experiments, including a class of backgrounds that can peak beneath the signal. A new experiment with a significantly improved reduction in backgrounds would provide greatly reduced statistical and systematic errors leading to a definitive result for the $\pi^0 2\gamma$ decay width. More importantly, the two-photon invariant mass spectrum, $d\Gamma/dM_{2\gamma}$, will provide key guidance for understanding the underlying dynamics.

A very recent result comes from the A2 collaboration at MAMI [84]. They have measured the $\eta \to \pi^0\gamma\gamma$ decay width with a 9% total uncertainty based on analysis of 1.2×10^3 $\eta \to \pi^0\gamma\gamma$ decays. This is a significant improvement over previous measurements. They also determined the 1-D projection of the Dalitz distribution, $d\Gamma/dm^2(\gamma\gamma)$, which is even more important than the decay width for constraining dynamics. As stated in the article [84], the 21% per bin experimental uncertainties on the new MAMI $m_{\gamma\gamma}$ distribution are too large to rule out any of the theoretical calculations. (See Fig. 12). However, the uncertainties lie tantalizingly close to allowing one to distinguish between VMD and more subtle dynamics. A next generation measurement should have error bars that are at least a factor of 2 smaller than the latest MAMI result. The projected errors

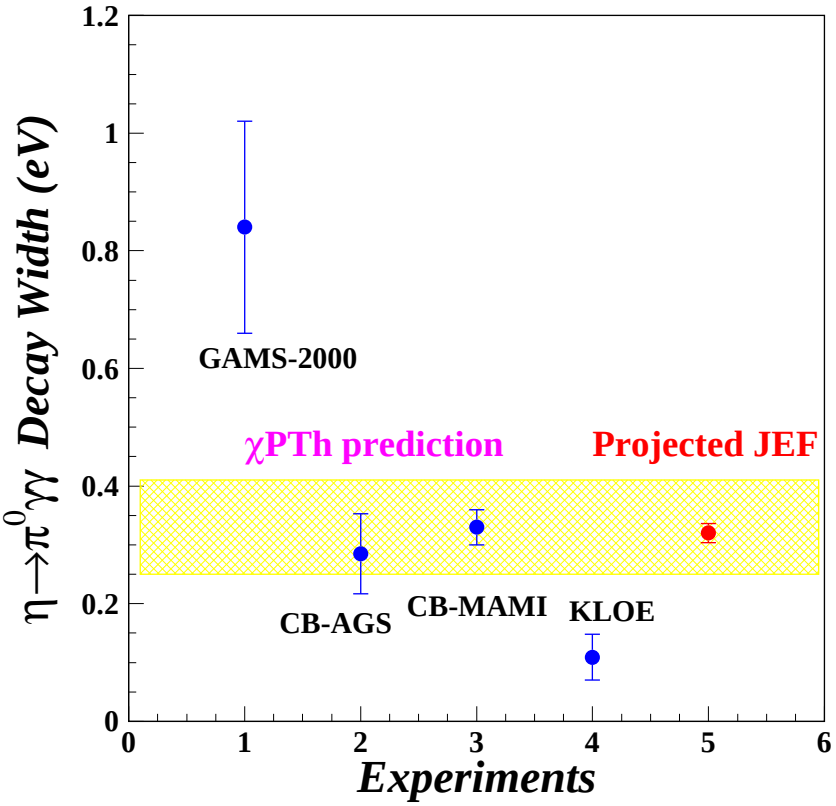

FIG. 11: Experimental results on the decay width of $\eta \to \pi^0\gamma\gamma$. [68], [85][86], [84], [88]. The yellow band is the most recent unitary ChPT calculation by Oset *et al.* The partial decay width is predicted to be [66] $\Gamma = (0.33 \pm 0.08)\,\mathrm{eV}$. The uncertainty comprises both the propagated experimental errors on the vector meson coupling constants, as well as estimates of neglected decay mechanisms. The new CB-MAMI total uncertainty is 9%. Our expected total error of 5% from section VI B 1 (in red) is arbitrarily plotted at the CB-MAMI value. We anticipate that our systematic error will be dominated by the PrimEx-eta uncertainty of 3.2% on $\Gamma(\eta \to 2\gamma)$.

of JEF for 100 days of running of 9% per bin in the $m_{\gamma\gamma}$ certainly fit the bill.

The uncertainty of the MAMI result was limited by large backgrounds from $\eta \to 3\pi^0$ and $\gamma p \to \pi^0\pi^0 p$ leaking into their 4γ final state data sample, also shown in Fig. 2 of reference [84]. The JEF experiment is projected to operate at much higher figure of merit due to greatly reduced

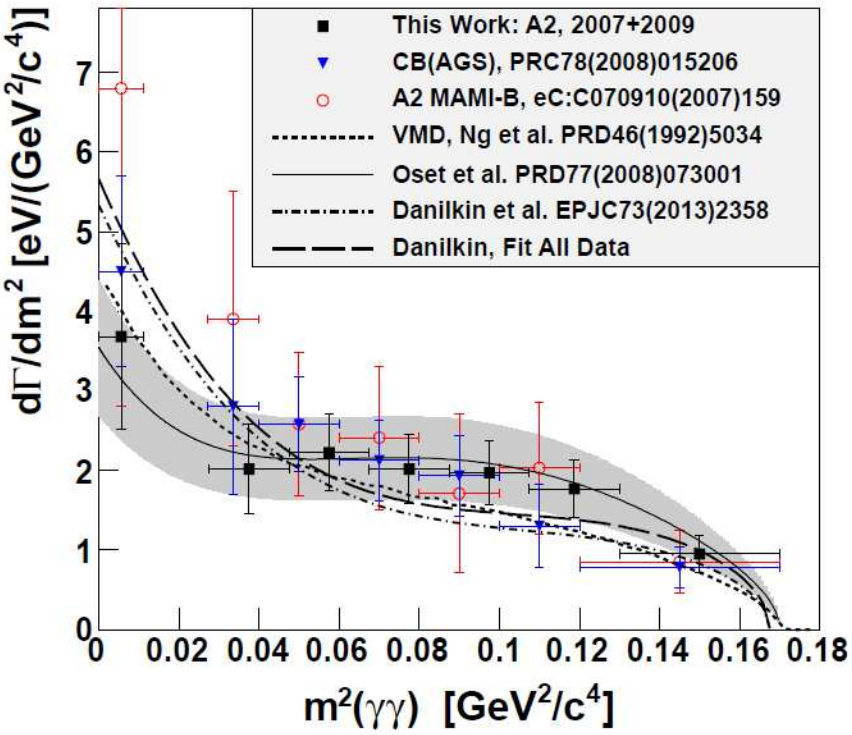

FIG. 12: Comparison of the existing experimental results (A2 at MAMI and CB at AGS) of $d\Gamma(\eta \to \pi^0\gamma\gamma)/dm^2(\gamma\gamma)$ with theoretical predictions. (Figure from reference [84].) The black error bars are typically about 21%.

background (although the number of signal events would be comparable). Our goal is to have sufficient sensitivity directly measuring the $\eta \to \pi^0\gamma\gamma$ Dalitz distribution to distinguish the interference between the vector and scalar contributions by a significant reduction in the background, shown in Figures 2 and 10. This will have a big impact on our understanding of the meson dynamics at $\mathcal{O}(p^6)$ of ChPT.

C. Determination of the quark mass ratio from $\eta \to 3\pi$

1. $\eta \to 3\pi$ *theory*

The two $\eta \to 3\pi$ decay channels arise from a small isospin-breaking term in the QCD Lagrangian, thereby providing one of the best ways to determine the up-down quark mass difference. [55][59]. This mass difference is a fundamental parameter of the SM which cannot be directly observed

due to confinement. To lowest order in ChPT, the $\eta \to 3\pi$ amplitude is proportional to the mass difference[94]:

$$\mathcal{A}(s,t,u) \propto B_0 \frac{m_u - m_d}{3\sqrt{3}F_\pi^2} = -\frac{1}{\mathcal{Q}^2}\frac{m_K^2}{m_\pi^2}(m_K^2 - m_\pi^2), \tag{4}$$

where B_0 is a mass-related parameter in the theory, F_π is the charged pion decay constant, and for the charged channel $s = (p_{\pi^+} + p_{\pi^-})^2$, $t = (p_{\pi^-} + p_{\pi^0})^2$, and $u = (p_{\pi^+} + p_{\pi^0})^2$. The decay width is therefore proportional to $\mathcal{Q}^{-4}$.

An estimate for $\mathcal{Q}^2$ can be obtained by using the mass difference between neutral and charged kaons:

$$\mathcal{Q}^2 = \frac{m_K^2}{m_\pi^2}\frac{m_K^2 - m_\pi^2}{\left(m_{K^0}^2 - m_{K^+}^2\right)_{QCD}}. \tag{5}$$

Here

$$\left(m_{K^0}^2 - m_{K^+}^2\right)_{QCD} = \left(m_{K^0}^2 - m_{K^+}^2\right)_{experiment} - \left(m_{K^0}^2 - m_{K^+}^2\right)_{EM}. \tag{6}$$

The electromagnetic contribution is estimated using Dashen's theorem relating the charged-neutral kaon mass difference to the charged-neutral pion mass difference:

$$\left(m_{K^0}^2 - m_{K^+}^2\right)_{EM} = \left(m_{\pi^0}^2 - m_{\pi^+}^2\right)_{EM}. \tag{7}$$

which yields $\mathcal{Q}_\mathcal{D} = 24.2$. The value for $\mathcal{Q}_\mathcal{D}$ leads to a serious underestimate in lowest order ChPT of the decay width for the $\pi^+\pi^-\pi^0$ channel ($\Gamma = 66$ eV compared to the PDG value of 300 eV [95]). Agreement improves after including one loop and two loop corrections, but since these rescattering effects are comparable in magnitude to the tree-level estimate[96], it is clear the convergence of the chiral series in this application is poor.

Dispersion relations allow for an evaluation of rescattering effects to all orders [108–110]. This is not completely independent from ChPT because a numerical evaluation based on the dispersive representation requires an input about the subtraction constants—this input can be provided fully or at least in part by ChPT. Furthermore, there is hope that by isolating the large rescattering corrections, the chiral series for the remainder will again be found to be more well-behaved.

In the mid 90's, when the first calculations of the $\eta \to 3\pi$ amplitude based on dispersion relations were made, there was no alternative to getting the input on the subtraction constants from ChPT. In the meanwhile a few experiments have measured the Dalitz plot for this decay, thereby obtaining

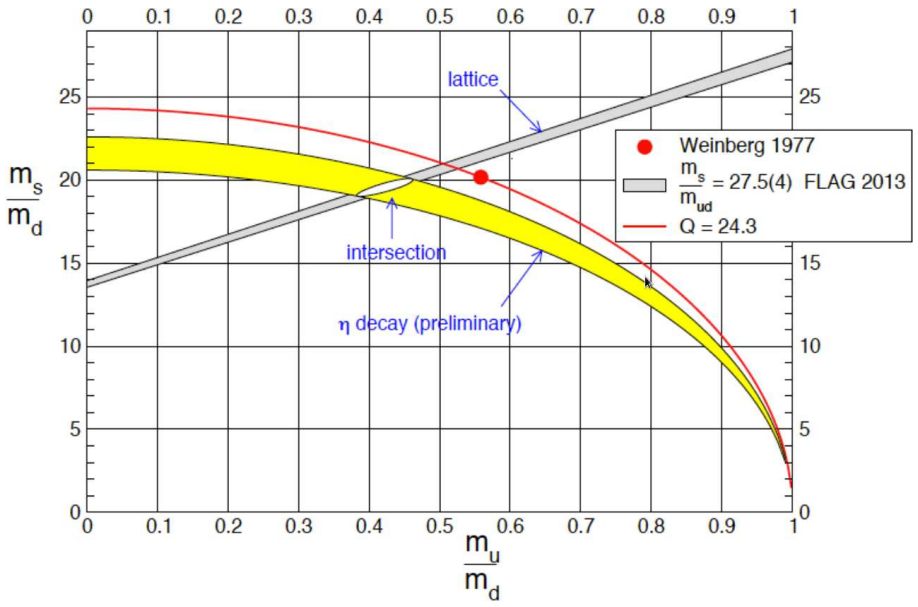

FIG. 13: Relationship between m_s/m_d and m_u/m_d.[21]

important information on the momentum dependence of the differential decay rate. This information can be used to determine or to at least constrain a subset of the subtraction constants. As it has been shown by S. Lanz, this experimental information on the subtraction constants has a strong impact on the extraction of $m_u - m_d$ from this decay. As first reported in his PhD thesis, the value of $Q \equiv (m_s^2 - \hat{m}^2)/(m_d^2 - m_u^2)$ extracted from the same $\eta \to 3\pi$ decay rate changes from 22.6 to 21.8, a shift of about one sigma of the early dispersive evaluations. Such a dispersive analysis is still in progress [107]. Preliminary results can be found in the conference proceedings of the latest Chiral Dynamics Workshop [111].

The preliminary result for the up-to-down quark mass ratio is shown in Figure 13, where the red curve represents the result using the Dashen theorem. The decays $\eta \to 3\pi$ constrain the quark masses through the Leutwyler ellipse

$$(\frac{m_s}{m_d})^2 \frac{1}{\mathcal{Q}^2} + (\frac{m_u}{m_d})^2 = 1. \tag{8}$$

Lattice QCD including photons by the FLAG collaboration has determined m_s and $(m_u + m_d)/2$ from measured values of the light meson masses. This constraint appears as a diagonal linear band. The intersection of the line and the ellipse in Figure 13 gives m_u/m_d (as well as m_s/m_d) and thus the difference $m_u - m_d$.[21]

To determine the subtraction constants for the dispersion analysis, the Dalitz distribution is used

as input. For the "charged" channel $\eta \to \pi^+\pi^-\pi^0$, the Dalitz plot is typically described in terms of two variables:

$$X = \sqrt{3}\frac{T_+ - T_-}{Q_\eta} = \frac{\sqrt{3}}{2m_\eta Q_\eta}(u-t), \tag{9}$$

$$Y = \frac{3T_0}{Q_\eta} - 1 = \frac{3}{2m_\eta Q_\eta}\left((m_\eta^2 - m_{\pi^0}^2)^2 - s\right) - 1, \tag{10}$$

where T_0, T_+, and T_- are the kinetic energies (in the η rest frame) of π^0, π^+, and π^-, respectively, and $Q_\eta = m_\eta - 2m_{\pi^+} - m_{\pi^0}$. (See Figure 14.) The Dalitz distribution is described in terms of several parameters[96]:

$$\Gamma(X,Y) \propto 1 + aY + bY^2 + cX + dX^2 + eXY + fY^3 + gX^3 + hX^2Y + lXY^2 \cdots. \tag{11}$$

Terms odd in X would require C violation. Once charge conjugation symmetry has been shown to hold within the precision of the dataset, one can set $c = e = g = l = 0$. The most recent experimental measurement in this channel was performed by the KLOE collaboration[97]. They obtained

$$\begin{aligned} a &= -1.090 \pm 0.005(stat)^{+0.008}_{-0.019}(syst) \\ b &= 0.124 \pm 0.006(stat) \pm 0.010(syst) \\ d &= 0.057 \pm 0.006(stat)^{+0.007}_{-0.016}(syst) \\ f &= 0.14 \pm 0.01(stat) \pm 0.02(syst) \end{aligned}$$

with all other coefficients consistent with zero within errors.

The disadvantage of experimentalists presenting their Dalitz distribution results using only the above format is that the correlations are missing. Our theory colleagues therefore prefer to work with binned $\Gamma(X,Y)$ data. KLOE is currently performing a new analysis, and a better use of their measurement will be possible.

For the neutral-only channel $\eta \to 3\pi^0$, the quantity $Z \equiv X^2 + Y^2$ is frequently used. The neutral Dalitz distribution is then parameterized as:

$$\Gamma(Z) \propto 1 + 2\alpha Z + 2\beta Z^{3/2} sin(3\phi) + 2\gamma Z^2 + \cdots, \tag{12}$$

where higher order terms involving products of X and Y have been omitted. The variable Z ranges from $Z = 0$ when all three π^0's have the same energy $E_i = m_\eta/3$, to $Z = 1$ when one of the π^0's is

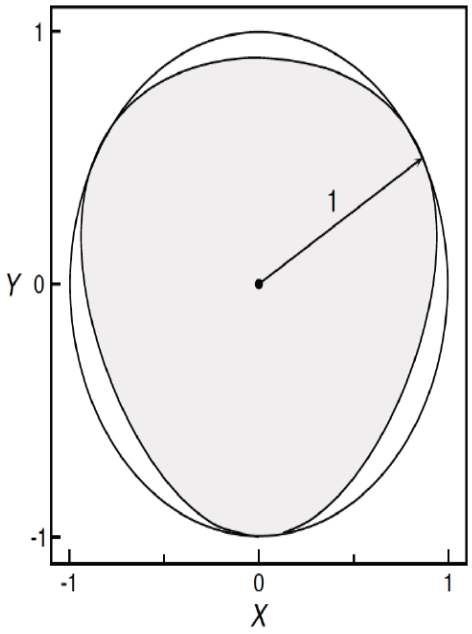

FIG. 14: The phase space limits for the $\eta \to 3\pi$ Dalitz distribution lie within the unit circle $X^2 + Y^2 = 1$ using the variables X and Y from equations 9-10. The variable Z used for $\eta \to 3\pi^0$ is defined $Z \equiv X^2 + Y^2$. [21]

at rest. In lowest order, this distribution should be uniform however, the π-π final state interaction and its strong energy dependence cause a small non-uniformity. The β and γ coefficients have not been determined experimentally, but there is good experimental agreement on α, the PDG average being $\alpha = -0.0315 \pm 0.0015$[95]. Hence the small slope parameter α has been determined with a relative error of $\sim$5%.

The amplitudes for the charged $\mathcal{A}_c$ and neutral $\mathcal{A}_n$ channels are directly related to each other:

$$\mathcal{A}_n(s,t,u) = \mathcal{A}_c(s,t,u) + \mathcal{A}_c(t,u,s) + \mathcal{A}_c(u,s,t). \tag{13}$$

The consequence of this is that the slope parameter α from the Dalitz plot of the $3\pi^0$ channel is constrained by the parameters a, b, and d from fits to the $\pi^+\pi^-\pi^0$ Dalitz distribution[96]:

$$\alpha \leq \frac{1}{4}\left(b + d - \frac{1}{4}a^2\right). \tag{14}$$

Within the framework of non-relativistic effective field theory, Schneider, Kubis, and Ditsche[104] were able convert this upper limit into an equality; unfortunately, using the Dalitz parameters from KLOE in this approach leads to a value for α that disagrees with the data. Clearly there is need for

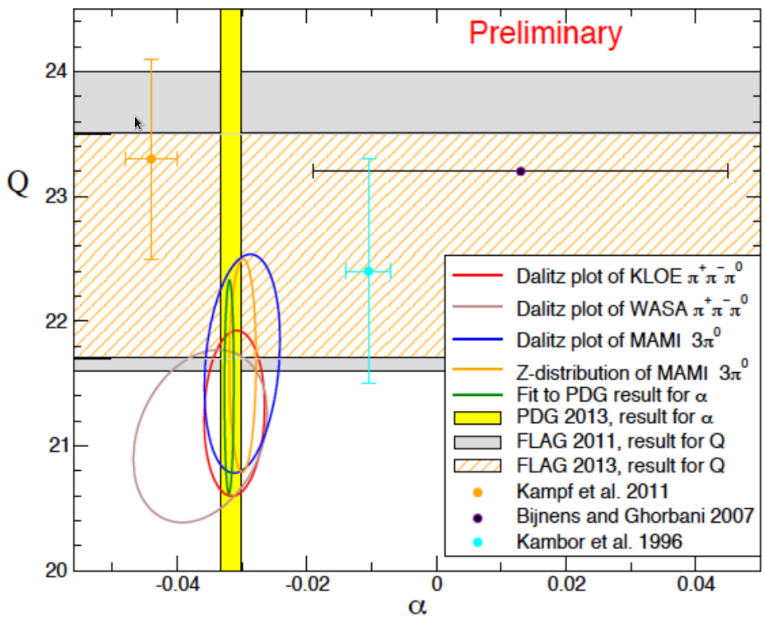

FIG. 15: Relationship between $\mathcal{Q}$ and the Dalitz parameter α from the $1 + 2\alpha Z$ fit to data.[21]

more experimental data to resolve this discrepancy. The JEF experiment will be able to measure both sets of parameters from the charged and neutral channels at the same time.

Electromagnetic corrections have also been evaluated at NLO in ChPT [105, 106]. Different kinds of effects are to be distinguished: those triggering the decay directly, which are small; kinematic effects due to the charged-to-neutral pion mass difference [104]; and conventional radiative corrections due to real- and virtual-photon effects. Even though suppressed they play an important role at the current level of precision. Indeed they are essential if one wants to bring the different determinations of $\mathcal{Q}$ based on the two channels into agreement. This has been shown in ongoing analysis and is still unpublished [107]. We stress that such an analysis was made *a posteriori* on the data and is therefore far from optimal. A proper correction of the electromagnetic effects can only be made directly by the experimentalists as they analyze the data. This requires a close collaboration with theorists and in particular the implementation of the relevant theoretical formulae in the Monte Carlo used for data analysis. For past experiments this is not possible anymore.

A plot showing the current status of the determination of $\mathcal{Q}$ given the experimental value of α and data from the "charged" channel is shown in Figure 15. Note that the best value for $\mathcal{Q}$ appears to be significantly smaller than the result using Dashen's theorem.

2. The World $\eta \to 3\pi$ dataset

The largest $\eta \to 3\pi$ datasets are summarized in Table II. The charged channel has a richer Dalitz distribution than the neutral channel. From the JEF event projections in Table VII, we expect to increase the world charged 3π dataset by a factor of about 2.8, significantly reducing the statistical error over the Dalitz distribution. Although the preliminary WASA dataset is much smaller than either the published or preliminary KLOE datasets, it provides a valuable cross-check that systematic errors have been estimated correctly. There appears to be some tension between the published KLOE result and the preliminary WASA result in the bY^2 term. [130] (Systematic errors for the larger, preliminary KLOE dataset are still being determined.) Our dataset would provide a more precise cross-check on the high statistics KLOE datasets.

The world dataset for $\eta \to 3\pi^0$ has been extensively investigated by the Crystal Ball collaboration at MAMI. For the neutral channel, Bose symmetry simplifies the form of the Dalitz distribution. From the JEF event projections in Table VII, we expect to increase the world neutral 3π dataset by a factor of about 2.6, significantly reducing the statistical error over the Dalitz distribution. We would also provide the first neutral 3π dataset with over a million events not taken on the Crystal Ball.

In terms of systematic errors, our simulations in Figure 42 suggest we will have a flatter acceptance compared to KLOE. This is presumably because our boost makes us more efficient in the larger Z region where one of the pions has a small energy in the η CM frame. The fit range caused the largest systematic uncertainty for the slope parameter α determination in the recent KLOE result [103].

D. Search for new C violating, P conserving interactions

Another approach to searching for BSM physics is to look for violations of symmetries at a level which is unexpected from SM sources. Assuming CPT is a good symmetry, Table III classifies forces in the SM according to their properties under charge conjugation (C) and parity (P). In the upper right quadrant of Table III, we encounter CP violation in which C is conserved but P is violated. The SM background here for flavor-conserving processes is extremely small since it

TABLE II: Event sizes of recent, large 3π datasets, both published and preliminary. Our projection for these non-rare channels is based on 100 days of JEF running plus 200 days of already approved GlueX-IV running. (See Table VII for details.)

Channel	Experiment	Number of Events
$\eta \to \pi^0\pi^+\pi^-$		
	KLOE [98]	1.3×10^6
	KLOE prelim. [130]	4.5×10^6
	WASA prelim. [130]	0.15×10^6
		World Total = 6×10^6
		(Our Projection: 16.5×10^6)
$\eta \to 3\pi^0$		
	Crystal Ball at MAMI [100]	3×10^6
	Crystal Ball at MAMI [101]	1.8×10^6
	Crystal Ball at BNL [99]	1×10^6
	KLOE [103]	0.6×10^6 [a]
	WASA [102]	0.12×10^6
		World Total = 6.5×10^6
		(Our Projection: 16.9×10^6)

[a] medium purity

occurs at two-loop level. However, larger contributions for EDMs could in principle arise at one-loop level from SUSY. For $\eta \to 2\pi$, calculations with an extended Higgs sector found 12 orders of magnitude enhancement in the C,PV,CPV decay compared to the base SM prediction, but the predicted BR of $O(10^{-15})$[122] is still far below the sensitivity of any forseeable experiment. While the motivation for improved $\eta \to 2\pi^0$ measurements does not currently appear strong, and thus has been de-emphasized in the current version of our proposal, we will lower the BR upper limit by over an order of magnitude as a by-product of our $\eta \to \pi^0 2\gamma$ analysis.

A less constrained, and therefore much more interesting, possibility is that of C violation with P conservation (the lower left quadrant in Table III). Under CPT this is of course equivalent to T violation with P conservation. The magnitude of such a new interaction is *indirectly* constrained by EDM measurements since a new CV,P,CPV interaction could mix with the usual weak interaction to yield the effective C,PV,CPV interaction needed to produce an observable EDM. However,

indirect constraints from EDMs turn out to be hierarchically ambiguous[37], so *direct* constraints on C violation with P conservation with sensitivity as close as possible to the weak scale would be very interesting.

1. *The C non-invariant decay $\eta \to 3\gamma$*

Few systems in nature are suitable for tests of the non-invariance of the charge conjugation operation C. It not only requires a particle of good C (or self-conjugate composite system), the decay into a state of opposite C must be blocked *only* by C invariance [95]. Experimental precision is limited by the need to first produce these unusual systems, then search for final states with opposite C in the face of SM backgrounds.

It is useful to have an estimate for the SM background in $\eta \to 3\gamma$. The only known source of C violation is the weak interaction, in which C violation is normally accompanied by P violation. Scaling the $\pi^0 \to 3\gamma$ calculation of Dicus [119] to the larger mass of η, one can estimate $\Gamma(\eta \to 3\gamma)/\Gamma(\eta \to 2\gamma) = 10^{-24}$. Despite the enormous expected enhancement in this branching ratio due to the larger η mass, and the considerable uncertainty in the estimates due to the choice of effective quark mass in the loops, the SM background for $\eta \to 3\gamma$ is effectively zero for any forseeable experiment. Thus any non-zero result in $\eta \to 3\gamma$ would require a new source of C violation.

As a by-product of the $\eta \to 3\gamma$ analysis, we will improve the upper limits on another C violating

TABLE III: Matrix of C and P symmetries. Assuming invariance under CPT, then interactions fall into one of only four combinations. The off-diagonal combinations involve CP violation, with EDM's most important for constraining new C,PV,CPV interactions, while η decays directly constrain new CV,P,CPV interactions.

	P	PV
C	C, P, CP Strong, EM $\eta \to 2\gamma$, $\eta \to 3\pi^0$, etc.	C, PV, CPV Weak (at 2-loop level) EDMs, $\eta \to 2\pi$
CV	CV, P, CPV Weak (at 2-loop level) $\eta \to 3\gamma$, $\eta \to 2\pi^0\gamma$, etc.	CV, PV, CP Weak PV experiments, μ and β decay asymmetries

"3γ" final state, $\eta \to \pi^0\gamma$. However, since the latter is also forbidden by the conservation of angular momentum we assume it will serve as an experimental control.

Status of $\eta \to 3\gamma$ tests of C non-invariance

Before showing our plot comparing different experiments, we must digress to explain the Figure of Merit (FOM) for measuring forbidden decay channels. A tentative signal for a SM forbidden η decay would appear as an excess at the η mass that is statistically unlikely (10% probability or lower). To a useful approximation, the branching ratio (BR) upper limits in published work can be simply estimated by $BR < 2\frac{\sqrt{N_{bkg}}}{N_\eta \times Acceptance}$ where N_{bkg} is the number of background events in the signal window, and the factor of 2 corresponds to roughly 90% CL. However, this equation gives a misleading impression since the number of background and signal events are linearly proportional if pile-up does not dominate. If we define the background fraction $f_{bkg} \equiv N_{bkg}/(N_\eta \times Acceptance)$, then the estimated BR upper limit expression becomes

$$BR < 2\sqrt{\frac{f_{bkg}}{N_\eta \times Acceptance}} \tag{15}$$

from which it is clearer that the FOM the experimenter needs to maximize in this case is

$$FOM \equiv N_\eta \times Acceptance/f_{bkg}. \tag{16}$$

Equation 15 highlights the level of experimental effort needed to reduce BR upper limits. Because of the square root dependence, an order of magnitude improvement in the BR upper limit requires improvements in experimental FOM which can only be expected perhaps once per generation.

Figure 16 shows the BR upper limits for $\eta \to 3\gamma$ from several experiments [121] [38] along with their effective number of η's and background fractions. These measurements have been limited mostly by background rather than by the number of effective η decays. Since the improved technology in our experiment will reduce the background from continuum $2\pi^0$ production with 1 missing photon, and the background from $\eta \to 3\pi^0$ with 3 missing photons[2], we expect to improve the BR upper limit by one order of magnitude. (See section VI B 4.)

[2] The background from photon splitting in $\eta \to 2\gamma$ has been easy to remove in most experiments, with low cuts losses, by rejecting close showers in the calorimeter.

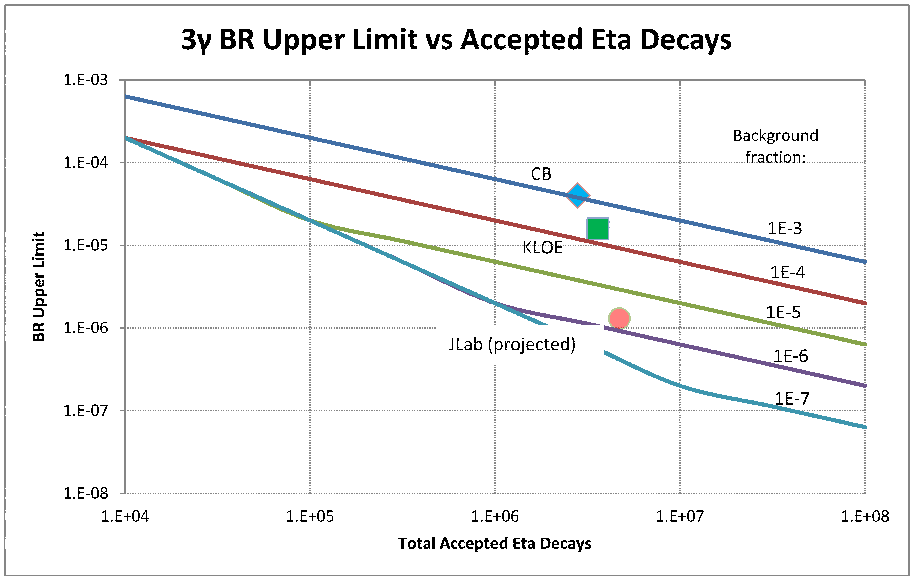

FIG. 16: The branching ratio upper limits and figures of merit for $\eta \to 3\gamma$ measurements by KLOE [121] and the Crystal Ball at BNL [38] plus a projection for the JLab Eta Factory.

2. Other C non-invariant observables

We will also search for the C violating decays $\eta \to 2\pi^0\gamma$ and $\eta \to 3\pi^0\gamma$, which were previously measured in reference [38]. We expect to make a large improvement in the former channel since it leads to 5 photons, hence the sensitivity of previous experiments has been limited by the missing photon background from $\eta \to 3\pi^0$. Finally, a by-product of our analysis of $\eta \to \pi^0\pi^+\pi^-$ (used to extract $m_u - m_d$ as already discussed in section II C), will be improved constraints on C violating asymmetries in the Dalitz distribution. All four decay channels in our campaign to improve direct limits on CV, PC, interactions in η decays are listed in Table I.

E. Opportunistic physics

The P violating and C conserving decay $\eta \to 2\pi^0$

A by-product of the analysis of our low background $\eta \to$ "4 γ" dataset will be $\eta \to 2\pi^0$. This channel would violate P while conserving C and thus violate CP, and has already been discussed above in the introduction of section II D. Neutron EDM measurements appear to tightly constrain

new, flavor-conserving sources CP violation that might be observed in $\eta \to 2\pi^0$. However, since Baryogenesis requires an additional source of CP violation to account for the dominance of matter over anti-matter in the universe, we should take the opportunity to dramatically reduce the BR upper limit for one of the few tests of CP in the flavor-conserving sector that exists. Figure 17 shows the BR upper limits for several experiments along with the effective number of η's in their experiments as well as their background fractions. These measurements have been limited both by backgrounds and the number of effective η decays. This proposal presents an opportunity to reduce the BR upper limit of $\eta \to 2\pi^0$ by 1.5 orders of magnitude. (See section VI B 5.)

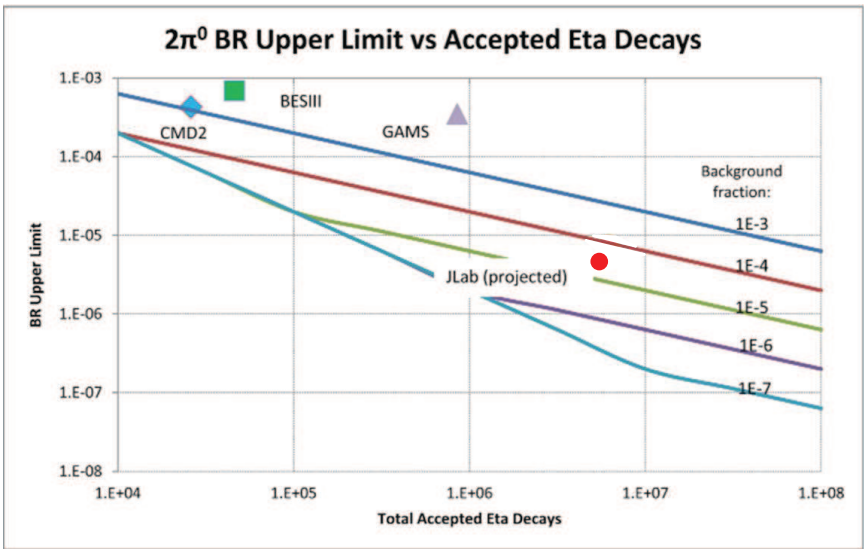

FIG. 17: The branching ratio upper limits for $\eta \to 2\pi^0$ measurements by GAMS [117], CMD-2 [113], and BES-III [115] plus a projection for the JLab Eta Factory.

F. Future extensions to η'

The η' meson measurements for the same channels as for η measurements could be a valuable addition to the data set. In most channels, the physics input will be the same (quark mass ratios, lepto-phobic dark-sector B-boson), providing complementary information to η measurements. These studies are of great interest because of the special property of the η' that distinguishes it

from the other Goldstone Bosons, namely that its mass does not vanish in the chiral limit: the η' receives the main contribution to its mass by the mechanism of the Axial Anomaly, and the rest of it is contributed by the quark masses. The η' meson is the heaviest of the three flavor-neutral low lying 0^{-+} mesons. It mixes with the η due to $SU(3)$ symmetry breaking and with the π^0 due to isospin breaking. Although it is rather heavy, there are several strong indications that it is an approximate Goldstone Boson (GB). One limit in QCD, where the η' becomes a GB on the same footing as the GB octet, is the large N_c limit. That limit has been used to formulate an effective theory which includes the η' [128]. Combining the $1/N_c$ and the chiral expansions thus allow one to study low energy processes involving the η' in a systematic way. As an example, the role of the η' in the decays of the η and π^0 has been analyzed along those lines [129], where the mentioned mixings are calculable at the lowest order of the expansion, and can be determined more precisely at the next sub-leading order. For instance, the $\eta' - \eta$ mixing angle is 10 ± 2^o, and the $\eta' - \pi^0$ mixing angle turns out to be 0.75 ± 0.2^o, both in the scheme of reference [129].

The dominant decay of the η' is into $\eta\pi\pi$, followed by the unnatural parity decays into $\rho^0\gamma$, $\omega^0\gamma$, and $\gamma\gamma$. All these decays are fairly accurately known. Other suppressed decays are of great interest, such as the $\eta' \to \pi^+\pi^-\pi^0$ which is driven by symmetry breaking effects due to $m_u - m_d$, which has been measured with about 10% error in the width. Another decay of interest is $\eta' \to \pi^0\gamma\gamma$. Both of those decays would be accessible with experiments similar to the one in this proposal. Of particular interest is a more detailed knowledge of the η' through its as yet unknown low energy constants, which require the experimental measurement of the mentioned processes as well as other ones which remain to be observed due to their small branching fractions. As an example, the measurement of $\eta' \to 3\pi$ impacts on the knowledge of two low energy constants, the L_{18} and L_{25} defined in Ref. [128].

In the theoretical realm, the η' has been addressed by several groups, in particular the decays $\eta' \to \eta\pi\pi$ and $\eta' \to 3\pi$. As in the case of the similar three body η decays, final state interactions must play an important role, and several works have addressed that problem. Since the two body rescattering occurs in S-wave, scalar meson dominance has been proposed [132], and also unitarization schemes based on an effective chiral Lagrangian [133]. The latter has been applied to a possible extraction of the quark mass ratio $\mathcal{Q}$ from $\eta' \to 3\pi$ [134] . Finally the first study of the decays $\eta' \to \pi^0\gamma\gamma$ and $\eta' \to \eta\gamma\gamma$ has only recently been undertaken [135]. It is of high interest to pursue further theoretical advances in η' physics, and that interest will certainly be significantly

reinforced by the current and future experimental efforts.

The current experimental efforts in η' physics are mainly concentrated at KLOE, BESIII where the most accurate $\eta' \to 3\pi$ has been measured, [130] and MAMI where measurements of $\eta' \to \eta\pi\pi$ have been carried out and forthcoming measurements of $\eta' \to 3\pi$ [131]. Compared to the other facilities, JLab is currently the only place where one can perform both η and η' measurements with similar rates, kinematics, and systematics.

III. CONTROLLING BACKGROUNDS IN RARE NEUTRAL DECAYS

Several key features of our proposal which suppress backgrounds while maintaining a high η production rate are:

(1) the 12 GeV high intensity tagged photon beam in Hall D to produce η mesons on a 30 cm liquid hydrogen target through the $\gamma p \to \eta p$ reaction,

(2) placing a central core of high-resolution, high-granularity $PbWO_4$ crystals in the forward calorimeter (an upgrade called FCAL-II) to reduce the missing photon background from the large $\eta \to 3\pi^0$ branch,

(3) measurement of the recoil p with the GlueX start counter and central drift chamber to establish coplanarity of the recoil proton and η from $\gamma + p \to \eta + p$ (thus over-determining the kinematics),

We will also benefit from using flash ADCs on every crystal for sub-nsec coincidence timing of showers and pile-up rejection, plus the short scintillation decay time of lead tungstate ($\sim$ 20 ns) which is about one order of magnitude shorter than NaI(Tl) used in the Crystal Ball calorimeter.

In the following sections, we show detailed simulations for the challenging rare decay $\eta \to \pi^0 2\gamma$. The BR of this channel is 2.7×10^{-4}, corresponding to a very small partial width of only $\Gamma = 0.35$ eV. We will demonstrate the ability of Hall D's kinematics and our proposed calorimeter upgrade to dramatically reduce backgrounds for this channel compared to other facilities. Once having shown the great promise for reducing the missing photon background in the "4γ" sector, we will make much simpler background estimates in the sensitivities section for the "3γ" sector.

To show that the lead tungstate upgrade for the central region of FCAL is essential for the rare decay part of our program, two options for the forward calorimeter were initially considered in the simulation. One was the the standard GlueX lead glass calorimeter (FCAL) with a round front face of 240 cm in diameter and block sizes of 4.0cm x 4.0cm, and the other was an upgraded version with a $PbWO_4$ crystal central region with an active area of 118×118 cm^2 (FCAL-II) and crystal sizes of 2.05cm x 2.05cm. (More details of FCAL-II will be described in section V.)

Our simulations show that the electromagnetic background plays no significant role in either the online trigger rate or in the offline accidental background. (See Appendix C for detail). In the

following discussion, we focus on the hadronic background only.

A. The $\eta \rightarrow 3\pi^0$ Background

Previous $\eta \rightarrow \pi^0\gamma\gamma$ experiments [68][86][88][84] found the dominant background to be from $\eta \rightarrow 3\pi^0$ which has a branching ratio three orders of magnitude larger than the desired $\eta \rightarrow \pi^0\gamma\gamma$ decay. Obviously, for a 6γ decay to be a background to a 4γ process, two photons must effectively be undetected while the event nevertheless passes the cuts used to define a good signal. There are three contributing cases [68]: (1) two soft photons can fall out of the geometrical acceptance or below threshold of the detector, or (2) four photons can merge into what appears to be two showers, or (3) a combination of soft photon losses and photon mergings.

The first mechanism (the loss of photons) affects the majority of published η rare decay experiments because their η's had small or modest boost. In that case, decays frequently produce low energy γ's whose omission allows the the $\eta \rightarrow 3\pi^0$ background to pass missing energy or η invariant mass cuts. The second mechanism, the merging of photons, is a problem when individual crystals subtend too large a solid angle, a feature of the legacy Crystal Ball calorimeter which was not optimized for η decay experiments. Both mechanisms can be greatly suppressed by increasing the energy of the η mesons while maintaining sufficient granularity in the calorimeter.

The advantage of using highly boosted η's can be seen by comparing spectra from two older experiments as shown in Figure 18 and Figure 19 (Left). The invariant mass spectrum from GAMS shows a narrow peak from $\eta \rightarrow \pi^0\gamma\gamma$ which is 7x larger than a smoothly falling background. [68] In that experiment, the η's were produced by a high energy π^- beam (30 GeV/c). The decay photons from η decays in flight were detected in the forward direction by a calorimeter consisting of a 48 x 32 array of lead glass modules. Because of the boost, when a photon is truly lost, the effect on the η mass reconstruction is relatively large thus the background from missing photons in $\eta \rightarrow 3\pi^0$ events is generally shifted out of the η signal window.

In the Crystal Ball at AGS [86], KLOE[88], and Crystal Ball at MAMI[84] program, the η's were produced with little boost. Under these circumstances, the background from $\eta \rightarrow 3\pi^0$ is broadly peaked near the η mass as can be seen in Figure 19 (Left).[3] Sideband subtractions alone are

[3] See also Figure 10(a) in reference [85].

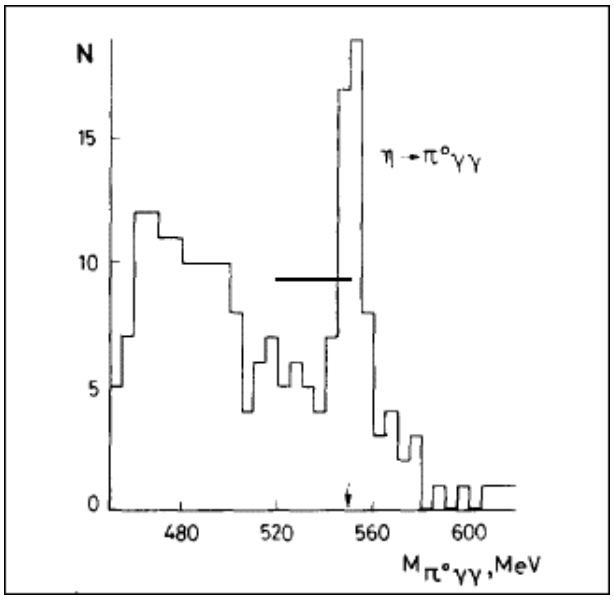

FIG. 18: Invariant mass spectrum for the $\pi^0\gamma\gamma$ reaction measured by the GAMS collaboration [68] from decay of η's with an energy of roughly 30 GeV.

therefore unreliable and one must rely on simulations of shower merging probability. Under such background conditions it is already difficult to accurately determine the simple branching ratio; the measurement of $d\Gamma/dM_{\gamma\gamma}$ with sufficient precision to probe the dynamics of the $\eta \to \pi^0 2\gamma$ decay is even more difficult.

Simulations were made to compare the ability of the existing FCAL and upgraded FCAL-II to suppress the missing photon background from $\eta \to 3\pi^0$ (using only the central regions containing lead glass or PWO, respectively). Four-photon invariant mass distributions for the signal $\eta \to \pi^0\gamma\gamma$ and the background $\eta \to 3\pi^0$ are reconstructed. Figure 20 is for events in the high resolution core of FCAL-II, while Figure 21 is for FCAL, with both located 6m downstream of the target. The signal to background ratio for the high resolution core of FCAL-II is two orders of magnitude better than FCAL.

We also studied the situation where the existing lead glass FCAL would be moved 3 m further downstream from the target (the maximum possible distance allowed in Hall D) to reduce photon merging and improve the angle resolution. While the signal to background ratio improved to 0.5, this is still 1.5 orders of magnitude worse than FCAL-II and not good enough for clear signal separation. **Thus, the upgrade of FCAL to FCAL-II is essential for rare η decays to**

neutral modes, and all subsequent plots will assume the hybrid FCAL-II configuration.

In summary, Hall D kinematics combined with a forward calorimeter upgrade will tightly manage the potential background from missing photons in the copious $\eta \to 3\pi^0$ channel. This leaves a small peaking background in the invariant mass spectrum that we will be able to accurately simulate and subtract.

B. The $\gamma + p \to 2\pi^0 + p$ (Continuum) Background

The remaining historically dominant background has been non-resonant multiple π^0 production. The production of $\gamma p \to 2\pi^0 p$ has been studied using different beam types and targets at low beam energies [123][124]. In our forward, high energy kinematics, the η carries almost the full beam

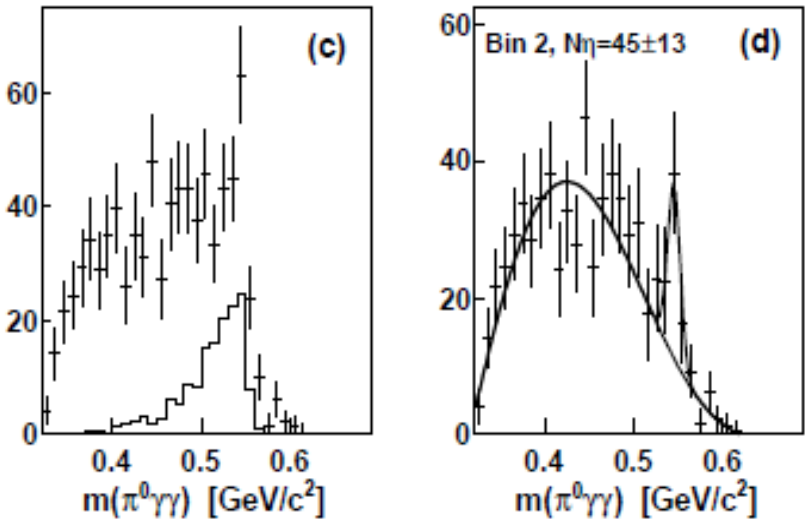

FIG. 19: Invariant mass spectrum for the $\pi^0\gamma\gamma$ system measured by the MAMI collaborations [84] (for a representative bin in the Dalitz distribution, $m^2(\gamma\gamma) = 0.0375 \pm 0.01$). Left - Spectrum after randoms subtraction. The solid line is the expected background from $\gamma p \to \eta p \to 3\pi^0 p$ after all cuts. Compare to the previous figure from GAMS. Right - After subtraction of the $\gamma p \to \eta p \to 3\pi^0 p$ background. The signal has been fitted by a Gaussian.

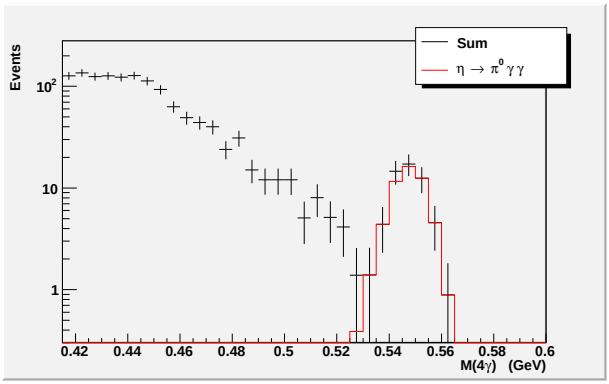

FIG. 20: Monte Carlo simulation of $M_{4\gamma}$ reconstructed in the high resolution $PbWO_4$ central region of the proposed FCAL-II. The only background considered here is from $\eta \rightarrow 3\pi^0$. The red curve is the signal from $\eta \rightarrow \pi^0\gamma\gamma$. Black points are the signal plus background. The signal to background ratio for $\pm 3\sigma$ around the η mass peak is 10:1.

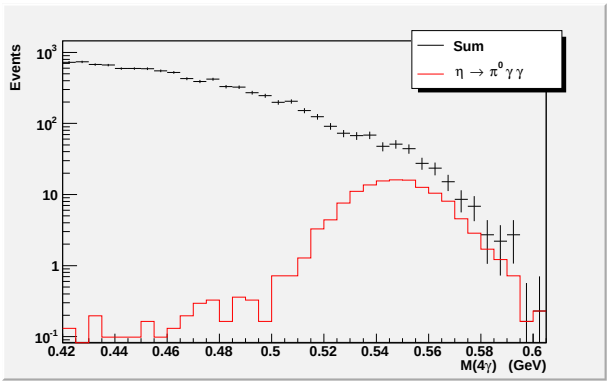

FIG. 21: Same conditions as the previous figure but using a current Hall D forward lead glass calorimeter (FCAL). The signal to background ratio is 0.1.

energy. This means that the elasticity, defined as

$$EL \equiv \frac{\Sigma E_\gamma}{E_{tagged\gamma}} \tag{17}$$

is approximately 1 for fully contained η decays produced by the exclusive $\gamma + p \rightarrow \eta + p$ production channel.[4] Requiring that the elasticity be near 1 (or the missing energy be near 0) greatly inhibits nature's ability to mimic a signal from complex backgrounds.

Three other kinematical variables used for event selection are the invariant mass $M_{4\gamma}$, missing energy ΔE, and the co-planarity $\Delta\phi$. The missing energy here is $\Delta E \equiv E_\eta + E_p - E_{beam} - M_p$. The co-planarity $\Delta\phi$ is the azimuthal angle difference between the proton and the reconstructed η, $\Delta\phi \equiv \phi_\eta - \phi_p$. The event selection windows for these variables correspond to $\pm 3\sigma$ (unoptimized) of the corresponding resolutions and are listed in Table IV.

A Monte Carlo simulation was performed for the $\gamma p \rightarrow 2\pi^0 p$ reaction using the PYTHIA event generator incorporating both non-resonant production of the two-pion pairs and production through resonances such as $\gamma + p \rightarrow \pi^0 + \Delta^+ \rightarrow 2\pi^0 + p$. Figure 22 shows the 4γ invariant mass distributions

[4] This is a legacy missing energy-like cut used in some of our early plots. It was more appropriate for PrimEx kinematics where the recoil proton carried away negligible energy.

	$M_{4\gamma}$ (GeV)	Elasticity	ΔE (GeV)	$\Delta\phi$ (deg)
FCAL(Pb glass)	[0.500, 0.595]	≥ 0.92	[-0.8 ,0.8]	[-5, 5]
FCAL-II (PWO)	[0.526, 0.569]	≥ 0.95	[-0.36,0.36]	[-5, 5][a]

[a]A smaller range could have been used due to the better PWO resolution.

TABLE IV: Event selection ranges used in the analysis.

for the $\eta \to \pi^0\gamma\gamma$ signal and the three backgrounds ($\eta \to 3\pi^0$, $\gamma p \to 2\pi^0 p$, and the "other hadronic backgrounds" that will be discussed in the next section). The statistics is normalized to one day of data taking, while the cuts are listed in Table IV. The projected signal to background ratio is approximately 3:1. The $2\pi^0$ continuum background appears to play a small role near the η mass signal window in Hall D kinematics.

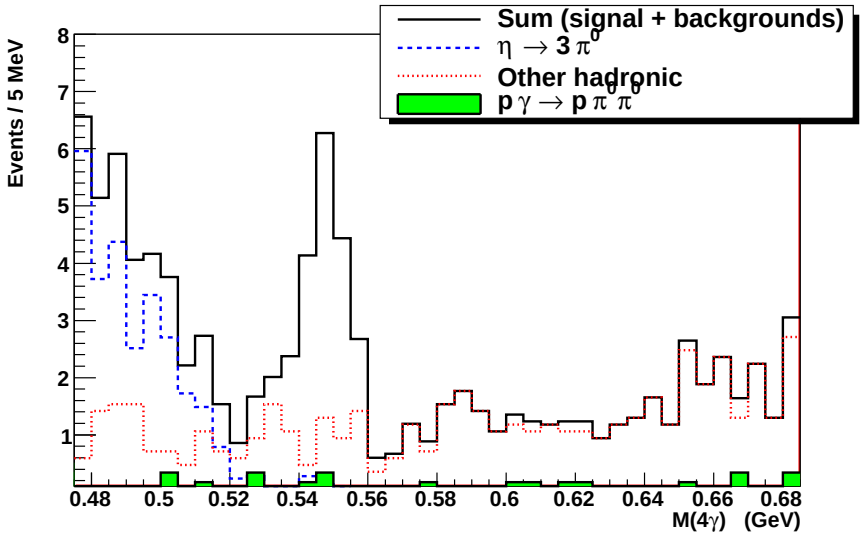

FIG. 22: Invariant mass ($M_{4\gamma}$) for FCAL-II including the signal channel $\eta \to \pi^0 2\gamma$ and essentially all significant background channels. The solid black curve is the sum of signal and background channels. The blue dashed curve is for $\eta \to 3\pi^0$; the solid green area is for $\gamma p \to 2\pi^0 p$, and the red dotted curve is for other hadronic backgrounds predicted by PYTHIA. All rates are normalized using estimated cross sections to 1 beam day. Cuts for FCAL-II listed in Table IV have been applied. This was a successful proof of principle cuts study; further improvements can be expected with optimized cuts. Our projected Signal/Background compares extremely favorably to the data from MAMI in Figure 19 (Left).

C. Other Hadronic Background

Essentially all remaining hadronic background contributions to the $\eta \to \pi^0\gamma\gamma$ signal channel were studied using a Pythia event generator adapted to GlueX energies. The background was simulated in the photon beam energy range between 9 GeV and 12 GeV. The total photoproduction cross section for this energy range is about 120 μb. The analysis was carried out in two steps:

First, we identified all possible decay channels that can contribute as a background to the "4γ" final state using 28 million Pythia events. Generated events were passed through the detailed GlueX Geant simulation and were reconstructed using official FCAL and PWO calorimeter cluster reconstruction programs. Since the backgrounds from $\gamma p \to \pi^0\pi^0 p$ and $\gamma p \to p\eta$ (followed by $\eta \to 3\pi^0$ decays) have been discussed in Sections II.A and B, we excluded them from this study. We observed that the dominant background originates from multiple photon final states such as $p\ 4\pi^0$, $p3\pi^0\gamma$, $p\ 2\pi^0\ \gamma$, $p\ 2\pi^0\ 2\gamma$, and $p\ 2\pi^0\ K_L$. Similar to the case of the $p\eta$ ($\eta \to 3\pi^0$) background described in Section II.A, these channels can either lose photons outside the calorimeter acceptance or produce overlapping clusters, leading to the reconstruction of a "4γ" final state.

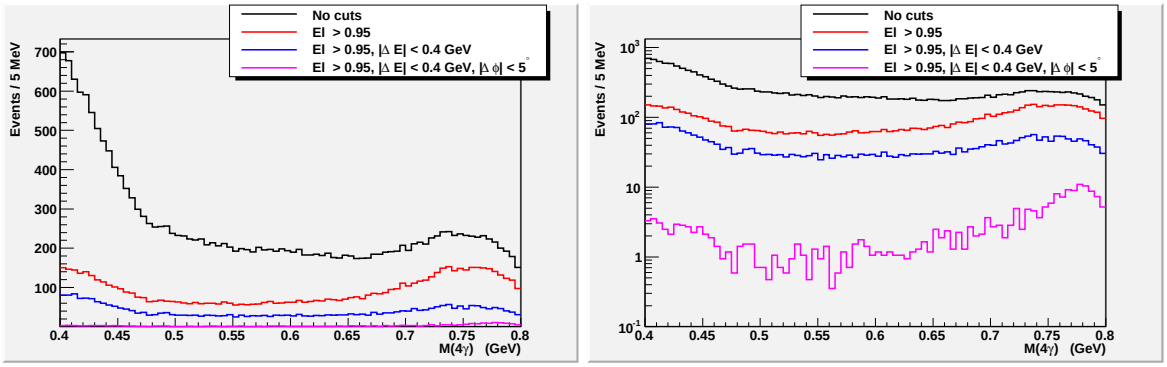

FIG. 23: 4γ invariant mass distribution for "other hadronic background" events reconstructed with the PWO region of FCAL-II. (Left - linear scale; Right - log scale) Different curves correspond to various cuts applied during the reconstruction: no cuts (black); elasticity cut (red); elasticity and ΔE cuts (blue); elasticity, ΔE, and $\Delta\phi$ cuts (purple).

Subsequently, we generated a MC sample with five times larger statistics for these selected background channels. The invariant mass distribution for events reconstructed with the PWO calorimeter (FCAL-II) is presented in Fig. 23 which shows the effect of subsequent cuts. The majority of the background events are suppressed by the elasticity/missing energy cut(s). Such background events

must have started at higher invariant mass and migrated into the η invariant mass window by losing an O(100) MeV photon out of the PWO calorimeter acceptance. (Using the lead glass section of FCAL-II as a veto would almost certainly reduce this background further.) The addition of the co-planarity cut suppresses the remaining background by an order of magnitude. The contribution of the "other hadronic background" estimate after cuts is also shown as the red dotted curve in Figure 22.

We conclude that the JEF configuration and preliminary cuts are sufficient to manage all the dominant backgrounds, and note that there is room for further improvement with optimized cuts.

IV. REFERENCE DESIGN AND HALL D BASE EQUIPMENT

We propose to use a 9.0–11.7 GeV incoherent tagged photon beam in Hall D to produce η mesons at small angles via the $\gamma + p \rightarrow \eta + p$ reaction. The majority of decay photons from the η's will be detected in an upgraded Forward Calorimeter (referred to as FCAL-II) in which the central lead glass blocks will be replaced with smaller, higher resolution $PbWO_4$ crystals. For not-too-small η angles, the low energy recoil protons will be detected by the start counter and central drift chamber of the GlueX solenoid detector to help suppress backgrounds. As shown in Figure 24, the experimental apparatus includes: (1) a high energy photon tagger; (2) a pair spectrometer for photon flux monitoring; (3) a 30 cm liquid hydrogen target; (4) the GlueX solenoid detector; (5) an upgraded forward multichannel electromagnetic calorimeter.

The parameters for the reference design of the experiment are summarized in Table V. Details of each instrument are discussed below.

A. High Energy Photon Tagger

Hall D has constructed a 12 GeV tagged photon beam line. While details of the design can be found in reference [136], the main features are:

1. Photon energy detection from 70% to 75% of the primary electron beam energy with energy resolution of about 0.5% (r.m.s.) of the primary beam energy. A counting rate of at least 5×10^6 electrons per second per 0.1% energy bin over this range of photon energies.

2. Additional capability for photon energy detection from 25% to 97% of the primary electron beam energy. Capable of pre-collimated intensities up to 150MHz/GeV for high intensity running, with 50% sampling of 60 MeV energy bins below 9 GeV and full coverage in 10-30 MeV wide energy bins above 9 GeV photon energy.

TABLE V: Parameters for the reference design of the JEF experiment.

Parameter	**Value**
Solenoidal Field	2.1 T
Photon Beam Energy Range	9 - 11.7 GeV
Beam Current	400 nA
Radiator Thickness (Au)	2.5 x 10^{-4} X_0
5 mm diam. Collimator Transmission	30%
Tagged Photon Rate on Target (9-11.7 GeV)	$\sim$5 x 10^7 Hz
LH_2 Target Length	30 cm (3.46 % R.L.)
LH_2 Target Thickness	1.28 x 10^{24} protons/cm^2
Cross Section for Forward $\gamma p \rightarrow \eta p$	$\sim$70 nb
Scintillator in FCAL-II	$PbWO_4$
Outer Active Dimensions of $PbWO_4$	118cm x 118cm
Outer Active Radius of FCAL-II	120cm
Beam Hole Dimensions in FCAL-II	12cm x 12cm
$PbWO_4$ Crystal Dimensions	2.05cm x 2.05cm x 18cm
Number of Optically Isolated Crystals	3445
Distance Target Center to FCAL-II Front	$\sim$6 m
Proton-tagged η Production Rate	3.4 Hz
LH_2 Production Request	100 days
Proton-tagged η's Produced in 100 Days	2.9 x 10^7
Total Beam Request	130 days

The tagging spectrometer is an Elbek-type spectrometer. The 12 GeV electrons pass through the radiator target where a small fraction undergo bremsstrahlung. The electrons then pass through a focusing quadrupole and are bent by the 6 meter long tagger magnet. The majority of the electrons do not significantly radiate and are bent 13.4° to the electron beam dump. A large vacuum vessel is integrated into the magnet and extends to the spectrometer focal plane so the only multiple scattering occurs in the radiator and in the exit window, preserving the resolution.

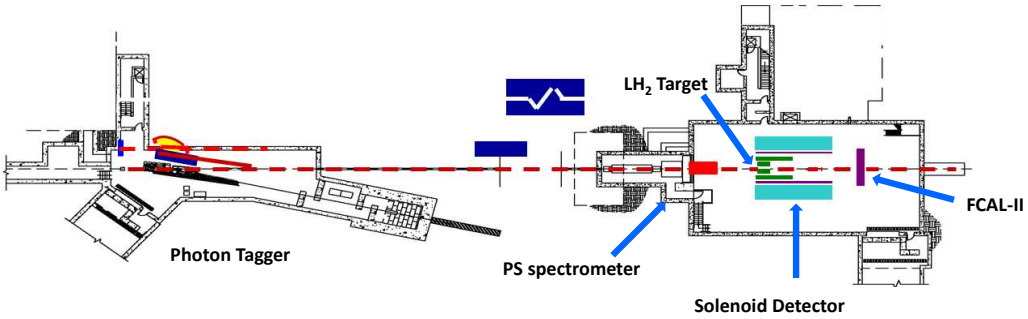

FIG. 24: Top view of the experimental setup for η rare decays measurements. This includes: (1) a high energy photon tagger; (2) a pair spectrometer; (3) a solenoid detector with a physics target; (4) a forward $PbWO_4$ crystal calorimeter.

The spectrometer detectors are positioned immediately outside the focal plane to determine the momentum of electrons that produce bremsstrahlung photons in the radiator. The photon energy, E_γ, is determined by the difference between the initial electron beam energy and the energy of the post-bremsstrahlung electron deflected towards the focal plane.

The detector package is divided into two parts: (1) a set of 218 fixed scintillation counters spanning the photon energy range from 3.0 to 11.7 GeV, and (2), a movable "microscope" of 500 scintillating fibers optimized for coherent photon beam operation spanning the energy range from 8.1 to 9.1 GeV.

The fixed array provides access to the full tagged photon spectrum, albeit at a modest energy resolution of $\sim 0.1\%$ and reduced rate capability. These detectors are well suited for running with a broadband incoherent bremsstrahlung source. The microscope provides energy resolution better than 0.07% in order to run in coherent mode at the highest polarization and intensities. Using the microscope, the source is capable of producing collimated photon spectral intensities in excess of 2×10^8 photons/GeV, although accidental tagging rates will limit normal operation to somewhat less than this.

For the proposed η rare decays measurement, we will use an incoherent bremstrahlung photon beam in an energy range from 9.0 GeV to 11.7 GeV. The current design of the fixed scintillation counters in this energy range with 10-30 MeV wide energy bins is sufficient.

B. Beam Collimation

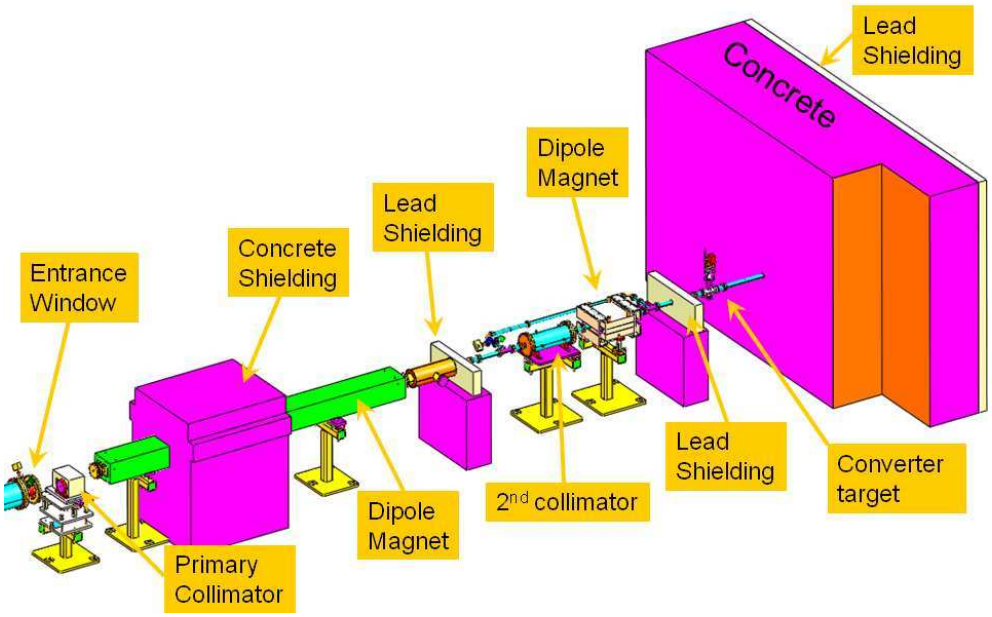

FIG. 25: The layout of the collimator cave.

A 12 GeV electron beam interacting with a thin radiator produces the photon beam. The characteristic opening angle for bremsstrahlung photons is $m_e/E = 42$ μrad. After 76 meters of drift in vacuum, the photon beam enters the collimator cave from the left through a thin 250 μm Kapton window 8″ (203mm) in diameter and immediately interacts with the primary collimator.

The layout of the collimator cave is shown in Figure 25. The primary collimator consists of two main components: an active collimator which measures the centroid of the photon beam and a hybrid tungsten-lead passive collimator. The size of the passive collimator has a couple of options from 3.4 mm to 5.0 mm in diameter. The active collimator is electrically isolated, has an inner aperture of 5 mm, and is precisely mounted in front of the primary collimator. The purpose of the active collimator is to measure the position of the centroid of the photon beam with an accuracy of 200 μm. The tungsten passive collimator is surrounded by 8″ of lead for additional shielding. A large flux of background particles are generated in the passive collimator and some lie along the photon beam. A sequence of sweeping magnets after the collimator removes the unwanted charged particles from the photon beam.

A second collimator is located following the lead shielding wall of the first collimator. This collimator is made of stainless steel and is 20″ long and 8″ in diameter. A 1 cm hole is bored along the axis of the collimator and is designed so that the effective aperture can be adjusted to 6, 8, or 10 mm by inserting stainless steel tubes. The purpose of this collimator is to scrape off photons which were produced by small angle scattering on the bore of the primary collimator. A second sweeping magnet is mounted directly after the second collimator. The specification of the tolerance on this alignment during beam operation is a circle of radius 200 microns. The size of the beam spot on target is defined by the primary collimator. We plan to use a 5 mm diameter primary collimator in the proposed experiment.

C. Pair Spectrometer and Total Absorption Counter

The most important diagnostics for the photon beam flux are the count rates in the tagger's fixed hodoscope array and the microscope. By detecting the electrons that undergo bremsstrahlung, one determines precisely the energy spectrum of the photon beam in front of the collimators. The photon flux on the target however is only a fraction of the tagged photons because of collimation. For example, a 5 mm diameter primary collimator will pass about 30% of the photons. It is proposed to use pair production, a well understood QED process, as the basis for the relative photon flux determination. An additional calibration measurement is needed to determine the pair spectrometer's absolute efficiency. This is done with dedicated calibration runs at low beam intensity with a total absorption counter (lead glass detector) inserted in the beam after the spectrometer.

The pair spectrometer consists of a thin foil converter (1×10^{-3} radiation length thick) placed in the photon beam following the last collimator (at 0.5 m distance upstream of the front end of the pair spectrometer magnet) to generate electron/positron pairs. These are swept away from the photon beam by a strong magnetic field (1.8 T) and are subsequently detected by identical left and right arm detector packages located symmetrically on either side of beam line. The photon energy is then simply the sum of the electron and positron energies. Each detector package covers the electron or positron energy from 3 GeV to 6.25 GeV. It consists of a front detector array for fine position resolution and a back scintillating hodoscope array to provide 200 ps time resolution to form the pair production trigger.

Our proposed experiment will use the incoherent photon beam at the highest possible energy (E_γ=9–11.7 GeV). We will measure branching ratios by normalizing to the $\eta \to \gamma\gamma$ channel. The design specification for the pair spectrometer is to monitor the beam flux at $\sim$ 1% level, which exceeds our requirements.

D. Target

We propose to use the standard Hall D liquid hydrogen target with 30 cm length, corresponding to approximately 3.46% radiation lengths. Hall D is using a cryogenic target system similar to what has been developed for Hall B [137]. The upstream end of the target has an inner diameter of 5.51 cm, tapering down to 4.0 cm inner diameter on the downstream end of the target. The reason for the taper is to allow boil off gas to escape the target. The radius on the endcaps is 4 cm. The target cell is constructed from 5 mil kapton.

During the proposed experiment, target temperatures and pressures will be written into the data stream. Since significant target heating does not occur for a real photon beam, the target density can be deduced from the equation of state and the target pressure-temperature data. However, as we are measuring a branching ratio rather than an absolute cross section, we are insensitive to changes in target density.

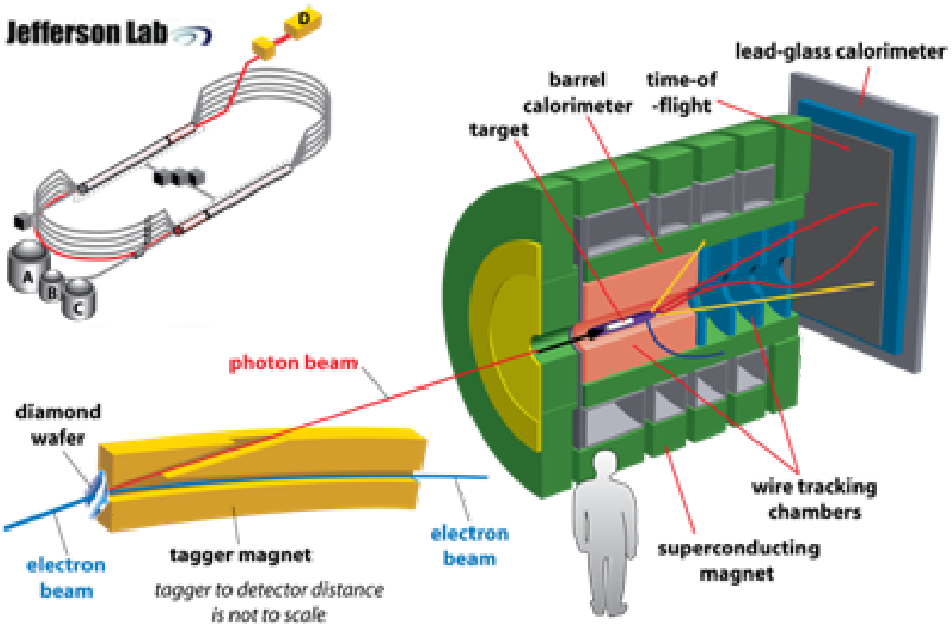

FIG. 26: The cross-sectional view of the complete original GlueX detector. The apparatus is described in detail in Section IV E.

E. The Gluex solenoidal detector

The photon beam used in this experiment will be produced in the tagger hall and travel 76 m, after which the beam will pass through a collimator. The photons then interact in a liquid hydrogen target. Outside the target, there is a scintillator-based start counter, the central drift chamber (CDC), and the lead scintillating fiber barrel calorimeter (BCAL) all inside a 2.1 T solenoid [140]. Most particles exiting the solenoid in the forward direction will strike a time of flight (TOF) wall. The complete GlueX apparatus is depicted in Figure 26.

Solenoid

The solenoid magnet creates a 2.1 T magnetic field at the center of the magnet oriented parallel to the beamline [141]. The magnet is 4.65 m long, has an inner diameter of 1.85 m, and an outer diameter of 3.76 m. The self inductance of the coil is 26.2 H hence at the nominal current of 1500 A the stored energy is 29.5 MJ.[5] The solenoid consists of 4 separate superconducting toroidal coils and cryostats and was recycled from previous experiments. It will be ready to run Fall 2014 at

[5] The maximum solenoid current is presently limited to 1350A due to concerns about quenching.

1350 A.

Central Drift Chamber (CDC)

The Central Drift Chamber (CDC) consists of 3522 1.5 m long straw tubes [143]. The straws are oriented in two directions: axial (12) and stereo (16), in order to provide better spatial resolution in the z or longitudinal coordinate. The CDC is a large cylinder surrounding the target and start counter with an inner radius of 10 cm and an outer radius of 60 cm. The expected position resolution of the CDC is 150 μm. For the nominal position for the LH_2 target, the angular coverage of the CDC is 6° to 165°.

The CDC allows us to detect recoil protons. A cut on the coplanarity of the η and recoil proton is very helpful in reducing backgrounds.

Start Counter

The start counter is a barrel hodoscope consisting of 30 scintillators surrounding the target that will be used in conjunction with the tagger to measure the beam bucket of the associated event [142]. The detector is a 40 cm long cylinder with a 16 cm cone that tapers toward the beamline on the downstream end of the target. The start counter accepts charged particles at angles between 3° and 134° over the full length of the target. The start counter is self-supporting as to not introduce additional material in the path of the particles.

The start counter will be useful in flagging the presence of extra charged particles, and will provide large pulses with good timing resolution for recoil protons.

Barrel Calorimeter (BCAL)

The barrel calorimeter (BCAL) is a lead-scintillating fiber sampling calorimeter that lines the inside of the solenoid. Each individual module consists of layers of corrugated lead sheets, interleaved with planes of 1 mm, round, Kuraray SCSF-78MJ scintillating fibres, bonded to the lead grooves using optical epoxy [144]. The complete detector consists of 48 identical wedge-shaped modules with each module occupying 7.5° of azimuthal angle. Each module is 3.9 m long and 22.46 cm thick, and once assembled into the final ring shape, the BCAL has an inner radius of 65 cm and an outer radius of 90 cm. The entire BCAL resides within the 2.1T magnetic field and will be read out by about 4,000 field-insensitive, large-area (1.44 cm^2 each) silicon photomultiplier arrays.

BCAL will be invaluable for allowing us to veto rare decay candidates with a soft π^0 that might otherwise escape our missing energy cut.

Time of Flight (TOF)

The time of flight (TOF) detector wall is an array of 2.54 cm thick and 6 cm wide scintillator paddles [145]. The paddles are read out on each end by PMTs, except in the middle where the beamline only allows single ended readout. There is a horizontally oriented wall and a vertically oriented wall to provide additional location information for a total of 92 paddles. The TOF detector covers angles of 1° to 11°, providing an overlap with the start counter of angles 3° to 11°. The primary purposes of the TOF detector are to determine charged track multiplicity, provide excellent TOF information with respect to the accelerator RF beam bucket, and to help distinguish neutral vs charged tracks.

V. UPGRADED CALORIMETER FCAL-II

A. General description

The η signal is primarily identified by reconstruction of the invariant mass,

$$M_{inv}^2 \equiv p^2 = (\Sigma E_\gamma, \Sigma \overrightarrow{P}_\gamma)^2 \tag{18}$$

from the summed 4-momenta of the decay photons detected in the forward multi-channel calorimeter. The relative error in invariant mass reconstruction is approximately given by the quadrature sum of the relative errors in energy and angle as can be surmised from the formula for reconstruction with two photons

$$M_{inv} = 2\sqrt{E_{\gamma 1} E_{\gamma 2}} \times \sin \alpha/2 \tag{19}$$

where α is the opening angle between the photons. We require percent-level resolution in shower energy reconstruction and, given a typical shower separation of 10's of cm, mm-scale resolution in calorimeter hit position to determine the angle of the photon. The calorimeter energy resolution will dominate the invariant mass resolution. The contribution from the target length is quite modest even if the vertex is unknown, but we will detect the recoil proton.

To minimize shower merging and pile-up in the calorimeter, high-granularity and fast decay time are also critical. The scintillator $PbWO_4$ has highly desirable properties for use in an electromagnetic calorimeter, including a small Molière radius (2.1 cm), short radiation length (7.4 g/cm^2), and fast decay time (20 ns). It is also highly radiation resistant and available in large quantities. Based on these features, and the extensive experience of some of us with a smaller lead tungstate calorimeter employed in the PrimEx experiment, we propose to use $PbWO_4$ crystals inserted into the central region of an upgraded Hall D Forward Calorimeter (FCAL-II).

The new central lead tungstate section of FCAL-II will basically be a larger version of the lead tungstate core of the PrimEx HyCal calorimeter. It will consist approximately of a 59 element x 59 element matrix of optically-isolated crystals each of size $2.05 \times 2.05 \times 18$ cm^3. The crystal transverse dimensions of 2.05×2.05 cm^2 are comparable to the Molière radius of lead tungstate so that shower energy sharing between adjacent crystals can be used to determine the position of the shower with mm-scale accuracy at the energies of interest. The 18 cm thickness (20 radiation lengths) has been

shown by PrimEx to be sufficient to achieve the required energy resolution. A central $\sim 12 \times 12$ cm^2 hole will be left open to enable the photon beam and small angle electromagnetic background to pass downstream.

Scintillation light from the electromagnetic shower will be detected with Hamamatsu R4125HA photomultiplier tubes coupled to the back of the crystals with optical grease. A fiber optic cable will be glued to the front face of each module for the gain monitoring system. If instrumented as in the PrimEx HyCal, there will be a HV and two signal cables for each base (one for the anode and another for the dynode). The anode signals will each go to a flash ADC as discussed below. The dynode signals will be summed first in groups, and then groups will be summed to form a total calorimeter energy signal for use in the trigger and to provide a hardware timing reference. Alternatively, the trigger can be built from the Flash ADC data pipeline.

An exciting development in JLab's 12 GeV era is the standardization of most new detector readout systems to flash ADCs. By keeping the cost per channel to less than $300 (and the loaded cost per channel including VME crate, CPU, etc. to less than $400), a single channel of 12 bit, 250 MHz flash ADC (plus fairly cheap memory and processing power) can substitute for an older non-flash ADC, a TDC, and two delay lines. This saves money, space, procurement time, and labor. Sampling is continuous and deadtimeless. When a shower occurs, the 4 nsec samples will be recorded so that the pedestal (zero offset), the energy, and the time can be determined offline. Tests indicate the time resolution is significantly better than 1 nsec[146]. This will allow us to constrain all photons in the event to the same beam burst and so minimize accidental coincidences. Flash ADCs are not merely cost-effective substitutes for older technology, they have been used in rare decay experiments for decades because they allow one to sensitively flag pile-up and even scrutinize interesting events individually when desired. The combination of $PbWO_4$ crystals and a flash ADC on each channel will make FCAL-II truly a cutting edge calorimeter for the 21st century.

Several institutions on this proposal are also major players in the PrimEx collaboration and were heavily involved in the design and construction of the state-of-the-art, high-resolution, $PbWO_4$ crystal and Pb glass Hybrid Calorimeter (HyCal). That detector was used in both the PrimEx-I and PrimEx-II runs. Their experience will be very important for successfully realizing FCAL-II in Hall D. In Appendix section D, we will discuss the performance of the $PbWO_4$ calorimeter in the PrimEx-I and PrimEx-II experiments. The pile-up and photon merging in a cluster reconstruction

algorithm are described there as well.

B. Trigger and Data Acquisition

We will use the standard Hall D trigger and data acquisition system. The trigger will be based on a measurement of the total energy deposition in the FCAL-II calorimeter; events with the total energy less than a threshold value will be rejected.

The trigger rate as a function of the total energy threshold was studied using a Geant detector simulation. Two types of processes were considered: hadronic interactions plus the background originating from the pileup of electromagnetic interactions in the same 100 ns window. The expected trigger rates from hadronic and electromagnetic interactions for a conservative energy threshold of 5 GeV are estimated to be about 1 kHz and 2.5 kHz, respectively. This energy threshold provides 100% trigger efficiency for the signal decays under study produced at beam energies of at least 8 GeV.

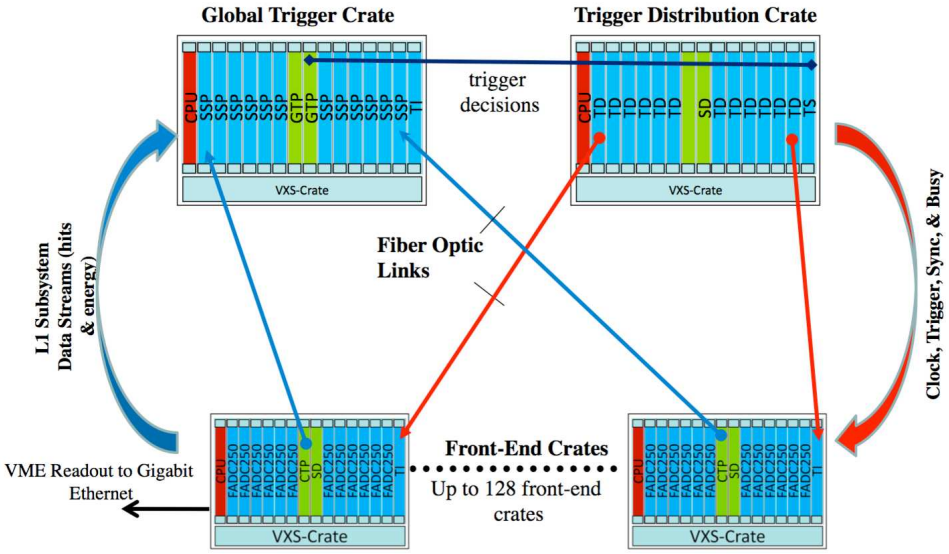

FIG. 27: Schematic of the integrated triggering and DAQ system. Fiber optics continuously stream digitized energy sum information from the CTP (crate trigger processor) module in the front-end crate to the SSP (subsystem processor module) in the Global trigger crate. Trigger decisions can then be made based on total energy sums in FCAL-II.

The GlueX trigger and DAQ architecture is shown in Fig. 27. The trigger logic is imple-

mented on special purpose programmable electronics boards developed at Jefferson Lab with Field-Programmable Gate Array (FPGA) chips. The electronics is based on pipelined FADC-250 boards running at a 250 MHz clock. The data from the front end calorimeter electronics is digitized and stored in the FADC-250 pipeline waiting for the readout. At the same time, energies from the 16 FADC-250 channels will be summed and forwarded to the Crate Trigger Processors (CTP) board positioned in the switch slot of the VXS crate. The CTP sums energies from all FADCs in the crate and sends the information via optical links to the Sub-System Processors (SSP). The SSP subsequently sums energies from all crates. The Global Trigger Processor (GTP) will make the trigger decision based on the total energy. When the trigger is issued, notification will be sent to the Trigger Interface board of each crate to initiate the event readout.

The algorithm running on the FADC-250 FPGA allows one to determine the time of a hit in the calorimeter with an accuracy of better than 1 ns by 'fitting' the leading edge of the electronics pulse. The readout information of each hit is coded in two 4 byte words representing the time and the energy integral. For the expected hit multiplicity, the event size is about 0.2 kByte and the data rate is about 800 kByte/sec. As the trigger rate is relatively small, the possibility exists to read out the FADC in the so-called Pulse Integral mode, i.e., read out digitized amplitudes for several FADC 4 ns time stamps around the signal pulse threshold crossing. The mode can allow one to analyze pulses offline. As an example, reading out FADC pulse amplitudes in an 80 ns time window will require 40 bytes of data resulting in a 2 kByte calorimeter event size and a total data rate of 8 MByte/sec. The trigger and the data rates can be handled by the electronics and the DAQ system. Data readout will be performed using the JLab CODA system.

C. FCAL-II Acceptance and High-Level Reconstruction

η rare decay events will be reconstructed from FCAL-II information, normalizing to $\eta \to \gamma\gamma$ decays measured simultaneously. Since our goal is to measure the branching ratios, knowledge of the absolute luminosity is not as important as in the PrimEx-eta program where the absolute decay width for $\eta \to \gamma\gamma$ will be determined. Our priorities are isolation of the signal with high efficiency while minimizing the background, specifically, optimizing the figure of merit $N_\eta \times Acceptance/\sqrt{N_{bkg}}$. To achieve this goal, one needs (1) the geometrical acceptance for each η decay channel under study,

(2) effective cut parameters and their resolutions.[6]

1. Calorimeter Geometrical Acceptance

One of the backgrounds for rare decays of the type $\eta \rightarrow$ "4γ" comes from the merging of showers in the calorimeter from $\eta \rightarrow 3\pi^0$. For fixed calorimeter size, as the distance between the target and calorimeter is varied, there is a trade-off between signal and this background. To check that FCAL is at an appropriate distance for a rare η decay to neutrals program, we examined the figure-of-merit (FOM) $FOM \equiv S/\sqrt{B}$ where S is the number of $\eta \rightarrow \pi^0 2\gamma$ signal events detected in the high resolution central region, and B is the number of background events from $\eta \rightarrow 3\pi^0$ within a $\pm 3\sigma$ window around the η invariant mass. Figure 28 shows that this FOM has a broad maximum near the standard distance of 5.6m, so our requirements are compatible with the standard FCAL distance.[7]

Channel	**PWO Acceptance**	**FCAL-II Acceptance**
$\eta \rightarrow$ "2γ"	43.9%	80.9%
$\eta \rightarrow$ "3γ"	28.7%	72.9%
$\eta \rightarrow$ "4γ"	18.4%	64.9%
$\eta \rightarrow$ "5γ"	12.8%	58.9%
$\eta \rightarrow$ "6γ"	7.3%	52.1%

TABLE VI: Summary of geometrical acceptances for the central high resolution region and entire FCAL-II for η decays. All calculations for photon beam energies of 9-11.7 GeV.

Eta decays to 2-6 photon final states were then simulated as a function of tagged photon beam energy for the PWO region only and for the entire FCAL-II. The result for $\eta \rightarrow$ "4γ" is shown in Figure 29. All results are summarized in Table VI. The average acceptance is 18% for 4γ for the high resolution central region but 65% for the entire FCAL-II. The geometrical acceptance decreases with increasing number of photons in the final state since there are more opportunities

[6] For this discussion, we will assume the signal is extracted from a series of cuts rather than a single cut on a likelihood parameter. No kinematic fitting has been assumed.

[7] Some of our early simulations were done at a distance of 6m. The FOM is essentially the same.

to lose a photon around the outer edges of the high resolution central region of the calorimeter. (Photon losses down the beam hole are quantitatively less important.)

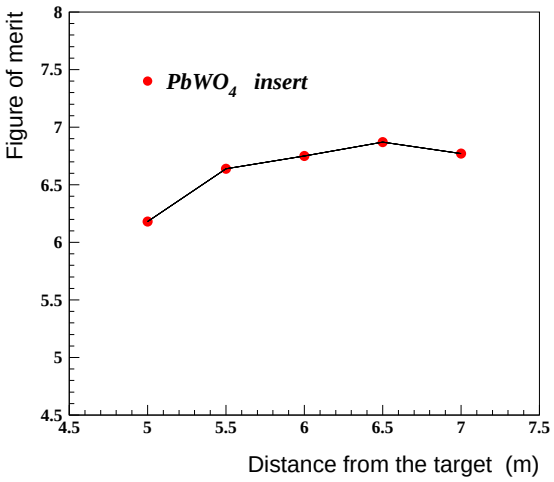

FIG. 28: The figure-of-merit $S/\sqrt{B}$ *versus* the distance between target and FCAL-II, where S is the accepted $\pi^0 2\gamma$ signal in the high resolution central region, and B is the background from shower merging from $\eta \to 3\pi^0$ which has a branching ratio 3 orders of magnitude larger. There is a broad plateau near the existing FCAL distance of 5.6m.

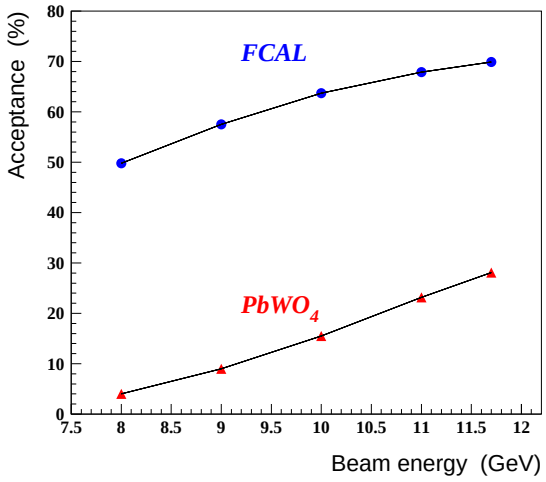

FIG. 29: The geometrical acceptance for the 4γ states ($\eta \to \pi^0 2\gamma$, etc.) *versus* the beam energy.

2. Calorimeter Resolutions in Missing Energy and Invariant Mass

There are two major calorimeter variables for the selection of η decay events. The first is the missing energy the resolution of which depends on the calorimeter energy resolution and, to a lesser extent, the tagger energy resolution. The second variable is the particle's invariant mass reconstructed from the decay of 2 or more photons. For both variables, energy resolution is important, but for the invariant mass the angle resolution is also critical. The photon angle is determined by the hit position on the calorimeter and the target position.

Simulations were performed for the high resolution $PbWO_4$ central region. Figure 30 shows the resolution in elasticity (the ratio of total energy deposited in FCAL-II to the tagged photon beam energy) for fully contained $\eta \to \pi^0 2\gamma$ decays. Resolutions for 2γ and 3γ final states are similar. (The peak elasticity is slightly less than 1 due to the missing energy carried away by the proton recoil.) Assuming a typical photon energy of 10 GeV, the elasticity resolution of 1.2% corresponds to a missing energy sensitivity of 120 MeV. This cut virtually ensures the forward neutral meson production was exclusive, suppressing feed-down from higher invariant masses with lost decay products. It is barely possible for a very soft additional π^0 to slip past this cut, but that could be vetoed using BCAL.

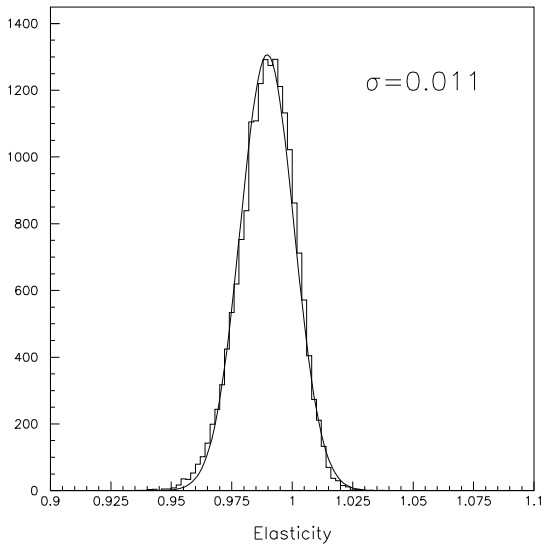

FIG. 30: Elasticity for $\eta \to \pi^0\gamma\gamma$. The resolutions for $\eta \to 2\gamma$ and $\eta \to 3\gamma$ are similar, 1.3% and 1.2%, respectively.

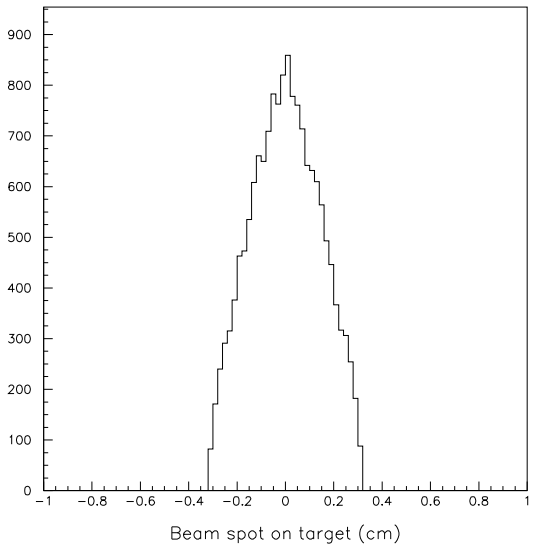

FIG. 31: The x (transverse) distribution of the interaction vertices in the target for a 5 mm diameter primary collimator. The beam spot size of less than 0.2cm (rms) makes a small contribution to the invariant mass resolution which is dominated by the calorimeter energy resolution.

In order to simulate the invariant mass resolutions, we have taken into account the beam spot size with a 5 mm diameter primary collimator, a 30 cm thick LH_2 target, 6 m distance between the FCAL-II and the target, and a photon beam in the energy range of 9-11.7 GeV. The size of the beam spot is directly correlated with the size of the primary collimator in the beam line. For illustration, Figure 31 shows the beam spot x (transverse) projection on the target for a 5 mm

diameter primary collimator.

The reconstructed η invariant mass resolution for the $\eta \to \pi^0\gamma\gamma$ reactions is shown in Figure 32. Resolutions for 2γ and 3γ final states are similar. Despite the high photon energy, the average rms resolution of 11 MeV is only 2% of the η mass. This is our most important cut variable to select η decay signals while suppressing continuum backgrounds. It will also be used to identify π^0's, ϕ's, etc., for calibration. Figure 33 shows that the invariant mass resolution of the π^0 from the $\eta \to \pi^0\gamma\gamma$ reaction is 3.8 MeV. This excellent π^0 resolution will help reduce combinatoric backgrounds. We note that the resolution can be improved an additional 35% using kinematical fits [150][151].

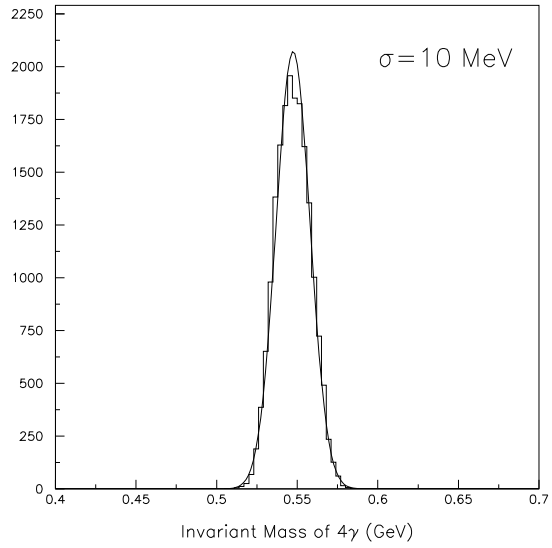

FIG. 32: Reconstructed four-photon invariant mass $M_{4\gamma}$ from the $\eta \to \pi^0\gamma\gamma$ reaction for the central high resolution section of FCAL-II. The resolution for 2γ and 3γ final states is similar, 12 MeV and 11 MeV, respectively.

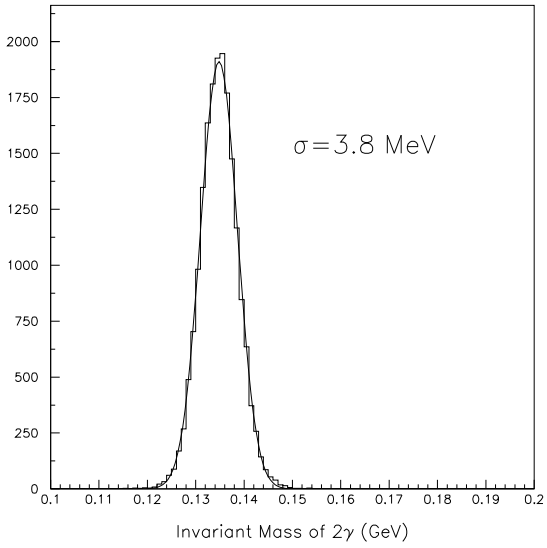

FIG. 33: Reconstructed two-photon invariant mass $M_{2\gamma}$ of the π^0 from the $\eta \to \pi^0\gamma\gamma$ reaction detected in the central high resolution section of FCAL-II. This excellent resolution will be useful for reducing combinatoric backgrounds.

3. Basic event selection for neutral decays

Event selection begins at the trigger level. Figure 34 shows the distribution of the energy deposited in FCAL-II from proton-tagged $\eta \to \pi^0\gamma\gamma$. Figure 35 shows the total energy spectrum in FCAL-II for one of the major inelastic reactions, $\gamma p \to \eta\pi^0 p$. As one can see from these two figures, an

FCAL-II threshold of about 8 GeV would safely select all signal events of interest while suppressing triggers from inclusive η production.

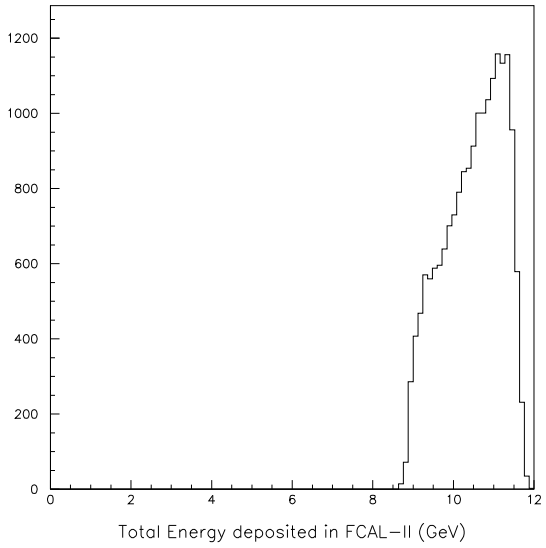

FIG. 34: Reconstructed total energy deposited in FCAL-II by $\eta \to \pi^0\gamma\gamma$. Nearly all events of interest deposit more than 8.5 GeV in the calorimeter. This energy threshold is simply explained by the minimum photon beam energy of 9 GeV less the sum of the η mass and proton recoil energy.

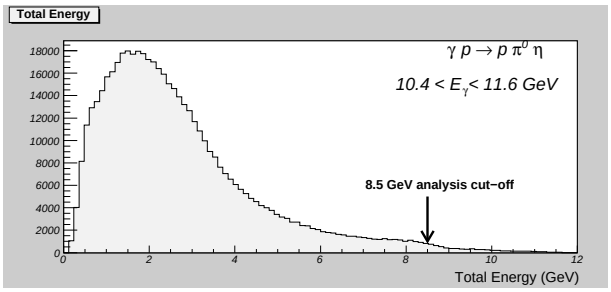

FIG. 35: Total energy deposited in FCAL-II by inelastic η production through the $\gamma p \to \eta\pi^0 p$ reaction.

In the off-line analysis, we will apply the following basic event selection criteria for tagged photon energies of 9-11.7 GeV: (0) single hit in the tagger for 9-11.7 GeV; (1) fiducial volume of FCAL-II for full shower containment (i.e., excluding the inner and outermost layers of crystals); (2) every shower in a candidate neutral meson must have good coincidence time with the hit tagger paddle (out of time showers must be dropped and the total energy recalculated); (3) there should be no significant missing energy (4) the invariant mass reconstructed must be consistent with the η mass.

Once an η has passed the above cuts, the detection of the recoil proton is in principle redundant. However, simulations have shown it will help reduce background to over-determine the kinematics, thus: (5) there must be a single recoil proton, and (6) the recoil proton and η must be co-planar.

The recoil protons of interest have polar angles of 55-78 degrees, with momenta of 0.3-1.4 GeV/c. (See Figure 36.) Tracking is not possible for recoil protons from the smallest angle η's because

those protons either range out before reaching the CDC or don't produce enough hits in the CDC for reconstruction. From Figure 37, one sees the tracking efficiency is currently about 70% for recoil proton momenta above 0.325 GeV/c (T_p = 55 MeV). We assume most of these events are recoverable. Reconstruction efficiency has dropped by about half at 0.275 GeV/c (T_p = 39 MeV) which is reasonably well understood in terms of the thickness of target and detector materials: the range of a 39 MeV proton is about 1.3 g/cm^2 of CH_2-equivalent.

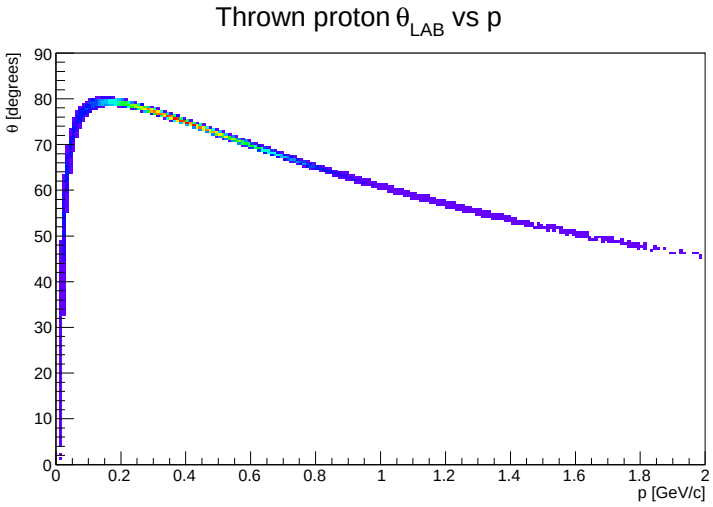

FIG. 36: Monte Carlo simulation of generated $\gamma + p \rightarrow \eta + p$ events showing the two-body kinematic relationship between proton angle and momentum.

In Figure 38 the η mass is reconstructed with roughly 100 MeV resolution from the proton recoil alone. Although this is by no means a clean η tag for rare decay studies, it will distinguish between π^0 and η production in the majority of cases reducing background in the final analysis. However, the more powerful proton cut variable appears to be on coplananarity (i.e., the difference of the azimuthal angles of the η and the proton). (See Figure 23.)

D. Major New Experimental Equipment (Cost, Manpower and Financial Resources, and Commitments)

Besides the Hall D base equipment, this proposal requires a major upgrade of the current FCAL to include high-resolution, high-granularity $PbWO_4$ crystals. An option which would preserve the large acceptance needed for the GlueX spectroscopy program, allow it to benefit from the better

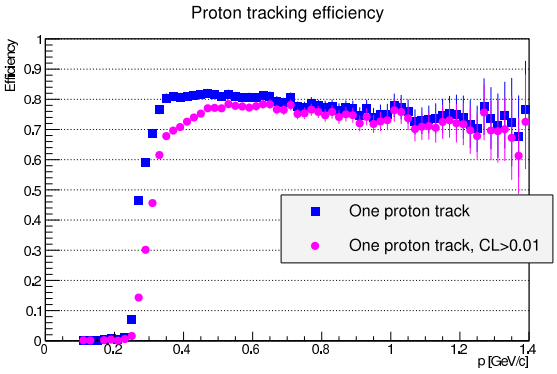

FIG. 37: The energy threshold for track reconstruction with recoil protons. Above 0.325 GeV/c, the inefficiency arises from finding more than one track. Such events are presumed recoverable.

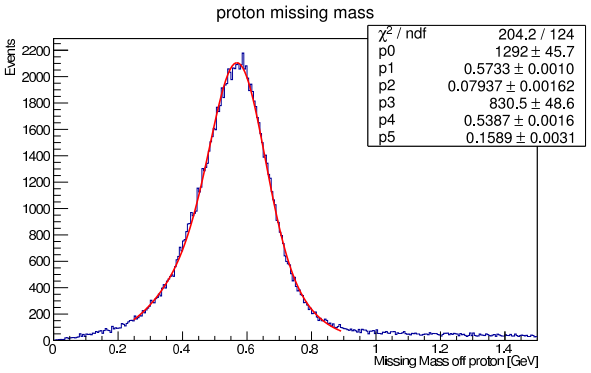

FIG. 38: Reconstructed missing mass using the recoil proton from the $\gamma p \to \eta p$ reaction.

properties of lead tungstate, and minimize overhead in configuration changes, is to insert the 118 × 118 cm^2 $PbWO_4$ crystals into the present Pb glass FCAL. This would make it a hybrid calorimeter, similar to a larger version of the state-of-art, high-resolution PrimEx calorimeter (HyCal) used in Hall B. Several institutions on this proposal were major players in the design and construction of HyCal and would play a leading role in developing the future FCAL-II. Previously, we successfully obtained the resources necessary to develop and construct HyCal from the NSF Major Research Instrumentation (MRI) program while establishing collaborations with Chinese institutions. The same strategy would be applied to the FCAL-II development.

The estimated total cost for 3445 $PbWO_4$ modules, including the crystal, PMT/base, flash ADC and HV is \$2.7M-\$4.6M depending on the assumptions for recycling existing equipment. (See "Response to PAC39 Issues and Recommendations" for details. [1]) Prof. X. Chen, a co-spokesperson on this proposal, will lead several Chinese institutes in applying for funds (\$0.5M-\$1.0M) from the Chinese National Science Foundation to cover the cost of the crystals. Prof. L. Gan (spokesperson of this proposal) will lead the US institutes in applying for a Major Research Instrumentation program (MRI) grant from the National Science Foundation (\$1.0M-\$3.5M) to cover the cost of PMT's, bases, possibly the Flash ADCs, plus small ancillary detectors. Three other co-spokespersons are JLab staff members and will help coordinate design and construction.

Since the new calorimeter would be incorporated into Hall D base equipment we would like the power supplies, cabling, possibly the Flash ADCs, and other readout support to come from JLab.

It is likely we will need design and engineering support for additional small detectors (e.g., cosmic tag, beam hole tag, etc.), as well as support from the Physics Division electronics group in designing low power PMT bases.

This experiment has the potential to add significant new manpower to the Hall-D effort, in particular from groups that have historically had little activity at Jefferson Lab. During the detector development and construction period, the Chinese team will be responsible for procuring and testing the $PbWO_4$ crystals. The US team will be responsible for the procuring and testing of the electronics. Several local universities near Jlab will play a major role in the detector assembly and testing.

VI. η PRODUCTION RATE, PROJECTED SENSITIVITIES, AND BEAM REQUEST

JEF's measurement sensitivities depend on the number of forward η's, the calorimeter acceptance, the efficiency including cuts, and the background. We address these in the following subsections.

A. Forward η production rates by $\gamma + p \rightarrow \eta + p$

For the electron beam current, radiator thickness, and energy range given in our reference design in Table V, the tagger rate is 1.6×10^8 Hz. Transporting all photons in vacuum, and using a 5 mm diameter primary collimator, $\sim 30\%$ of the γ's will reach the physics target for a tagged γ rate on target of 5×10^7 Hz.

The Hall D LH_2 target is 30 cm thick, or $1.28 \times 10^{24} protons/cm^2$. From reference [149], the average total cross section for $\gamma p \rightarrow \eta p$ in the 9 to 11.7 GeV photon energy range is ~ 70 nb. About 25% of these η's are produced at too small an angle to allow a proton tag. The total rate of $\eta(548)$ produced by forward $\gamma + p \rightarrow \eta + p$ with 75% proton detection is therefore:

$$N_\eta = N_\gamma \cdot N_p \cdot \sigma \cdot \epsilon = 3.4 Hz \;\; (2.9 \times 10^7 / 100 \; days). \tag{20}$$

Anticipating the FCAL-II channel-dependent acceptance results from the next section, the number of *effective* forward η's (proton-tagged $N_\eta \times Acceptance$) will be O(10^7) per year of JLab accelerator operations, several times the effective production rate of KLOE-I which employed $\phi \rightarrow \eta + \gamma$. This is the basis for our calling Hall D with FCAL-II an "η factory". [8]

B. channel rates and experiment sensitivities

Table VII estimates the number of events in 100 days. Some comments:

- The PDG branching ratio for the rare decay $\eta \rightarrow \pi^0 2\gamma$ is an average of several widely inconsistent measurements.
- The photon acceptance for the rare decay $\eta \rightarrow \pi^0 2\gamma$ is only for the $PbWO_4$ central region of FCAL-II and drops rapidly with decreasing photon beam energy. The number of rare decay

[8] Production rates for the $\eta'(958)$ are about 2/3 as large.[114] Our η' production rate is competitive with BES-III.

TABLE VII: For the JEF beam request of 100 days of production, total events expected for 9-11.7 GeV photon beam energy for the SM allowed channels of interest based on PDG branching ratios and the proton-tagged η rate from equation 20. Rare decays use only the high resolution PWO acceptance, while non-rare decays use the entire FCAL-II acceptance. (The values in parenthesis are for the GlueX photon energy bite of 8.4-9 GeV with the same tagged photon rate on target. The lower GlueX energy provides a higher forward cross section of 92 nb but with greatly reduced acceptance in the PWO region due to the smaller boost.)

Channel	**BR**	**Photon Acceptance**	**Tracking Effi.**	**Events per 100 days**
rare decay:				
$\eta \to \pi^0 2\gamma$	2.7×10^{-4}	0.184	—	1.4×10^3
		(0.07)		(0.72×10^3)
non-rare decays:				
$\eta \to 3\pi^0$	32.7%	0.542	—	5.1×10^6
		(0.470)		(5.9×10^6)
$\eta \to \pi^+\pi^-\pi^0$	22.9%	0.786	0.9	4.7×10^6
		(0.745)		(5.9×10^6)
$\eta \to 2\gamma$	39.4%	0.809	—	9.2×10^6
for normalization		(0.7)		(10.5×10^6)

events under JEF running conditions is more than twice that with GlueX running conditions, which motivates our beam request.

- The photon acceptance for the non-rare decays $\eta \to 3\pi$ uses the entire FCAL-II and is less sensitive to a decrease in photon beam energy during GlueX-IV running. The number of 3π events under JEF running conditions is roughly 20% less than with GlueX-IV running conditions.

- We will use $\eta \to \gamma\gamma$ decays for normalization (BR $= 39.43 \pm 0.26\%$ [8]). The statistical error will be about 0.3% per day.

1. Sensitivity of our Standard Model $\eta \to \pi^0 2\gamma$ measurement

The relative statistical error for the $\eta \to \pi^0 2\gamma$ signal including background fluctuations is

$$\frac{\Delta S}{S} = \frac{\sqrt{N_s + N_b}}{N_s} = \frac{1}{\sqrt{N_s}}\sqrt{1 + N_b/N_s} \tag{21}$$

where N_s is the number of signal events and N_b is the number of background events in the η invariant mass window after all cuts. Because setting $N_b = 0$ recovers the familiar expression $\Delta S/S = 1/\sqrt{N_s}$, the term $\sqrt{1 + N_b/N_s}$ can be considered the error magnification from the background. The figure of merit in this case, taken as the inverse error squared, is not N_s but rather $N_s/(1 + N_b/N_s)$. If backgrounds are large, as is the case in all previous measurements of this channel, one cannot characterize the quality of an experiment in terms of signal events alone.

In Table VII, we estimate we will acquire 1,440 doubly radiative η decay events in 100 days of proposed JEF running with an estimated Signal/Background ratio of 3:1. (See Figure 22 for results from our simulation and cuts study.) With this many events our statistical error on the $\eta \to \pi^0 2\gamma$ branching ratio, will be

$$\frac{\Delta S}{S} = \frac{1}{\sqrt{1,440}}\sqrt{1 + 1/3} = 3.0\% \tag{22}$$

with little error magnification from background. This is 3x smaller than the 9% statistics-dominated error from the recent MAMI result, mainly due to error magnification from their large backgrounds. [84]. To match JEF's projected figure of merit, a new MAMI experiment would have to increase the statistics they accumulated in 2007+2009 by an order of magnitude. (Even then, systematic errors from the large background subtraction would remain.)

Allowing for few percent relative acceptance uncertainties between $\eta \to \pi^0 2\gamma$ and the $\eta \to 2\gamma$ normalization channel, we project a final total error for the BR of about 4%. Anticipating that the dominant systematic uncertainty on the decay width for $\eta \to \pi^0 2\gamma$ comes from the absolute decay width of $\eta \to 2\gamma$, we project an uncertainty for the decay width of about 5%. [9] This 5% projection is plotted along with previous results for the $\eta \to \pi^0 2\gamma$ decay width in Figure 11.

As for the differential decay width, $d\Gamma/dM_{2\gamma}$, our average statistical error on each of 7 bins would be 7.9% (or 8.6% including the systematic error from normalization). This is typically over a

[9] The approved PrimEx Eta measurement, PR12-10-011, will reduce the error on $\Gamma_{\eta\to 2\gamma}$ to 3.2%.

factor of x2 smaller than the black error bars in Figure 12. Such precision is needed to search for dynamical details that go beyond VMD, as can also be seen comparing our projected error bars to theory curves in Figures 2 and 10. To summarize in the language of the older but simpler plot in Figure 2, the projected uncertainties would allow one to determine whether the expected amplitudes interfere constructively or destructively. There would certainly no longer be any question of factor of 2 ambiguities in the BR for this channel.

2. Sensitivity for leptophobic dark B boson search

$\eta \to \gamma + B(\to \gamma + \pi^0)$

To study the experimental reach for B-boson search, η's were simulated using the standard JEF configuration listed in Table V. Four photons from each η decay were detected by the forward calorimeter (FCAL-II). We required at least two out of four photons to hit the central $PbWO_4$ region. The reconstructed $\pi^0\gamma$ invariant mass resolution $\sigma(m_B)$ as a function of m_B is shown in Fig. 40.

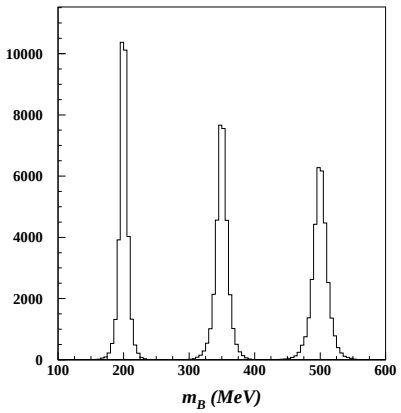

FIG. 39: The $M_{\gamma\pi^0}$ mass reconstruction for B-boson mass m_B at 200 MeV, 350 MeV, and 500 MeV.

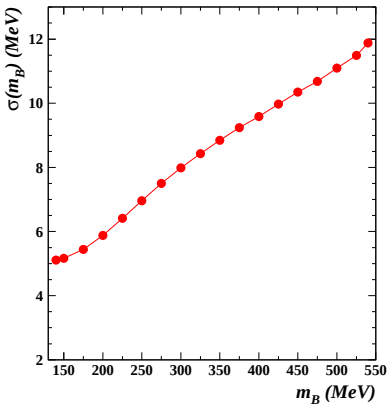

FIG. 40: The reconstructed B-boson mass resolution $M_{\gamma\pi^0}$ as a function of the generated B mass.

To quantify statistical sensitivity, we assume that the continuum background in the resonance search can be modeled by a smoothly varying function and subtracted. Exclusion power is then determined by the ratio of the potential signal within an invariant mass window to $\sqrt{N_{bin}}$, where

N_{bin} is the total background statistics in the same window. An invariant mass window is centered at m_B with a width of $\delta m_B = 2.5\sigma(m_B)$.

The statistics of signal and background in a $\pi^0\gamma$ invariant mass window δm_B are calculated by:

$$S = N_\eta \cdot \varepsilon_\eta \cdot BR(\eta \to B\gamma) \cdot BR(B \to \pi^0\gamma) \cdot \xi_s \tag{23}$$

$$N_{bin} = N_\eta \cdot \varepsilon_\eta \cdot BR(\eta \to \pi^0\gamma\gamma) \cdot \xi_b, \tag{24}$$

where N_η is total number of η's anticipated in the experiment; $\varepsilon_\eta \sim 75\%$ is the η tagging efficiency by measuring the recoil proton; $BR(\eta \to B\gamma)$, $BR(B \to \pi^0\gamma)$, and $BR(\eta \to \pi^0\gamma\gamma)$ are the branching ratios for the corresponding decays. The ξ_s is a fraction of signal events ($\eta \to B\gamma \to \pi^0\gamma\gamma$) that have a reconstructed $\pi^0\gamma$ invariant mass within the signal window and ξ_b is the fraction of background events($\eta \to \pi^0\gamma\gamma$) that have a reconstructed $\pi^0\gamma$ invariant mass within the same window. The ξ_s and ξ_b are calculated with Monte Carlo data samples and shown in Fig. 41, the detector acceptance and efficiency being taken into account. The kinematic distribution of $\eta \to \pi^0\gamma\gamma$ is based on the phase space. In addition, both combinations of reconstructed $\pi^0\gamma$ pair from the final state are included in this calculation. For certain values of m_B, one can do better than this by only taking the higher or lower energy single photon to reconstruct B. For example, for a large B mass ($m_B \sim 500$ MeV), the single photon from B decay will have a higher energy than the other single photon not from B; while for a small B mass ($m_B \sim 200$ MeV), the signal photon from B decay will have lower energy compared to the other single photon not from B . Therefore, one may further reduce the background fraction ξ_b at both low and high ends of the m_B range.

The sensitivity is calculated by:

$$\frac{S}{\sqrt{N_{bin}}} = \sqrt{N_\eta \cdot \varepsilon_\eta} \cdot \frac{BR(\eta \to B\gamma) \cdot BR(B \to \pi^0\gamma)}{\sqrt{BR(\eta \to \pi^0\gamma\gamma)}} \cdot \frac{\xi_s}{\sqrt{\xi_b}} \tag{25}$$

Events from multi-photon final states other than $\eta \to \pi^0\gamma\gamma$ can leak into the signal region. We estimate the level of this background to be $\sim 20\%$ relative to $\eta \to \pi^0\gamma\gamma$. (See Figure 22.) Addition of this background changes the experimental reach for α_B by about 10%, which is not visible in Fig. 8.

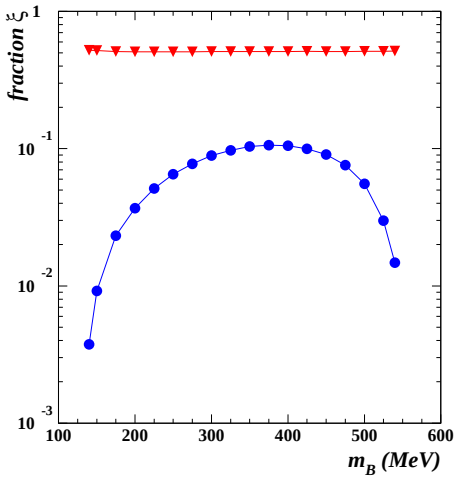

FIG. 41: The red triangles are the fraction of signal events ($\eta \to B\gamma \to \pi^0\gamma\gamma$) that have a reconstructed $\pi^0\gamma$ invariant mass within the signal window. The blue dots are the fraction of background ($\eta \to \pi^0\gamma\gamma$) events that have a reconstructed $\pi^0\gamma$ invariant mass within the same window.

3. Sensitivity for quark mass ratio determination in $\eta \to 3\pi$

In order to study the acceptance for the "charged" channel, 100,000 $\eta \to \pi^+\pi^-\pi^0$ events were generated with a Regge-based model[149] for the η production cross section using the JEF running conditions. The η decayed via three-body phase space. All of the final state particles, including the recoil proton, were reconstructed and a kinematic fit was applied to the full event. The product of $acceptance \times efficiency$ over the Dalitz plot variables X and Y was calculated. Since the experimental distributions must be corrected for $acceptance \times efficiency$, flatter distributions imply smaller experimental systematic errors. The anticipated JEF distributions for the charged 3π channel are quite flat until large positive Y is reached (at which point most of the energy in the CM system is in the π^0, leaving the $\pi^+\pi^-$ pair with small relative energy).

A similar study was performed for the $3\pi^0$ channel. The efficiency for the Dalitz Z distribution is shown in Figure 42. JEF's flatter acceptance in Z should help us control systematic errors. Since the slope (or α parameter) is only about -3%, the bin-dependent $acceptance \times efficiency$ correction of 20% made by KLOE was quite significant.

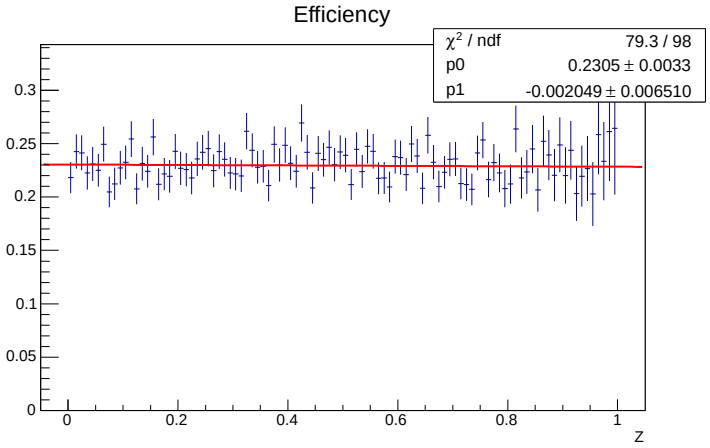

FIG. 42: For the $\eta \to 3\pi^0$ channel: Our projected $acceptance \times efficiency$ versus Z distribution is flat to better than 3 percent. (This simulation using GlueX reconstruction code includes the geometrical acceptance for FCAL, the 75% efficiency for getting a proton out of the target, and 75% for finding a single track. Our yield estimates in Table VII do not include the latter because we believe the "two tracks found" events are recoverable.)

The $\eta \to 3\pi$ acceptances from this study were used to calculate the event yields in Table VII. The world's largest $\eta \to 3\pi$ datasets were summarized in Table II. We anticipate being able to significantly reduce the statistical errors on the charged and neutral 3π channel Dalitz plot parameters.

4. Sensitivity for $\eta \to 3\gamma$ BR upper limit

Our Pythia analysis of the "3γ" background is in progress, but we can make inferences from a previous experiment. The dominant background in the Crystal Ball experiment at BNL [38] was continuum $2\pi^0$ production yielding an apparent "3γ" final state. As we have discussed, the missing energy cut in JEF will remove the majority of events which have truly lost a photon, hence we make an estimate assuming our dominant background arises from all 4-photon sources with $M_{4\gamma} = M_\eta$ followed by the merging of two showers.

From Figure 22, the entire Signal + Background of the "4γ" source term is $4/3 \times 1,440 = 1,920$ events in 100 days. The geometrical probability of two photons hitting the PWO and merging, assuming uniform illumination, is approximately $6cm \times 6cm/(118cm \times 118cm) = 0.26\%$. With 4

photons, there are 6 opportunities to merge showers, so the probability of at least one pair merging is 1.6%. This gives a "3γ" background estimate from shower merging of 1.6%*1,920 events = 31 events in 100 days.[10]

Several other backgrounds were considered, but can be completely excluded with efficient cuts: One such potential background is from photon splitting of $\eta \to 2\gamma$. (Photon splitting is where a shower is initiated by a single photon but reconstructs as a close pair.) This is easily dealt with by rejecting $\eta \to 3\gamma$ candidates with close showers. Another potential background is an $\eta \to 2\gamma$ event in random coincidence with electromagnetic background. Most of these events will consist of a low energy photon near the beam hole, and can be easily cut for example by rejecting all candidates where two of the three photons reconstruct to the η mass. Finally, there is a continuum 3γ background from the tails of the ρ or ω resonances extending down to the η invariant mass: $V \to P\gamma$ where P is either the η or π^0, followed by $P \to 2\gamma$. Such background can be suppressed simply by rejecting candidates with a photon pair that reconstructs to the η or π^0 mass.

To estimate our sensitivity as a BR upper limit, we furthermore assume the effective number of η's is reduced 75% by the above cuts, giving

$$BR(\eta \to 3\gamma) \leq 2 \times \frac{\sqrt{N_{bkg}}}{N_\eta * Acceptance} = 2 \times \frac{\sqrt{31}}{3 \times 10^7 \times 75\% \times 0.3} = 1.6 \times 10^{-6} \qquad (26)$$

which would be an order of magnitude better than the existing best result, 1.6x10^{-5}.

5. Opportunistic physics

The P violating and C conserving decay $\eta \to 2\pi^0$

The current experimental limit of 3.5×10^{-4} for the branching ratio for $\eta \to 2\pi^0$ was set by the GAMS-4π collaboration.[117] (For some other results, see references [115] and [113].) The limit on the *charged* channel $\eta \to \pi^+\pi^-$ from KLOE, 1.3×10^{-5} [118], is currently the best result for any $\pi\pi$ decay branch but is somewhat higher than our projection for $2\pi^0$. Accounting for identical particles in the neutral channel, this would imply an upper limit of 6.5×10^{-6} for $\eta \to 2\pi^0$. Our direct measurement of $\eta \to 2\pi^0$ will improve on this implied limit by about 25%.

[10] A more careful combinatoric analysis would reject events containing a π^0, reducing the background further.

TABLE VIII: Beam time request.

LH_2 production	100 days
Empty target and target-out runs	7 days
Tagger efficiency, TAC runs	3 days
FCAL-II commissioning, calibration, and checkout	12 days
Luminosity optimization (pile-up, accidentals studies)	8 days
Total	130 days

The acceptance of the P and CP forbidden $\eta \to 2\pi^0$ is $\sim 20\%$. The rare decay $\pi^0 2\gamma$ is now a background in the 4γ final state but is suppressed by cutting all events that are not consistent with two π^0's. At that point the remaining background will be dominated by the $2\pi^0$ continuum. According to our simulation, the background fraction f_{bkg} in our η invariant mass signal window is $\sim 4 \times 10^{-5}$. The estimated BR upper limit will be:

$$BR(\eta \to 2\pi^0) \leq 2 \times \sqrt{\frac{f_{bkg}}{N_\eta * Acceptance}} = 2 \times \sqrt{\frac{4 \times 10^{-5}}{3 \times 10^7 \times 0.2}} \sim 5 \times 10^{-6} \tag{27}$$

This is more than 1.5 orders of magnitude better than the existing upper limit for the neutral channel $\eta \to 2\pi^0$, bringing the sensitivity in this channel down to the level of the KLOE $\eta \to \pi^+\pi^-$ result. The results were summarized in Figure 17.

C. Beam Time Request

We request 100 days of beam time on the LH_2 target for the rare decay program, plus time for commissioning and overhead as outlined below. (GlueX running conditions have much lower figure of merit for our rare decay channels.) This will provide sufficient statistics on $\eta \to \pi^0\gamma\gamma$ events to precisely study the Dalitz plot of the 2γ invariant mass, as well as sensitively search for a leptophobic boson that couples to baryon number. In addition, we'll improve the upper limit on several SM forbidden channels by 1-1.5 orders of magnitude depending on the channel.

A summary of the requested beam time, specified for each major activity, is shown in Table VIII. To understand backgrounds from the target windows and beamline sources such as the collimators

(quasi-elastic protons, high energy neutrons, etc.) we need 7 days for both empty target and target-out runs. We will measure the tagging efficency with the Total Absorption Counter and the pair-spectrometer several times. This will be interspersed with production and requires minimal configuration changes, hence only 3 days are budgeted. Based on our experience from the first PrimEx experiment in Hall B, we need 12 days for commissioning, calibration, and general checkout of FCAL-II with beam. The majority of this time will be used for the gain calibration and trigger setup including threshold adjustment. To be able to achieve the greatest possible sensitivity in 100 days of production, we further require 8 days to find the luminosity that optimizes our figure of merit $N_\eta \times Acceptance \times Efficiency/\sqrt{N_{bkg}}$.[11]

This request is for dedicated beam time for the rare decay program. During GlueX running periods, we will utilize the $\eta \rightarrow 3\pi$ data for the photon beam energy range 8.4-9.0 GeV. This will be very important for the quark mass ratio analysis. This will also provide an opportunity to study backgrounds in preparation for rare decay measurements with the upgraded FCAL-II.

[11] Due to increasingly apparent synergies with GlueX running, the time requested for luminosity optimization has been reduced from 14 days in previous versions of this proposal to only 8 days in this version.

VII. SUMMARY

The availability of significantly boosted η's in Hall D, in combination with our proposed lead tungstate upgrade to the forward calorimeter, will improve the signal to background ratio for rare η decays to neutral channels with 3-5 photons by up to 2 orders of magnitude. For non-rare η decays, the combination of JEF and GlueX running will allow the collection of datasets competitive with KLOE-II. This will allow us to address a broad range of important physics topics, from a sensitive search for dark matter to a more precise determination of the quark mass ratio.

Our highest priority channel, $\eta \to \pi^0 2\gamma$, is central to *two* of our physics campaigns: the search for a leptophobic B boson, as well as testing models of ChPT at $\mathcal{O}(p^6)$. By-products of these coupled analyses will include improved limits on the CP violating channel $\eta \to 2\pi^0$ as well as the highly suppressed decay $\eta \to 4\gamma$. The expected dramatic reduction in background also applies to two channels in another physics campaign to improve direct limits on new C violating, P conserving interactions: $\eta \to 3\gamma$ and $2\pi^0\gamma$ (as well as our $\pi^0\gamma$ control).

Our emphasis and niche is in rare η decays to neutral modes, where because of our proposed technology we would have no competition. However, we have been persuaded to form a close collaboration with theorists to to reduce uncertainties on the quark mass ratio. We will increase the size of the world $\eta \to 3\pi$ datasets by about 2.7x for both the charged and neutral channels. (See Table II.) Over 2/3 of the new dataset would be obtained during 200 days of approved GlueX-IV running. Our systematic errors will cross-check other high precision datasets (KLOE in the case of the charged 3π channel, and MAMI in the case of the neutral 3π channel) and are expected to be significantly smaller due to our flatter acceptance over phase space.

The channels in the scope of this proposal are summarized in Table I, while event yields are summarized in Table VII. The parameters of the reference design were summarized in Table V. We estimate Hall D can produce 3×10^7 proton-tagged η's in 100 days in the forward, exclusive channel $\gamma + p \to \eta + p$ alone. Folding in the high resolution calorimeter acceptance, our expected number of $\eta \to \pi^0 2\gamma$ rare decay events will not only exceed that of published or preliminary datasets, but will have an order of magnitude larger figure of merit due to lower backgrounds. This high figure of merit will apply to all rare decays to all-neutral final states.

Appendix A: FCAL-II versus FCAL for hybrid meson decays

As was presented in previous sections, the inner part of the FCAL-II instrumented with $PbWO_4$ crystals provides a significantly better energy resolution for reconstructed photons compared with the FCAL. FCAL-II also allows for a better separation of potentially overlapping clusters. The better energy resolution will improve reconstruction for several of the hybrid meson decays of interest to GlueX which happen to be photon-rich.

As an example, we compared reconstructions in the FCAL-II and FCAL using $\gamma p \to \pi(1400)p$, $\pi(1400) \to \eta\pi^0$ decays. The invariant mass resolution of two photons originating from π^0 and η decays, as well as the fraction of events hitting the forward and the barrel calorimeters, are listed in Table IX. The invariant mass resolutions for FCAL-II are ∼30% smaller. The total energy resolution of reconstructed decays is found to be about a factor of 1.5 better for FCAL-II, specifically 169 MeV and 248 MeV for FCAL-II and FCAL, respectively. (See Fig. 43.) Improvements in the invariant mass resolution and energy resolution depend on the event topology and kinematics.

Some photon-rich hybrid decays will yield more than 4 photons in the final state. As an initial study, we subsequently generated $\gamma + p \to p + X(1600)$, $X(1600) \to \eta\pi^0\pi^0$ events, which contains one additional pion in the final state. Though these events have a more isotropic decay angular distribution, resulting in a smaller fraction of photons accepted in the inner, higher resolution part of the FCAL-II, the total energy resolution in the FCAL-II is about a factor of 1.35 better than that in FCAL.

Appendix B: Lead Tungstate vs Lead Glass Both at 6m

Comparison of lead tungstate vs lead glass for the central region of the forward calorimeter. See Figures 44 and 45.

	π^0		η	
	FCAL	FCAL-II	FCAL	FCAL-II
$M_{\gamma\gamma}$ mass resolution (MeV/c^2)	6.6	4.1	22.3	17

Two photons in Forward Calorimeter

Fraction of events	52%		32%	
$M_{\gamma\gamma}$ mass resolution (MeV/c^2)	6.2	3.2	19	12

One photon in Forward Calorimeter and one in BCAL

Fraction of events	20%		55%	
$M_{\gamma\gamma}$ mass resolution (MeV/c^2)	7.0	6.2	22.9	19.5

TABLE IX: Invariant mass $M_{\gamma\gamma}$ resolution of reconstructed π^0 and η mesons originating in $\gamma + p \rightarrow p\eta\pi^0$ reaction.

Appendix C: Electromagnetic Background

Monte Carlo simulations were done using the standard GlueX *sim-recon* package to estimate the trigger and accidentals rates coming purely from electromagnetic background. The simulation used the standard GlueX geometry which included the FCAL lead-glass calorimeter at its nominal position and the Forward Drift Chambers (FDC) installed, also in the nominal position. The simulation consisted of searching for photons in FCAL arising from the full beam photon spectrum at a rate consistent with 4×10^7 tagged γ/s running. A 100ns time window was used. The results shown here therefore consist of events where a single beam photon contributed to the detector response as well as events where multiple beam photons contributed. Note that in the offline analysis, showers will only be accepted if they are coincident within a single 2 nsec RF beam bucket, so the offline event rate from electromagnetic background will be far smaller than the trigger rate from this background.

Used in the study were two candidates for the GlueX level-1 trigger. These are defined as:
L1a : $(E_{BCAL} + 4 * E_{FCAL}) > 2GeV \& (E_{BCAL} > 200MeV) \& (E_{FCAL} > 30MeV)$
and

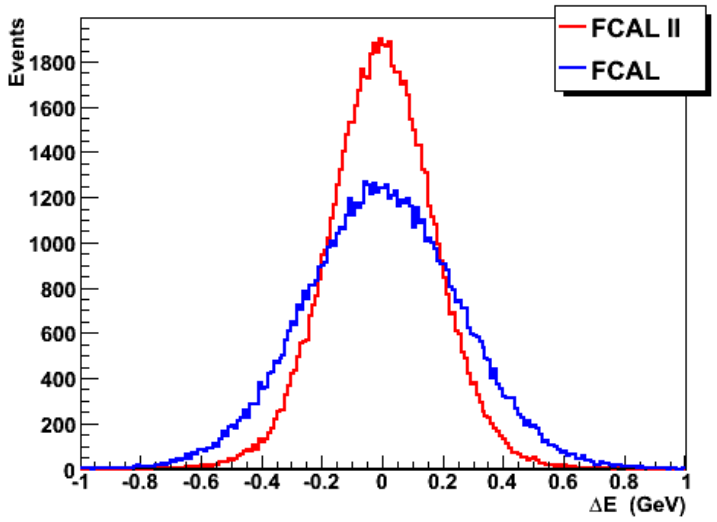

FIG. 43: Energy resolution of the reconstructed $\gamma + p \rightarrow p\eta\pi^0$ decays in the FCAL-II (red) and FCAL (blue).

L1b : $(E_{BCAL} + 4 * E_{FCAL}) > 2GeV \& (E_{BCAL} > 30MeV) \& (E_{FCAL} > 30MeV) \& (N_{SC} > 0)$ where SC indicates the Start Counter, and $BCAL$ is for Barrel Calorimeter. The reconstruction software requires FCAL cluster energies to be greater than 0.5 GeV. No other cuts are applied. Neither of these potential GlueX triggers is a close match to the JEF trigger (which will require the total energy in FCAL to exceed 8 GeV), but this existing simulation tool provides insight into how the electromagnetic background decreases rapidly with increasing energy.

Figure 46 shows the number reconstructed photons per event in the FCAL for events passing the level-1 triggers described above. Since both level-1 triggers require energy in the FCAL, the bin at $N_{photons} = 0$ is empty. Figure 47 shows the total reconstructed energy in FCAL for 5 seconds of real time. Under the level-1 trigger condition, the trigger rate due to electromagnetic background would be approximately $4.2kHz$, but with an 8 GeV threshold it will be less than 1 Hz hence negligible.

Figure 48 shows the invariant mass of all reconstructed FCAL photons for events with at least 4 reconstructed photons. The histogram has been scaled by the 5 seconds of beam time simulated to make the y-axis in units of trigger rate per 2MeV of invariant mass. Extrapolating Figure 48 to the η mass, the rate is about 6.7×10^{-6} Hz, roughly two orders of magnitude smaller than the expected $\eta \rightarrow \pi^0\gamma\gamma$ signal rate (2×10^{-4} Hz). Taking into account that the offline coincident time

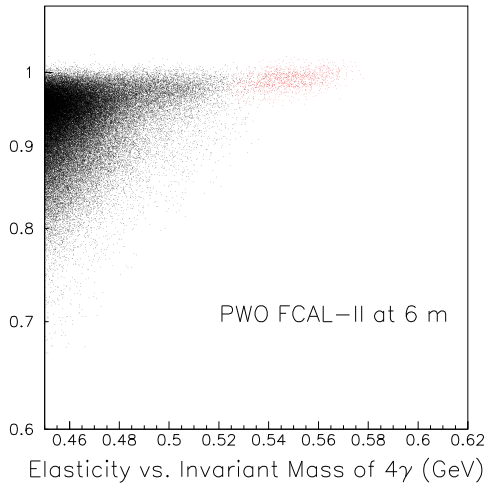

FIG. 44: Monte Carlo simulation assuming the $PbWO_4$ calorimeter in our reference design (the central part of FCAL-II). The vertical axis is the measured elasticity (a missing energy-like variable) while the horizontal axis is the reconstructed invariant mass, $M_{4\gamma}$. Signal events $\eta \to \pi^0\gamma\gamma$ appear as red dots while background $\eta \to 3\pi^0$ events are black.

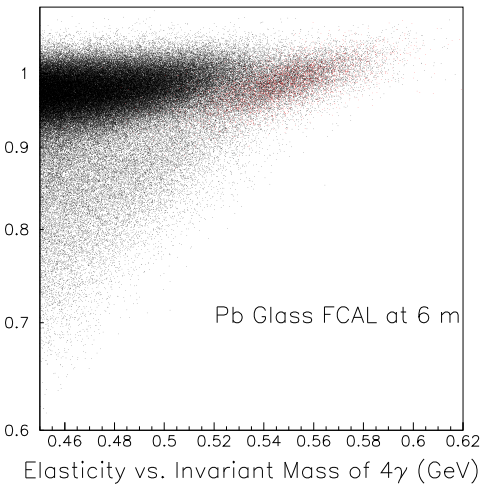

FIG. 45: Same conditions as the previous figure but using a current Hall D forward lead glass calorimeter (FCAL) at 6m.

window of 2 ns is much smaller than the 100 ns sampling window considered here, we conclude that beam related electromagnetic background plays no significant role in either the JEF online trigger rate or in the offline 4-photon accidentals background.

Appendix D: Performance of the PrimEx $PbWO_4$ Calorimeter (HyCal)

1. Energy and Position Resolutions

During the PrimEx-I experiment in 2004, calibration of HyCal was performed using a low intensity tagged photon beam with energies of $E_\gamma = 0.5 - 5.5$ GeV. After the center of each detector module was irradiated, the calorimeter was moved to scan the photon beam continuously across the entire front face of the calorimeter, row by row. The measured energy and position resolutions *versus* initial incident photon energy are shown in Figure 49 and Figure 50 respectively. Excellent energy and position resolutions were achieved which was crucial to achieving the good resolution in $M_{\gamma\gamma}$

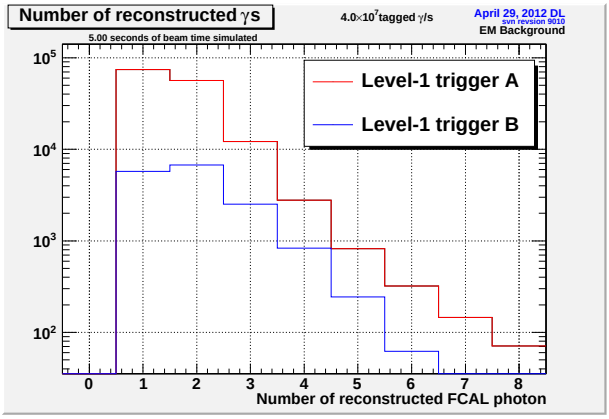

FIG. 46: Number of reconstructed photons in GlueX FCAL for events triggered by electromagnetic beam background.

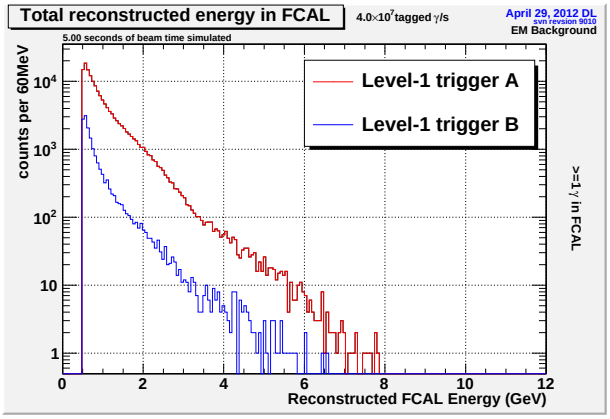

FIG. 47: Energy sum of all reconstructed photons in GlueX FCAL for events triggered by electromagnetic beam background.

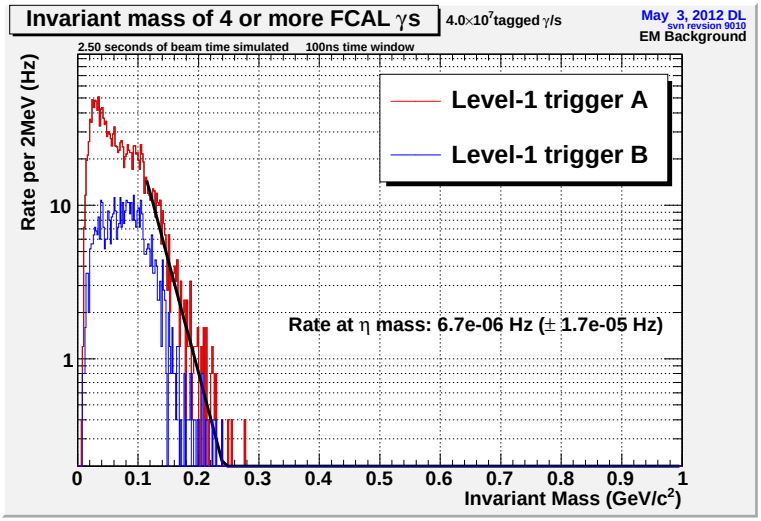

FIG. 48: Invariant mass of all reconstructed photons in GlueX FCAL for events triggered by electromagnetic beam background that have at least 4 reconstructed photons.

needed to isolate good π^0 events from background and to accurately determine the π^0 production angle used to identify the Primakoff peak. A 2.8% total uncertainty on the π^0 lifetime [147] was obtained in PrimEx-I, a factor of two and half more precise than the Particle Data Group average of several old experiments [148].

The PrimEx program proved the $PbWO_4$ material was highly radiation resistant. In terms of angle, the central beam hole in HyCal was more than 3x smaller than we plan for FCAL-II in Hall D

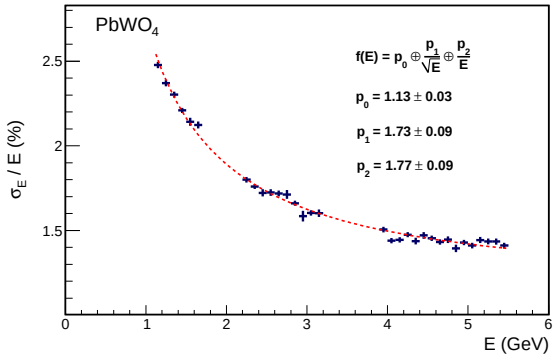

FIG. 49: Measured result for the $PbWO_4$ calorimeter energy resolution *versus* initial incident photon energy. (PrimEx-I calibration) Extrapolated to 10 GeV, the energy resolution will be 1.3% or 130 MeV.

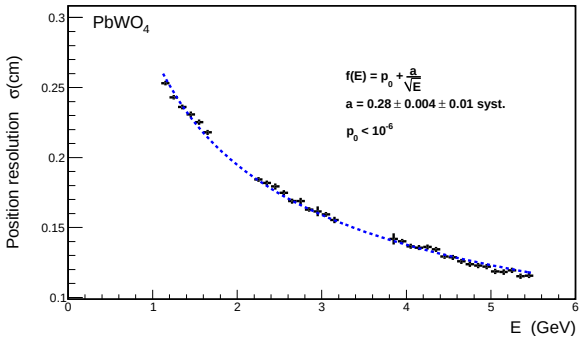

FIG. 50: Measured result for the $PbWO_4$ calorimeter position resolution *versus* initial incident photon energy. (PrimEx-I calibration) Extrapolated to 10 GeV, the position resolution will be 0.9mm.

(4.1×4.1 cm^2 at 7 m for Hycal versus 12x12 cm^2 at 6m for FCAL-II). HyCal was in the beam for more than three months at 7×10^7 γ's/sec on a 5% radiation length (R.L.) target during PrimEx-I and a 10% R.L. target in PrimEx-II. When calibration data were compared from the beginning and end of the program, the gain changes for $\sim$ 1200 channels were less than a few percent.

2. Pile-Up in the PrimEx $PbWO_4$

Another important issue in calorimetry is pile-up, the probability that any given event will appear in combination with clusters from a separate scattering event. In our rare-decay experiment, pile-up could cause $\eta \to 2\gamma$ events to look like $\eta \to 3\gamma$ events, or it could push $\eta \to 3\pi^0$ events with lost photons back into the elasticity cut. During both PrimEx-I and PrimEx-II, clock trigger events were used to open a 100 nsec wide ADC gate with minimal bias. Figure 51 and Figure 52 show the energy-dependent occupancy seen by PrimEx-II which ran at twice the planned JEF luminosity. The probability of a 100 MeV background event occuring during a high energy shower of interest was reduced an additional factor of 50 through the use of TDCs. Although the analysis of the PrimEx-II dataset is still ongoing, the effect on the detection efficiency due to piled-up events was less than 0.5% in the published PrimEx-I result.

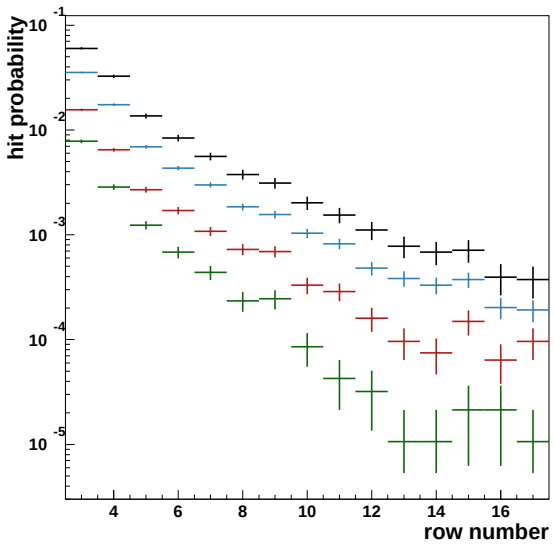

FIG. 51: Probability of a crystal module to register a hit in 100 nsec *versus* the distance from the beam axis in PrimEx-II (1 row = 2.05cm). Rows 1 and 2 are missing due to the beam hole. The black, blue, red and green data points are for the energy deposits in the counter greater than 10 MeV, 20 MeV, 50 MeV, and 100 MeV, respectively. The green points with 100 MeV threshold are most relevant. JEF will use a larger beam hole, effectively starting at row number 4, and run at half the PrimEx-II luminosity.

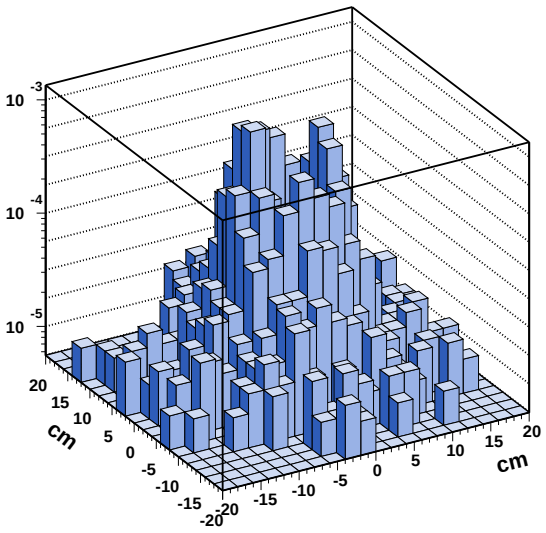

FIG. 52: The γ occupancy probability distribution on the HYCAL measured in PrimEx-II.

3. Photon Merging in a Cluster Reconstruction Algorithm

Recently, collaborator I. Larin developed a so called "Island Algorithm" for cluster reconstruction in the calorimeter to improve the efficiency of shower reconstruction and minimize overlapping showers. We discuss it here because it is relevant to the background in the 4γ channel due to photon merging from the large branch $\eta \to 3\pi^0$.

The algorithm follows three steps: (1) identifying a crystal cell with the maximum energy deposition; (2) declaring all surrounding connected cells as an initial "raw" cluster; (3) splitting the "raw" cluster into many hits based on the transverse shower profile function. The transverse shower profile function for the $PbWO_4$ crystal was measured with a 6×6 matrix $PbWO_4$ prototype detector in a

secondary electron beam. The x and y coordinate of incident beam were determined by a scintillating fiber detector located in front of the prototype calorimeter. The scintillating fiber detector consisted of two scintillating fiber arrays with a 0.6 mm resolution. Figure 53 shows the experimental result for a 2-dimensional shower profile, and Figure 54 shows the shower profile function extracted from the experimental data in Figure 53.

This newly developed cluster reconstruction algorithm was tested by mixing two hits from the PrimEx-II "snake scan" data. A 5 GeV hit was selected from the data as the stationary shower, while a second hit with energy of 1–5 GeV approached the stationary one. The "Island Algorithm" was applied to reconstruct the clusters. Any cases where the two hits were reconstructed as a single cluster were counted as inefficient.

Figure 55 and Figure 56 are the resulting two-cluster reconstruction efficiency *versus* the separation distance between two hits for the 2.05x2.05x18cm^3 $PbWO_4$ and 4x4x45cm^3 Pb glass, respectively. There is no merging of clusters in the $PbWO_4$ calorimeter when the showers are separated by at least 2.5cm, and the majority of close showers are identifiable as such even when their axes are as close as 1.25cm. In lead glass, showers begin to merge even when hits are separated by 6cm, although the majority of close showers can still be flagged as two hits when they are as close as 4.25cm. Using the separation at which 50% of two-cluster hits are reconstructed as a single hit, the use of lead tungstate can be expected to reduce merging probability by roughly $(4.25cm/1.25cm)^2 \sim 12$.

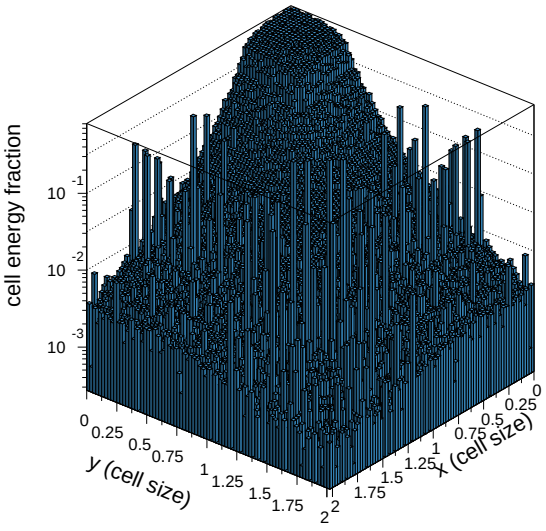

FIG. 53: The $PbWO_4$ calorimeter transverse shower profile measured from the PrimEx beam test.

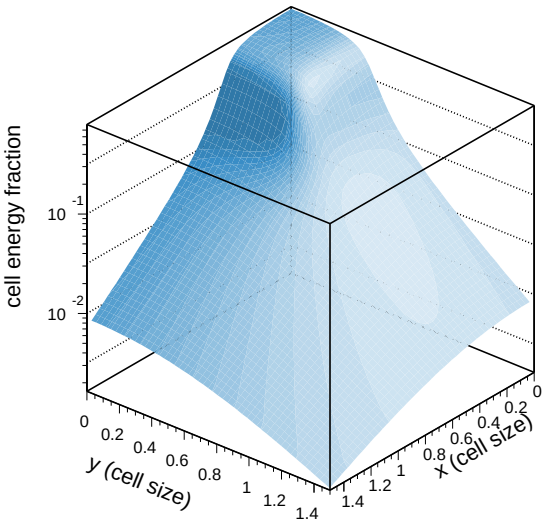

FIG. 54: The $PbWO_4$ calorimeter transverse shower profile distribution function extracted from the PrimEx beam test result shown in Figure 53.

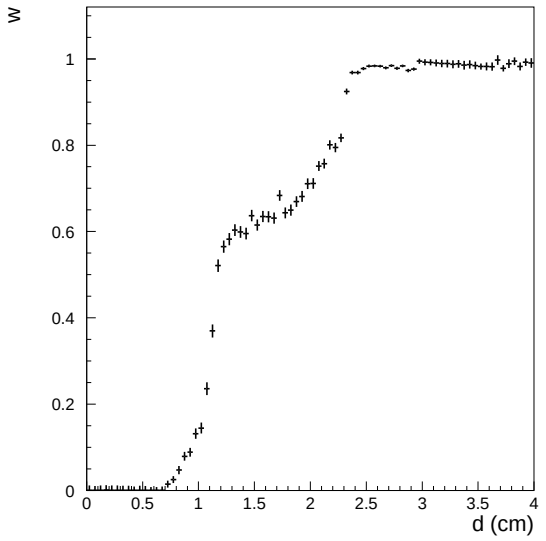

FIG. 55: The $PbWO_4$ calorimeter two-cluster reconstruction efficiency *versus* the separation distance between two showers.

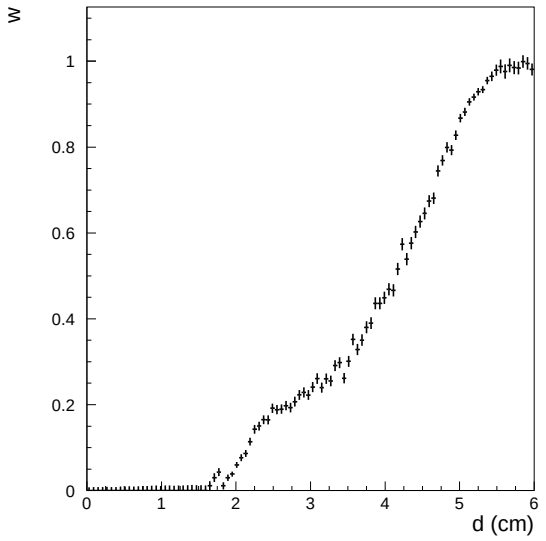

FIG. 56: The Pb glass calorimeter two-cluster reconstruction efficiency *versus* the separation distance between two showers.

[1] L. Gan *et al.*, "Symmetry Tests of Rare Eta Decays to All-Neutral Final States: the JLab Eta Factor (JEF) Experiment", available online at
`http://www.jlab.org/exp_prog/proposals/PR12-13-004.pdf` .

[2] Jefferson Lab PAC40 report, 2013. Available online at
`http://www.jlab.org/exp_prog/PACpage/pac.html`

[3] Workshop on "Hadronic Probes of Fundamental Symmetries", the Amherst Center for Fundamental Interactions (ACFI), University of Massachusetts, Amherst, MA, March 6-8, 2014. *https://www.physics.umass.edu/acfi/seminars-and-workshops/hadronic-probes-of-fundamental-symmetries* .

[4] Workshop summary for "Hadronic Probes of Fundamental Symmetries",
`http://www.physics.umass.edu/acfi/sites/acfi/files/workshop-documents/report-acfi-workshop_1.pdf`

[5] Sean Tulin, talk at ACFI workshop "Hadronic Probes of Fundamental Symmetries".

[6] S. Tulin, arXiv:1404.4370, accepted by Phys. Rev. D.

[7] P. Langacker, Rev.Mod.Phys., 81, 1199 (2009).

[8] J. Beringer *et al.*, (Particle Data Group), PRD 86, 010001 (2012).

[9] B. Dobrescu and C. Frugiuele, arXiv:1404.3947.

[10] H. Davoudiasl, H.S. Lee, and W. Marciano, arXiv:1402.3620, 2014.

[11] G.R. Farrar and G. Zaharijas, Phys.Rev.Lett. 96 (2006) 041302; M. Duerr and P.F. Perez, arXiv:1309.3970v2 [hep-ph] 7 Mar 2014; H. Davoudiasl *et al.*, Phys.Rev.Lett. 105:211304, 2010; K. Agashe and G. Servant, Phys.Rev.Lett. 93:231805, 2004; M.L. Graesser *et al.*, arXiv:1107.2666 [hep-ph].

[12] H. Davoudiasl and R.N. Mohapatra, Invited review, to appear in the New Journal of Physics focus issue on "Origin of Matter", arXiv:1203.1247v2 [hep-ph]; K.M. Zurek, Invited Review for Physics Reports, arXiv:1308.0338v2 [hep-ph]; K. Petraki and R.R. Volkas, Int. J. Mod. Phys. A 28, 1330028 (2013), arXiv:1305.4939v3 [hep-ph].

[13] A. E. Nelson and N. Tetradis, Phys.Lett. B221, 80 (1989).

[14] S. Rajpoot, Phys.Rev. D40, 2421 (1989); R. Foot, G. C. Joshi, and H. Lew, Phys.Rev. D40, 2487 (1989); X.-G. He and S. Rajpoot, Phys.Rev. D41, 1636 (1990); C. D. Carone and H. Murayama, Phys.Rev.Lett. 74, 3122 (1995), hep-ph/9411256; D. C. Bailey and S. Davidson, Phys.Lett. B348, 185 (1995), hep-ph/9411355; C. D. Carone and H. Murayama, Phys.Rev. D52, 484 (1995), hep-ph/9501220; A. Aranda and C. D. Carone, Phys.Lett. B443, 352 (1998), hep-ph/9809522; P. Fileviez Perez and M. B. Wise, Phys.Rev. D82, 011901 (2010), 1002.1754; M. L. Graesser, I. M. Shoemaker, and L. Vecchi (2011), 1107.2666.

[15] R. Barbieri and T. E. O. Ericson, Phys.Lett. B57, 270 (1975).

[16] A. Aranda and C. D. Carone, Phys.Lett. B443, 352 (1998), hep-ph/9809522.

[17] J. Bijnens, talk at "Hadronic Probes of Fundamental Symmetries" ACFI workshop.

[18] L. Ametller, J. Bijnens, and F. Cornet, Phys. Lett., B276, 185 (1992).

[19] B. Holstein, discussion at "Hadronic Probes of Fundamental Symmetries" ACFI workshop.

[20] J.N. Ng and D.J. Peters, Phys. Rev. D **47**, 4939 (1993).

[21] E. Passemar, talk at "Hadronic Probes of Fundamental Symmetries" ACFI workshop.

[22] J. Bijnens, G. Colangelo, and B. Kubis, "Comments on $\eta \to \pi^0\gamma\gamma$ and $\eta \to 3\pi$", May 27, 2014, a theory note following the ACFI workshop.

[23] R.J. Dowdall *et al.*, Phys. Rev. D 88, 074504 (2013).

[24] V. Lubicz, Kaon 2013 conference proceedings, available online at http://arxiv.org/abs/1309.2530 .

[25] M. Antonelli *et al.*, Eur. Phys. J. C (2010)**69**: 399-424. available online at http://www.lnf.infn.it/wg/vus/ .

[26] J. Bsaisou *et al.*, Eur.Phys.J. A49 (2013) 31.

[27] A. Ali *et al.*, Phys.Rev. D63 (2001) 014014.

[28] J. S. Bell and D. G. Sutherland, Nucl. Phys. B **4**, 315 (1968).

[29] D. G. Sutherland, Phys. Lett. **23**, 384 (1966).

[30] G. Colangelo, discussion at "Hadronic Probes of Fundamental Symmetries" ACFI workshop.

[31] Discussions at "Hadronic Probes of Fundamental Symmetries" ACFI workshop.

[32] S. Gardner, talk at "Hadronic Probes of Fundamental Symmetries" ACFI workshop.

[33] J.G. Layter *et al.*, Phys. Rev. Lett. **29** (1972) 316.

[34] J. Bernstein, G. Feinberg and T.D. Lee, Phys. Rev., B139, 1650 (1965).

[35] A.V. Tarasov, Sov. J. Nucl. Phys., 5, 445 (1967).

[36] M.J. Ramsey-Musolf, talk at "Hadronic Probes of Fundamental Symmetries" ACFI workshop.

[37] A. Kurylov, G. Mclaughlin and M. Ramsey-Musolf, phys. Rev., D63, 076007 (2001).

[38] B.M.K. Nefkens *et al.*, Phys. Rev. C **72**, 035212 (2005).

[39] Jlab 12 GeV upgrade white paper "The Science Driving the 12 GeV Upgrade of CEBAF".

[40] R. Essig, *et al.*, arXiv:1311.0029, 2013.

[41] B. Holdom, Phys. Lett., B166, 196 (1986).

[42] B. Batell, M. Pospelov, and A. Ritz, Phys.Rev. D80, 095024 (2009), 0906.5614.

[43] A. Artamonov *et al.* (BNL-E949 Collaboration), Phys.Rev. D79, 092004 (2009), 0903.0030.

[44] R. Dharmapalan *et al.* (MiniBooNE Collaboration) (2012), 1211.2258.

[45] H. Davoudiasl, H.-S. Lee, and W. J. Marciano, Phys.Rev. D85, 115019 (2012), 1203.2947.

[46] R. Essig, J. Mardon, M. Papucci, T. Volansky, and Y.-M. Zhong, JHEP 1311, 167 (2013), 1309.5084.

[47] R. Foot, G. C. Joshi, and H. Lew, Phys.Rev. D40, 2487 (1989)

[48] M. Williams, C. Burgess, A. Maharana, and F. Quevedo, JHEP 1108, 106 (2011), 1103.4556.

[49] M. Pospelov, colloquium presentation at Jlab, May 16, 2014.

[50] Proceeding for the 7th international workshop on chiral dynamics, Aug 6-10, 2012, Newport News, VA. http://www.jlab.org/conferences/CD12/program.html

[51] F. Niecknig *et al.*, Eur. Phys. J. C72: 2014, 2012.

[52] J. Bijnens and K. Kampf, Nucl.Phys.Proc.Suppl., **207-208**, 220 (2010).

[53] S. Cohen, H. Lin, J. Dudek, R. Edwards, arXiv:0810.5550 [hep-lat].

[54] N.H. Christ, *et al.*, Phys.Rev.Lett., **105**, 241601 (2010).

[55] B.R. Holstein, Phys. Scri. T99, 55 (2002).

[56] Private discussions with B.R. Holstein and J. Goity.

[57] M. Reece and L.T. Wang, JHEP 07, 051 (2009).

[58] M. Gell-Mann, R. J. Oakes, and B. Renner. Phys. Rev. 175 (1968) 2195.

[59] B.M.K. Nefkens and J.W. Price, Phys. Scr. **T99** (2002) 114. This review is especially valuable for tying BR upper limits to model-independent constraints on C and CP violation in the strong and EM amplitudes.

[60] S. Kullander *et al.*, Acta Physica Polonica B, Vol. 29 (1998) 97-111. This is an easy reading and insightful survey of the new physics potential of a broad, rare η decay program.

[61] M. Unverzagt, Nucl. Phys. B (Proc. Suppl.) 198 (010) 174-181.

[62] A. Kupsc *et al.*, Nucl. Phys. B (Proc. Suppl.) 181-182 (2008) 221-225.

[63] D. Babusci *et al.*, Phys.Lett. B720, 111 (2013).

[64] P. Adlarson *et al.*, Phys.Lett. B726, 187 (2013).

[65] M. N. Achasov, et, al., Nucl. Phys., B600, 3 (2001).

[66] E. Oset, J.R. Pelaez, L. Roca, Phys. Rev. D77, 073001 (2008).

[67] P. Ko, Phys. Lett. B349, 555 (1995); S. Bellucci and C. Bruno, Nucl. Phys. B452, 626 (1995); J. Bijnens, F. Fayyazuddin and J. Prades, Phys. Lett. B379, 209 (1996); J.N. Ng and D. J. Peters, Phys. Rev. D46, 5034 (1992); M. Jetter, Nucl. Phys. B459, 283 (1996); E. Oset, J.R. Relaez and L. Roca, Phys. Rev. D67, 073013 (2003).

[68] D. Alde et al., Yad. Fiz 40, 1447 (1984); D. Alde et al., Z. phys. C25, 225 (1984); L. G. Landsberg, phys. Rep., 128, 301 (1985).

[69] E. Oset, J. R. Peláez and L. Roca, Phys. Rev. D **67**, 073013 (2003) [hep-ph/0210282].

[70] M. Jetter, Nucl. Phys. B **459**, 283 (1996) [hep-ph/9508407].

[71] G. Ecker, J. Gasser, A. Pich and E. de Rafael, Nucl. Phys. B **321**, 311 (1989).

[72] D. Antreasyan *et al.* [Crystal Ball Collaboration], Phys. Rev. D **33**, 1847 (1986).

[73] T. Oest *et al.* [JADE Collaboration], Z. Phys. C **47**, 343 (1990).

[74] J. A. Oller and E. Oset, Nucl. Phys. A **629**, 739 (1998) [hep-ph/9706487].

[75] I. V. Danilkin, M. F. M. Lutz, S. Leupold and C. Terschlüsen, Eur. Phys. J. C **73**, 2358 (2013) [arXiv:1211.1503 [hep-ph]].

[76] G. Ecker, et. al., Nucl. Phys., B321, 311 (1989).

[77] J. Bijnens and G. Ecker, arXiv:1405.6488, 2014.

[78] J. Schwinger, Phys. Lett. B24 (1967) 473; J. Wess and B. Zumino, Phys. Rev. 163 (1967) 1727; S. Weinberg, Phys. Rev. 166 (1968) 1568.

[79] J. Bijnens and J. Gasser, Phys. Scripta, T99, 34 (2002).

[80] J. Bijnens et. al., Phys. Lett., B379, 209 (1996).

[81] L. Ametller, Phys. Scripta, T99, 45 (2002).

[82] L.M. Sehgal, Phys. Rev., D38, 808 (1988).

[83] J.N. Ng, et al., Phys. Rev., D46, 5034 (1992).

[84] B.M.K. Nefkens *et al.*, arXiv:1405.4904v1 [hep-ex] 19 May 2014.

[85] S. Prakhov et al., Phys. Rev. C72, 025201(2005).

[86] S. Prakhov et al., Phys. Rev. C78, 015206 (2008).

[87] S. Prakhov, Proceeding of the 11th International Conference on Meson-Nucleon Physics and the Structure of the Nucleon, Juelich, 2007, http://www.fz-juelich.de/ikp/menu2007/Program/ProgramSessions.shtml.

[88] B.Di Micco et al., Acta Phys. Slovaca 56, 403 (2006).

[89] T.D. Lee and C.N. Yang, Phys, Rev. 104, 254 (1956); Z.K. Silagadze, Phys. At. Nucl. 60, 272 (1997).

[90] C. Jarlskog and E. Shabalin, Phys. Rev. D52, 248 (1995)

[91] C. Jarlskog and E. Shabalin, Phys. Rev. D52, 6327 (1995).

[92] Particle Data Group, Phys. Rev., D66, (2002).

[93] C. Ditsche *et al.*, Eur. J. C (2009) 60: 83-105.

[94] B. R. Holstein, Phys. Scripta T **99**, 55 (2002) [hep-ph/0112150].

[95] Beringer et al.(Particle Data Group), PRD86, 010001 (2012) and 2013 partial update for the 2014 edition (URL:http://pdg.lbl.gov).

[96] S. Lanz, PoS CD **12**, 007 (2013) [arXiv:1301.7282 [hep-ph]].

[97] F. Ambrosino *et al.* [KLOE Collaboration], JHEP **0805**, 006 (2008) [arXiv:0801.2642 [hep-ex]].

[98] F. Ambrosino *et al.*, JHEP 0805: 006, 2008. [arXiv: 0801:2642]

[99] W.B. Tippens et al., Phys. Rev. Lett. 87 (2001) 192001.

[100] S. Prakhov et al., Phys Rev C 79 (2009) 035204.

[101] M. Unverzagt et al., Eur. Phys. J. A 39 (2009) 169.

[102] C. Adolph *et al.*, Phys. Lett. B 677 (2009) 24-29.

[103] F. Ambrosino *et al.*, Phys.Lett. **B694**, 16 (2010).

[104] S. P. Schneider, B. Kubis and C. Ditsche, JHEP **1102**, 028 (2011) [arXiv:1010.3946 [hep-ph]].

[105] R. Baur, J. Kambor and D. Wyler, Nucl. Phys. B **460**, 127 (1996) [hep-ph/9510396].

[106] C. Ditsche, B. Kubis and U.-G. Meißner, Eur. Phys. J. C **60**, 83 (2009) [arXiv:0812.0344 [hep-ph]].

[107] G. Colangelo, S. Lanz, H. Leutwyler and E. Passemar, work in progress.

[108] A. V. Anisovich, Phys. Atom. Nucl. **58**, 1383 (1995) [Yad. Fiz. **58N8**, 1467 (1995)].

[109] A. V. Anisovich and H. Leutwyler, Phys. Lett. B **375**, 335 (1996) [hep-ph/9601237].

[110] J. Kambor, C. Wiesendanger and D. Wyler, Nucl. Phys. B **465**, 215 (1996) [hep-ph/9509374].

[111] S. Lanz, PoS CD **12** (2013) 007 [arXiv:1301.7282 [hep-ph]].

[112] E.L. Bratkovskaya *et al.*, Phys. Lett. B 359 (1995) 217-222.

[113] R.R. Akhmetshin *et al.*, PLB 462 (1999) 380-388.

[114] S. Taylor, "Modelling η and η' Cross Sections", JEF Technical Note, February 10, 2014 . Available online at https://cnidlamp.jlab.org/RareEtaDecay/JDocDB/node/41 .

[115] M. Ablikim *et al.*, PRD **84**, 032006 (2011)

[116] "Photoproduction and Decay of Light Mesons in CLAS", M. Amaryan *et al.* JLab CAA-HS12-01, Newport News, VA, USA, 2012. Available online at http://www.jlab.org/Hall-B/general/caa.html

[117] A.M. Blik *et al.*, Physics of Atomic Nuclei, **70** (2007) 693-701.

[118] F. Ambrosino *et al.*, Phys. Lett. B 606 (2005) 276-280.

[119] D.A. Dicus, Phys. Rev. D 12 (1975) 2133-2136.

[120] J. McDonough et al, Phys. Rev. D 38 (1988) 2121.

[121] A. Aloisio et al., Physics Letters B 591 (2004) 49-54.

[122] C. Jarlskog *et al.*, Phys. Rev. D **52** 6327 (1995), and references.

[123] S. Prakhov *et al.*, Phys. Rev., **C69**, 042202 (2004).

[124] T. Matsumura *et al.*, Nucl. Phys., **A721**, 723 (2003).

[125] Proposal for the Wide Angle Shower Apparatus (WASA) at COSY-Juelich "WASA at COSY", arXiv:nucl-ex/0411038v1 19 Nov 2004

[126] P. Gauzzi, KLOE Results on Light Meson Spectroscopy and Prospects for KLOE-2, talk in Meson Production at Intermediate and High Energies, Nov 10-11, Messina, Italy. Available online at http://newcleo.unime.it/workshop2011/talks.html .

[127] M. Unverzagt, Rare Meson Decays, talk in Meson Production at Intermediate and High Energies, Nov 10-11, Messina, Italy. Available online at http://newcleo.unime.it/workshop2011/talks.html .

[128] R. Kaiser and H. Leutwyler, Eur. Phys. J. C **17**, 623 (2000) [hep-ph/0007101].

[129] J. L. Goity, A. M. Bernstein and B. R. Holstein, Phys. Rev. D **66**, 076014 (2002) [hep-ph/0206007].

[130] A. Kupsc, "Decays and transition form factors of π^0, η' and η' mesons", in "Hadronic Probes of Fundamental Symmetries" http://www.physics.umass.edu/acfi/.

[131] M. Unverzagt, "Light meson physics with the Crystal Ball at MAMI", in "Hadronic Physics Probes of Fundamental Symmetries" http://www.physics.umass.edu/acfi/.

[132] A. H. Fariborz and J. Schechter, Phys. Rev. D **60**, 034002 (1999) [hep-ph/9902238].

[133] B. Borasoy and R. Nissler, Eur. Phys. J. A **26**, 383 (2005) [hep-ph/0510384].

[134] B. Borasoy, U.-G. Meissner and R. Nissler, Phys. Lett. B **643**, 41 (2006) [hep-ph/0609010].

[135] R. Escribano, PoS CD **12**, 035 (2013).

[136] The Technical Design of the Hall-D Polarized Photon Beam at the Thomas Jefferson National Accelerator Facility, The GlueX Collaboration, Novermber 7, 2008.

[137] Jefferson Lab Hall D CDR, version 5.0.

[138] R. Bradford and R.A. Schumacher, CLAS-NOTE 2002-003, unpublished.

[139] R.A. Schumacher, CLAS-NOTE 99-010, unpublished.

[140] Mapping the Spectrum of Light Quark Mesons and Gluonic Excitations with Linearly Polarized Photons, The GlueX Collaboration, gluex.org, July 2006.

[141] Overview of Hall D solenoid refurbishment and testing, G. Biallas et al., September 2010.

[142] Start Counter Update, W. U. Boeglin et al., Florida International University, February 2008.

[143] The GLUEX Central Drift Chamber: Design and Performance, Y. Van Haarlem et al., NIM A, 622 (2010) 142–156.

[144] Performance of the prototype module of the GlueX electromagnetic barrel calorimeter, B. D. Leverington et al., NIM A, 596 (2008) 327–337.

[145] Time of Flight Detector, Conceptual Design Report, The GlueX Collaboration, March 2008.

[146] J.V. Bennett, M. Kornicer, and M.R. Shepherd, Precision timing measurement of phototube pulses using a flash analog-to-digital converter, NIM A622, 225 (2010).

[147] I. Larin et al., Phys. Rev. Lett., 106, 162303 (2011).

[148] K. Nakamura et al. (Particle Data Group), J. Phys. G 37, 075021 (2010).

[149] J.M. Laget, Phys Rev. **C72**, 022202 (2005).

[150] H. Beck et al., Nucl. Instr. Meth., A269, 568 (1988).

[151] Jlab proposal "A Precision Measurement of the η Radiative Decay Width"(E-10-011), 2010.

[152] A. Gasparian and L. Gan et. al., Jlab proposal PR-09-015, "A Precision Measurement of the η Radiative Decay Width via the Primakoff Effect" using the PrimEx PWO calorimeter (HyCal), `http://www.jlab.org/exp_prog/proposals/09/PR12-09-015.pdf, 2009.`